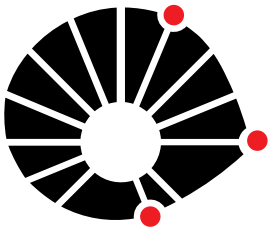

UNICAMP

UNIVERSIDADE ESTADUAL DE CAMPINAS

Instituto de Matemática, Estatística e Computação Científica

FELIPE ALVES RUBIO

Study of the antibody-dependent enhancement phenomenon during secondary dengue virus infection

Estudo do fenômeno reforço dependente de anticorpos durante uma infecção secundária por vírus da dengue

Campinas

2021

Felipe Alves Rubio

Study of the antibody-dependent enhancement phenomenon during secondary dengue virus infection

Estudo do fenômeno reforço dependente de anticorpos durante uma infecção secundária por vírus da dengue

Tese apresentada ao Instituto de Matemática, Estatística e Computação Científica da Universidade Estadual de Campinas como parte dos requisitos exigidos para a obtenção do título de Doutor em Matemática Aplicada.

Thesis presented to the Institute of Mathematics, Statistics and Scientific Computing of the University of Campinas in partial fulfillment of the requirements for the degree of Doctor in Applied Mathematics.

Orientador: Hyun Mo Yang

Este trabalho corresponde à versão final da Tese defendida pelo aluno Felipe Alves Rubio e orientada pelo Prof. Dr. Hyun Mo Yang.

Campinas

2021

Ficha catalográfica
Universidade Estadual de Campinas
Biblioteca do Instituto de Matemática, Estatística e Computação Científica
Ana Regina Machado - CRB 8/5467

R825s

Rubio, Felipe Alves, 1992-
Study of the antibody-dependent enhancement phenomenon during secondary dengue virus infection / Felipe Alves Rubio. – Campinas, SP : [s.n.], 2021.

Orientador: Hyun Mo Yang.
Tese (doutorado) – Universidade Estadual de Campinas, Instituto de Matemática, Estatística e Computação Científica.

1. Vírus da dengue. 2. Reforço dependente de anticorpos. 3. Algoritmo de Gillespie. I. Yang, Hyun Mo, 1959-. II. Universidade Estadual de Campinas. Instituto de Matemática, Estatística e Computação Científica. III. Título.

Informações para Biblioteca Digital

Título em outro idioma: Estudo do fenômeno reforço dependente de anticorpos durante uma infecção secundária por vírus da dengue
Palavras-chave em inglês:
Dengue virus
Antibody-dependent enhancement
Gillespie algorithm
Área de concentração: Matemática Aplicada
Titulação: Doutor em Matemática Aplicada
Banca examinadora:
Hyun Mo Yang [Orientador]
José Luiz Boldrini
Carlos Alberto dos Santos Braumann
Jose Fernando Fontanari
Artur César Fassoni
Data de defesa: 14-05-2021
Programa de Pós-Graduação: Matemática Aplicada

Identificação e informações acadêmicas do(a) aluno(a)
- ORCID do autor: https://orcid.org/0000-0002-3428-5919
- Currículo Lattes do autor: http://lattes.cnpq.br/0112134643398966

Tese de Doutorado defendida em 14 de maio de 2021 e aprovada

pela banca examinadora composta pelos Profs. Drs.

Prof(a). Dr(a). HYUN MO YANG

Prof(a). Dr(a). JOSÉ LUIZ BOLDRINI

Prof(a). Dr(a). CARLOS ALBERTO DOS SANTOS BRAUMANN

Prof(a). Dr(a). JOSE FERNANDO FONTANARI

Prof(a). Dr(a). ARTUR CÉSAR FASSONI

A Ata da Defesa, assinada pelos membros da Comissão Examinadora, consta no SIGA/Sistema de Fluxo de Dissertação/Tese e na Secretaria de Pós-Graduação do Instituto de Matemática, Estatística e Computação Científica.

Agradecimentos

Primeiramente agradeço à Deus, pois sem Ele não teria concluído essa longa jornada.

À minha família, que sempre me apoiou e incentivou a continuar os estudos. Em especial à meu pai e minha noiva Vivian, que sempre estiveram ao meu lado nos momentos que mais precisava.

Ao meu orientador Prof. Hyun, que sempre foi paciente e contribuiu muito nesta pesquisa. Agradeço por todo conhecimento transmitido durante nossas reuniões e conversas no laboratório, sempre foram momentos de muito aprendizado.

Aos meus amigos do laboratório EPIFISMA: Josi, Thomas, Luis Pedro, Caren, Geisel, Evandro, Luiz Fernando, Miller e Roberta obrigado pela amizade, encorajamento nos momentos difíceis da pesquisa e por todo o aprendizado durante nossas conversas nos seminários.

À Universidade Estadual de Campinas (UNICAMP), e principalmente ao Instituto de Matemática, Estatística e Computação Científica (IMECC) pela oportunidade, apoio e aprendizado ao longo desses quatro anos.

Aos professores do IMECC, que contribuiram muito na minha formação. Em especial, agradeço ao Prof. Wilson e ao Prof. Joni pelos ensinamentos nas disciplinas de Biomatemática, que me fizeram enxergar as infinitas possibilidades desta área da Matemática. Aos funcionários da secretaria de pós-graduação, da biblioteca do IMECC e da limpeza.

O presente trabalho foi realizado com apoio da Coordenação de Aperfeiçoamento de Pessoal de Nível Superior – Brasil (CAPES) – Código de Financiamento 001.

Resumo

Existem quatro sorotipos do vírus da dengue, os quais têm infectado milhares de pessoas todos os anos, apresentando-se desde formas assintomáticas até casos graves, que muitas vezes pode levar a morte. Uma infecção primária pelo vírus da dengue fornece proteção ao longo de toda a vida para reinfecções de mesmo sorotipo, e apenas uma proteção parcial nos primeiros meses para os demais sorotipos. Uma das hipóteses de aumento da gravidade da dengue em infecções secundárias é que os anticorpos liberados durante a infecção secundária poderiam reforçar a doença, este fenômeno é conhecido como "reforço dependente de anticorpos" (ADE). Neste trabalho são apresentados dois modelos matemáticos compostos por equações diferenciais ordinárias não-lineares para descrever o fenômeno ADE. No primeiro modelo, estudou-se a dinâmica entre as células-alvo, o vírus da dengue e as células plasmáticas. O objetivo é analisar o efeito da capacidade de suporte para a proliferação das células plasmáticas. Conclui-se que se o número básico de reprodução, R_0, for menor do que a unidade e se a proliferação das células plasmáticas for menor do que um valor limiar, o vírus da dengue será eliminado. No entanto, mesmo que o número básico de reprodução seja menor do que um, mas com uma alta proliferação das células plasmáticas é possível a ocorrência de ADE. Em suma, o modelo sugere que quanto maior for a proliferação das células plasmáticas maior será a possibilidade de ocorrência do ADE. Para este modelo também fez-se uma comparação entre a abordagem determinística e estocástica considerando o algoritmo de Gillespie para simulação estocástica. Por fim para o segundo modelo, estudou-se de maneira mais detalhada o fenômeno ADE, com enfoque em analisar a influência do aumento da produção das células B e T de memória. Observou-se que a proliferação das células B de memória é a principal responsável pela ocorrência do ADE. Por outro lado, a memória imunológica das células T tem um papel fundamental para o controle e possível eliminação do vírus.

Palavras-chave: Vírus da Dengue. Reforço dependente de anticorpos. Células B de mémoria. Células T de memória. Simulação estocástica. Algoritmo de Gillespie.

Abstract

There are four serotypes of dengue virus, which have infected thousands of people every year, ranging from asymptomatic forms to severe cases, which often can lead to death. Primary infection with the dengue virus provides lifelong protection against the same serotype reinfections, and only partial protection in the first months for other serotypes. One of the hypotheses of increasing the severity of the dengue disease in secondary infections is that the antibodies released during the secondary infection could reinforce the condition; this phenomenon is known as antibody-dependent enhancement (ADE). This work presents two mathematical models composed of ordinary nonlinear differential equations to describe the ADE phenomenon. In the first model, the dynamics between the target cells, the dengue virus, and the plasma cells were studied. The purpose is to analyze the effect of the carrying capacity for the proliferation of plasma cells. It is concluded that if the basic reproduction number, R_0, is less than one and if the expansion of plasma cells is less than a threshold value, the dengue virus will be eliminated. However, even if the basic reproduction number is less than one, but with a high proliferation of plasma cells, the ADE occurence is possible. In short, the model suggests that the higher the increase of plasma cells, the vaster the possibility of ADE occurrence. For this model a comparison was also made between the deterministic and stochastic approaches considering the Gillespie algorithm for stochastic simulation. Finally, in the second model, the ADE phenomenon was studied in more detail, with a focus on analyzing the influence of increased production of memory B and T cells. It was observed that the proliferation of memory B cells is the main responsible for ADE occurrence. On the other hand, the immune memory of T cells plays a crucial role in controlling and possibly eliminating the virus.

Keywords: Dengue virus. Antibody-dependent enhancement. Memory B cells. Memory T cells. Stochastic simulation. Gillespie algorithm.

Lista de ilustrações

Lista de tabelas

Sumário

Introdução

A Dengue é uma das arboviroses mais comum no mundo, o vírus da Dengue (DENV) é transmitido durante a picada do mosquito fêmea, principalmente das espécies *Ae. aegypti* e *Ae. albopictus*. A Dengue é amplamente distribuída em regiões tropicais e subtropicais, fatores como chuva, temperatura, humidade relativa favorecem o desenvolvimento e a proliferação dos vetores transmissores da doença. Segundo a Organização Mundial de Saúde, esses mosquitos infectam aproximadamente 390 milhões de pessoas por ano. Nos dois últimos anos, cerca de 2,5 milhões de casos de Dengue foram reportados no Brasil.

Há quatro sorotipos distintos do vírus, DENV-1, DENV-2, DENV-3 e DENV-4, os quais possuem 60%-80% de homologia entre si. Infecções primárias por DENV fornecem uma imunidade por toda a vida contra este mesmo sorotipo. Entretanto, a imunidade cruzada para outros sorotipos fornece somente uma proteção parcial e temporária. Infecções secundárias por outros sorotipos aumentam o risco de desenvolver a forma severa da doença. Os mecanismos envolvidos no processo da severidade da dengue não são totalmente compreendidos. A imunidade cruzada pode ser o principal desafio para a criação de uma vacina tetravalente efetiva contra o DENV.

Os anticorpos de um sorotipo específico do vírus da dengue têm um papel importante no controle da infecção viral. No entanto, em alguns casos esse agente protetivo pode contribuir para a replicação do vírus. Esse fenômeno é conhecido como reforço dependente de anticorpos (ADE, em inglês), que é o objeto de estudo deste trabalho. Este fenômeno foi primeiramente descrito por Hawkes em 1964, e somente em 1977 o ADE obteve relevância científica com a associação entre o conceito de reforço e da dengue severa detalhada por Halstead and O'rourke.

O fenômeno ADE pode ser explicado da seguinte forma: quando uma pessoa é infectada pela primeira vez por algum sorotipo da dengue, a resposta imune humoral do hospedeiro produz anticorpos neutralizantes específicos contra esse sorotipo da primeira infecção. Após essa infecção primária ser eliminada, células plasmáticas produzem anticorpos específicos contra o sorotipo primário, os quais persistem no organismo devido a memória imunológica. Se esta pessoa é infectada uma segunda vez com um sorotipo diferente, anticorpos da infecção primária se ligam ao vírus formando o complexo imune, mas não conseguem neutralizá-lo. Além disso, macrófagos são recrutados para eliminar este complexo imune. Eles internalizam o vírus não neutralizado e se tornam infectados durante o processo de eliminação do complexo. Há evidências que os receptores-Fc, os quais são proteínas na superfície de algumas células como macrófagos e monócitos que

se ligam ao complexo imune podem facilitar a entrada do vírus na célula e reforçar a replicação viral.

Nesta tese, propomos e analisamos dois modelos matemáticos compostos por Equações Diferenciais Ordinárias para descrever a interação de células específicas e o DENV na ocorrência do fenômeno ADE.

No Capítulo 1, consideramos um modelo matemático para estudar a interação entre DENV, células plasmáticas e macrófagos. Neste primeiro modelo analisamos o efeito da capacidade de suporte da proliferação de células plasmáticas.

No Capítulo 2, foi proposto a comparação de duas abordagens de modelagem matemática: determinística e estocástica. Para isto, consideramos o modelo determinístico proposto no Capítulo 1 e a algoritmo de simulação estocástica proposto por Gillespie (2).

No Capítulo 3, apresentamos o segundo modelo matemático com o propósito de estudar o efeito da proliferação das células B e T de memória durante uma infecção secundária por vírus heterólogo.

As conclusões gerais e perspectivas futuras são apresentadas no Capítulo 4. Os Capítulos 1 a 3 foram escritos em inglês em formato de artigo para publicação em periódicos internacionais.

1 A mathematical model to describe antibody-dependent enhancement and assess the effect of limiting cloning for plasma cells in heterologous secondary dengue infection

Abstract. We propose a mathematical model to study the antibody-dependent enhancement (ADE) phenomenon. Here we explored the interaction between macrophages, dengue virus, and plasma cells, especially the effect of a limitation on plasma cell proliferation, which occurs due to immunological memory. We determine the existence regions for the equilibrium points of the model and their stability. Numerical simulations show that ADE can occur even when the value of R_0 is less than one. Sensitivity analysis was performed to analyze the most influential parameters on the thresholds R_0 and Q.

Keywords: Mathematical modeling. Sensitivity analysis. Antibody-dependent enhancement. Severe dengue.

1.1 Introduction

Dengue disease is one of the most common arboviruses in the world; the dengue virus is transmitted by *Aedes* mosquito bite. In tropical and subtropical regions, the *Aedes* mosquito is widely distributed, mainly *Ae. aegypti* and *Ae. albopictus*. These mosquitoes infect approximately 390 million people every year (3). Between 2010 and 2016, more than 100 thousand dengue cases were reported to the World Health Organization (WHO) as suspected or confirmed case in Brazil and Mexico.

There are four serotypes of dengue virus (DENV), DENV1 - DENV4, which have 60%-80% homology to each other (4, 5). The main difference between them lies in the subtle discrepancies in surface proteins of different dengue subtypes. These subtle discrepancies generate a cross-reaction that can contribute to the severity of the dengue infection. In general, a person that gets infected with a dengue virus for the first time experiences an asymptomatic or milder infection. This first DENV infection leads their immune system to mount a defense against all serotypes for only 2-3 months; after this, it provides protection only for the Dengue-specific serotype. When this short time wanes, patients with secondary dengue infections are at higher risk of severe disease (6).

The mechanisms involved in the dengue severity process are barely understood.

Cross-reaction may be the main challenge for creating an effective tetravalent vaccine. Borges et al. (2019) showed that post-vaccination enhanced DENV infection in macaques could be detected in their model. It shows that a vaccine might increase the risk of severe dengue in vaccinated individuals. Thus, it is essential to understand cellular mechanisms associated with the DENV infection process and how to fight against this pathogen.

Antibodies of a specific dengue-virus serotype play a vital role in viral infection control. However, this protective agent may play a beneficial role in virus replication; this phenomenon is known as Antibody-Dependent Enhancement (ADE). Hawkes described it in 1964 (8); however, only in 1977, the ADE phenomenon had scientific relevance with the association between the concept of reinforcement and severe dengue detailed by Halstead and O'rourke (1977).

The primary target cells of DENV are macrophages, dendritic cells, and monocytes. Monocytes can control viral replication through phagocytosis, innate and adaptative system stimulation, and antigen presentation during DENV infection (10). After the first dengue infection, a person is protected from having a new infection with the same serotype because memory cells can act quickly and provide an adaptative response (11). These cells can remain in the body for many years or even throughout a lifetime (12). However, DENV infection control is not effective when a person gets a secondary DENV infection but with a different dengue virus serotype from the primary infection.

The specific antibodies of the primary DENV infection start acting on the secondary virus because they suppose it is the same primary dengue virus. This false recognition induces a reinforcement of the new virus. More severe dengue cases have been reported in secondary infections, such as dengue hemorrhagic fever (DHF) and dengue shock syndrome (DSS), which often can lead the patient to death. (4).

Here we propose a mathematical model to describe the ADE phenomenon in secondary dengue infection. We consider that plasma cells produce specific antibodies to the antigen of the primary DENV infection. We also consider that they do not start producing the specific antibodies to the second dengue infection antigen at the beginning of secondary DENV infection. In a simple way, we consider only the plasma cells, macrophages, and the dengue virus as dynamical variables to investigate this phenomenon.

The paper is structured as follows. In section 1.2, a mathematical model is described. In section 1.3, the analysis of the model is presented. We analyzed the existence regions of the equilibrium points and their stability. In Section 1.4, numerical simulations are performed to test the properties of the equilibrium points related to stability. Section 1.5 provides a sensitivity analysis of the parameters R_0 and Q to evaluate the most influential parameters on these thresholds. Section 1.6 shows a discussion about the ADE phenomenon dynamics. Conclusion is presented in Section 1.7.

1.2 Mathematical modeling

We propose a mathematical model that considers only four compartments to study the ADE phenomenon. Memory B cells quickly differentiate into plasma cells in contact with DENV (13). Plasma cell concentration is denoted by B, which releases specific antibodies against the DENV of the primary infection. We assumed that plasma cells are maintained at a constant reposition rate K_B and death rate μ_B. In the DENV presence, they have a proliferate rate $\alpha_B\,(1 - B/K)\,V$, with K being the carrying capacity for plasma cell proliferation.

The antibodies released by plasma cells can bind to the free DENV and form the antibody-antigen complex. The naive macrophages, which are denoted by S, are maintained constant through the repositioning rate K_S and death rate μ_S. These cells are responsible for intake free virus by phagocytosis (11). The per-capita rate α_V describes this process. Moreover, macrophages also can neutralize the virus by opsonization and internalization of the immune complex. This process is facilitated by Fc-receptors, which are proteins found on the surface of specific cells, including macrophages (14). It is described by the per-capita engulfment rate α_C. We consider that each naive macrophage engulfs N immune complexes.

However, facing a secondary dengue infection, the macrophages cannot neutralize the antigen. In fact, among these macrophages, a portion ρ will become infected, which are denoted by I, contributing to virion production. The virion concentration is denoted by V.

We assume that some infected macrophages can neutralize the immune complex and return to the naive class, which occurs at a rate σ. They also have a higher per-capita mortality rate $\mu_I = \mu_S + \mu_a$, where μ_a is the additional mortality due to DENV infection. These infected macrophages release new virions at a per-capita virion production rate γ, and μ_V represents the per-capita death rate of the virions. Also, the DENV can infect others cells, but here we are interested in investigating only the infection in macrophages. Since many antibodies can bind to the free DENV to form the immune complex, there would be a small amount of free DENV to infect other cell types. So, we are considering that most of the DENV infection occurs via macrophages.

Considering all the hypothesis above, we have the following system of nonlinear ordinary differential equations,

$$\begin{aligned}
\frac{dB}{dt} &= K_B + \alpha_B \left(1 - \frac{B}{K}\right) BV - \mu_B B \\
\frac{dS}{dt} &= K_S + \sigma I - (\rho \alpha_C BV + \mu_S) S \\
\frac{dI}{dt} &= \rho \alpha_C BVS - (\sigma + \mu_I) I \\
\frac{dV}{dt} &= \gamma I - N \alpha_C BVS - (\alpha_V S + \mu_V) V.
\end{aligned} \tag{1.1}$$

Figure 1.1 shows a flow chart for model (1.1).

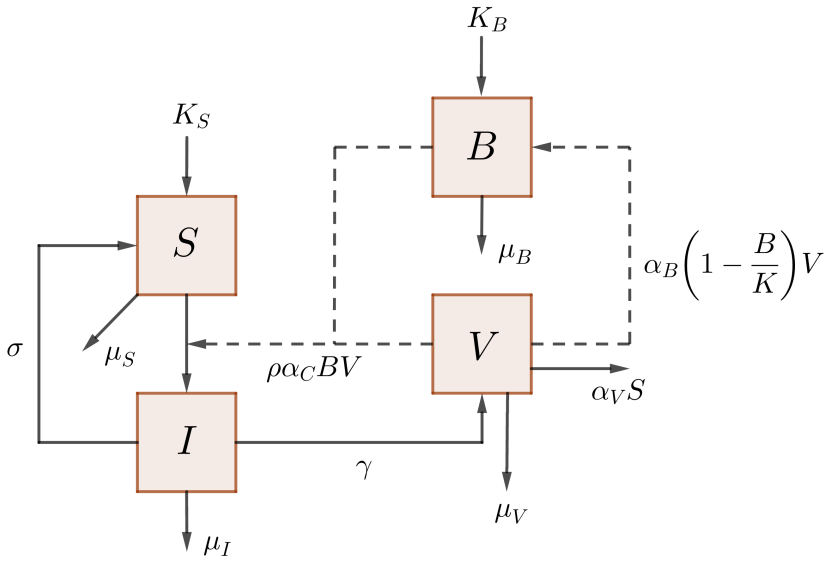

Figure 1.1 – Flow chart for model (1.1). The solid arrows mean a change of state, while dashed arrows represent only interference between the cells.

Table 1.1 describes the variables of model (1.1), and their respective unit (*vol* means an arbitrary volume unit). A summary of the parameters and their meanings can be found in Table 1.2.

Variable	Meaning	Unit
B	Plasma cells	$[B]/vol$
S	Naive macrophages	$[M]/vol$
I	Infected macrophages	$[M]/vol$
V	Virions	$[V]/vol$
t	Time	T

Table 1.1 – Description of variables of the model (1.1).

Parameter	Meaning	Value	Unit	Reference
K_B	Production rate at rest of plasma cells	40.0	$[B]\,vol^{-1}T^{-1}$	(15)
μ_B	Per-capita mortality rate of plasma cells	0.02	T^{-1}	(16)
α_B	Per-capita proliferation rate of plasma cells	$^*3.0 \times 10^{-11}$	$[V]^{-1}\,volT^{-1}$	Assumed
K	Carrying capacity for proliferation of plasma cells	$^*8.0 \times 10^{3}$	$[B]\,vol^{-1}$	Assumed
K_S	Production rate of naive macrophages	6.8×10^{3}	$[M]\,vol^{-1}T^{-1}$	(17, 18)
μ_S	Per-capita mortality rate of naive macrophages	0.017	T^{-1}	(17)
α_C	Per-capita engulfment rate of antigen-antibody complex	$^*2.0 \times 10^{-9}$	$[B]^{-1}\,[V]^{-1}\,vol^2T^{-1}$	Assumed
ρ	Fraction of infected macrophages	$^*3.6 \times 10^{-5}$	-	(15)
σ	Per-capita recovery rate of infected macrophages	0.2	T^{-1}	(15)
μ_I	Per-capita rate mortality of infected macrophages	0.2	T^{-1}	(19)
γ	Per-capita releasing rate of virions by infected macrophages	6.12×10^{4}	$[M]^{-1}\,[V]\,T^{-1}$	(20, 17)
α_V	Per-capita phagocytosis rate by naive macrophages	8.0×10^{-6}	$[M]^{-1}\,volT^{-1}$	(15)
μ_V	Per-capita inactivation of virions	3.3	T^{-1}	(21)
N	Number of antigen-antibody complex engulfed by macrophages	3.0	$[M]^{-1}\,[V]$	(15)

Table 1.2 – Parameter description and values adopted in simulations of the model (1.1). (We used $vol = mm^3$ and $T = day$. *Value allowed to vary.)

The solutions of the system (1.1) with an initial condition in Ω, which is given by

$$\Omega = \left\{ P = (B, S, I, V) \in \mathbb{R}^4_+ : B \geqslant \frac{K_B}{\mu_B}, S + I \leqslant \frac{K_S}{\mu_S}, V \leqslant \frac{\gamma K_S}{\mu_V \mu_S} \right\}, \tag{1.2}$$

are always positively limited.

Proposition 1.1. *The set Ω is positively invariant with respect to system (1.1), considering $\mu_I > \mu_s$ and $K > (K_B/\mu_B)$.*

Proof: See appendix 1.A. □

1.3 Model Analysis

We determine the equilibrium points of the system (1.1) and their stability. The equilibrium points are found, taking the derivatives of the system (1.1) equal to zero. Supposing $V = 0$ in (1.1) we obtain the virions-free equilibrium (VFE) point, which is denoted by P^0, and assuming $V > 0$ in (1.1), the virions-presence equilibrium (VPE) point, which is denoted by P^*, is established. Through bifurcation diagrams, we show the existence regions for P^* and its stability.

1.3.1 Virions-free equilibrium point - P^0

The VFE point P^0 has the coordinates $(B^0, S^0, I^0, V^0) = (K_B/\mu_B, K_S/\mu_S, 0, 0)$. The characteristic polynomial of the Jacobian Matrix of system (1.1) evaluated at this point is $p(\lambda) = (\lambda - \mu_B)(\lambda - \mu_S)(\lambda^2 + p_1\lambda + p_0)$, in which

$$p_1 = \sigma + \mu_I + \mu_V + S^0\alpha_V + N\alpha_C B^0 S^0$$
$$p_0 = (\sigma + \mu_I)(S^0\alpha_V + \mu_V)(1 - R_0),$$

and

$$R_0 = \alpha_C \frac{K_B}{\mu_B}\frac{K_S}{\mu_S}\left[\frac{\dfrac{\gamma\rho}{\sigma + \mu_I} - N}{\alpha_V \dfrac{K_S}{\mu_S} + \mu_V}\right]. \tag{1.3}$$

The threshold R_0 displays a net amount of new virions produced by one invasive virus in the early stages of secondary DENV infection. Biological details of this parameter are found in Gómez and Yang (2019).

Thus, to guarantee the local stability of P^0, we need that all eigenvalues of Jacobian Matrix evaluated at P^0 have a negative real part (22), that is, all roots of $p(\lambda)$ have a negative real part. As follows, using Routh-Hurwitz criteria, the local stability of P^0 is asserted in Theorem 1.1.

Theorem 1.1. *The VFE point P^0 is locally asymptotically stable (LAS) if $R_0 < 1$ and unstable if $R_0 > 1$.*

Proof: *The Routh-Hurwitz criteria for a second-degree polynomial are $p_1 > 0$ and $p_0 > 0$. Since all parameters are non-negative, it is easy to see that p_1 is positive and $p_0 > 0$ when $R_0 < 1$. So, the local asymptotic stability of P^0 is assured if $R_0 < 1$ and if $R_0 > 1$ the VFE point P^0 is unstable.* □

1.3.2 Virions-presence equilibrium point - P^*

The VPE point $P^* = (B^*, S^*, I^*, V^*)$ is obtained by solving a system equivalent to the system (1.1), given by

$$\begin{cases} 0 = K_B + \alpha_B \left(1 - \dfrac{B^*}{K}\right) B^* V^* - \mu_B B^* \\ 0 = K_S - \mu_S S^* - \mu_I I^* \\ 0 = \rho \alpha_C B^* V^* S^* - (\sigma + \mu_I) I^* \\ 0 = \rho \gamma I^* - N(\sigma + \mu_I) I^* - \rho \alpha_V S^* V^* - \rho \mu_V V^* \end{cases} \tag{1.4}$$

We found the coordinates,

$$\begin{aligned} S^* &= S^0 - \frac{\mu_I}{\mu_S} I^* \\ I^* &= \frac{\mu_B \rho \left(B^* - B^0\right) \left(\alpha_V S^0 + \mu_V\right)}{(\sigma + \mu_I) \alpha_B B^* \left(1 - \dfrac{B^*}{K}\right) \left[\dfrac{\rho \gamma}{(\sigma + \mu_I)} - N\right] + \dfrac{\mu_B \rho \alpha_V \mu_I}{\mu_S} \left(B^* - B^0\right)} \\ V^* &= \frac{\mu_B}{\alpha_B} \frac{\left(B^* - B^0\right)}{\left(1 - \dfrac{B^*}{K}\right) B^*}, \end{aligned}$$

and B^* is the root of the polynomial $z(B^*)$, which is given by

$$z(B^*) = b_2 B^{*2} + b_1 B^* + b_0 \tag{1.5}$$

with coefficients

$$\begin{aligned} b_2 &= -\frac{R_0}{K} \\ b_1 &= R_0 + \frac{B^0}{K} - Q \\ b_0 &= B^0(Q - 1), \end{aligned}$$

and

$$Q = \frac{K_B \mu_V \mu_I \rho \alpha_C}{\alpha_B (\alpha_V K_S + \mu_V \mu_S)(\sigma + \mu_I)}.$$

The parameter Q can be interpreted as the ratio between the mortality rate of infected macrophages and the proliferation rate of plasma cells; it is called ADE weakening factor during DENV infection (15).

Notice that, for $K >> 1$ we can assume $z(B^*) = (R_0 - Q)B^* - B^0(Q - 1) = 0$. Thus, we get only one steady state $P^* = (B^*, S^*, I^*, V^*)$ where $B^* = B^0(Q-1)/(R_0 - Q)$ and $B^0 = K_B/\mu_B$, which is the same steady state P^* presented in Gómez and Yang (15).

The VPE point P^* stability is determined by analyzing the characteristic polynomial of the Jacobian Matrix of the system (1.1) evaluated at this point, given by

$$q(\lambda) = \lambda^4 + q_3 \lambda^3 + q_2 \lambda^2 + q_1 \lambda + q_0, \tag{1.6}$$

wherein the coefficients are defined in Appendix 1.B. Due to the complexity of the coefficients in $q(\lambda)$, we analyze with more details the existence regions for P^* and its respective stability with respect to the parameters Q and R_0.

1.3.2.1 Existence regions for the VPE point and its stability

To analyze the VPE existence regions, we explore the existence regions for B^* varying R_0 and Q. As we presented in the previous section, the equation (1.5) shows a second-degree polynomial with coefficients $b_j,\ j = 0, 1, 2$. Descartes' rule of signs provides that $z(B^*)$ can have only one positive root when $Q > 1$ and zero or two positive roots if $0 \leqslant Q < 1$. However, we are interested only in roots belonging to the interval $[B^0, K[$ to obtain all non-negative equilibrium variables.

Notice that, for $Q = 0$, we have the following roots for $z(B^*)$: $B_1^* = K$ and $B_2^* = B^0/R_0$. According to the value of R_0, B_2^* may be higher or less than B^0 or K. Figure 1.2 shows all the possibilities of position for this specific root.

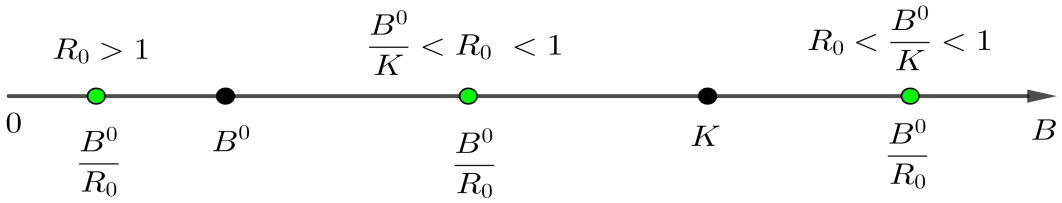

Figure 1.2 – Position of the root $\dfrac{B^0}{R_0}$ when $Q = 0$, according to the value of R_0.

So, we start from $Q = 0$ and analyze the existence regions for B^* varying the parameter Q and considering three cases: (a) $R_0 < (B^0/K) < 1$, (b) $(B^0/K) < R_0 < 1$, and (c) $R_0 > 1$.

1.3.2.2 (a) Case 1: $R_0 < \dfrac{B^0}{K} < 1$

When $R_0 < (B^0/K) < 1$, the value of the root (B^0/R_0) is greater than K, so the bifurcation diagram is located above the range $[B^0, K[$ when $0 \leqslant Q < 1$. Besides that, for $Q > 1$, there is only one positive root, which is less than B^0. Thus, there is no positive root belonging to $[B^0, K[$, which implies that the plasma cell dynamics can converge to B^0 because of $R_0 < 1$. Figure 1.3 shows this behavior.

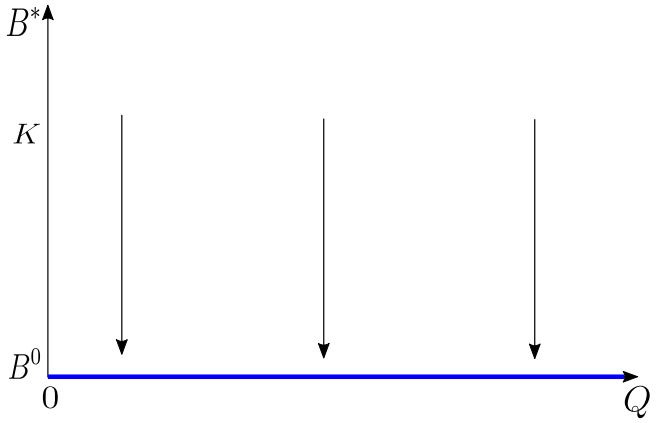

Figure 1.3 – Bifurcation diagram for B^* with respect to Q when $R_0 < \dfrac{B^0}{K}$.

1.3.2.3 (b) Case 2: $\dfrac{B^0}{K} < R_0 < 1$

In this case, there may be two VPE points, which we will denote by $P_-^* = (B_-^*, S_-^*, I_-^*, V_-^*)$ and $P_+^* = (B_+^*, S_+^*, I_+^*, V_+^*)$ with $B_-^* \leqslant B_+^*$. Consider $Q = \hat{Q}_{+,-}$, with

$$\hat{Q}_{+,-} = R_0 + \frac{B^0}{K} - 2R_0\frac{B^0}{K} \pm 2\frac{\sqrt{\phi}}{K}, \tag{1.7}$$

and $\phi = B^0R_0(R_0 - 1)(B^0 - K)$. Notice that, $\phi > 0$ because of $R_0 < 1$ and $B^0 < K$. For $Q = \hat{Q}_{+,-}$, the two positive roots for $z(B^*)$ are the same, which is denoted by $B_+^* = B_-^* = B^*$. However, when $Q = \hat{Q}_+$, the root B^* does not belong to $[B^0, K[$, because

$$B^* = \frac{K}{2} + \frac{B^0}{2R_0} - \frac{\hat{Q}_+K}{2R_0} = B_0 - \frac{\sqrt{\phi}}{R_0},$$

which is less than B^0. On the other hand, if $Q = \hat{Q}_-$, the root B^* is higher than B^0 because of

$$B^* = \frac{K}{2} + \frac{B^0}{2R_0} - \frac{\hat{Q}_-K}{2R_0} = B_0 + \frac{\sqrt{\phi}}{R_0}.$$

Therefore, if $0 \leqslant Q < \hat{Q}_-$, there are two positive roots for $z(B^*)$, which are B_+^* and B_-^*, but if $\hat{Q}_- < Q < 1$, there is no root belonging to the interval $[B^0, K[$. We cannot state if the roots belong to the interval $[B^0, K[$; we only know that they are higher than B^0 when $0 \leqslant Q < \hat{Q}_-$. On the other hand, if $(B^0/K) < R_0 < 1$, we have that $(B^0/K) \in [B^0, K[$, so the two roots will be in $[B^0, K[$. Figure 1.4 shows a bifurcation diagram for B^*, according to the value of Q and considering $(B^0/K) < R_0 < 1$.

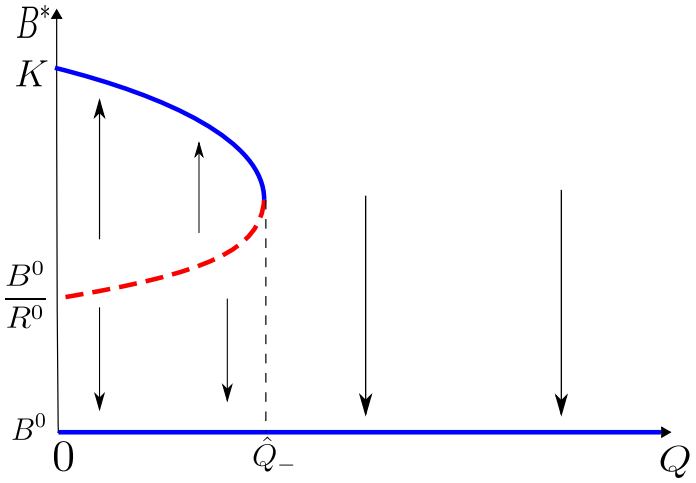

Figure 1.4 – Bifurcation diagram for B^* with respect to Q when $\frac{B^0}{K} < R_0 < 1$.

Concerning the stability of VPE points, P_-^* and P_+^*, through numerical simulations, we verified that the coefficients q_1 and q_0 of the characteristic polynomial $q(\lambda)$ are negative for P_-^*. For P_+^*, all Routh-Hurwitz criteria were satisfied. Figure 1.5 shows all steady states and their respective stability, according to the value of Q and $(B^0/K) < R_0 < 1$. We fixed $B^0 = 2000$, $K = 8000$, and $R_0 = 0.1$. Numerically we verified the real part of all eigenvalues of the Jacobian Matrix of the system (1.1) evaluated at point P^*. If all eigenvalues had the negative real part, we mark the coordinate of the VPE in blue, representing that it was stable. Otherwise, we designed this point in red color to represent instability. In all bifurcation diagrams that show a numerical example of the behavior for B^* according to the value of Q, we use red and blue colors to represent the stability of the point B^*.

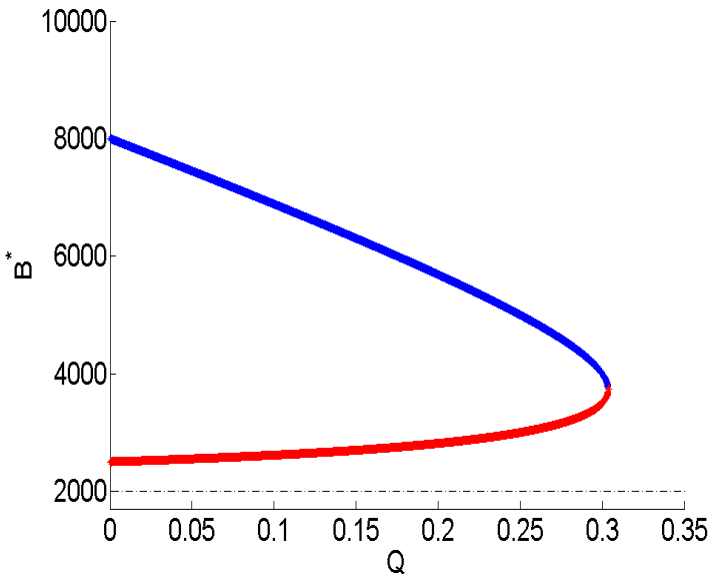

Figure 1.5 – Bifurcation diagram for B^* according to the value of Q, with $B^0 = 2000$, $K = 8000$, and $R_0 = 0.1$.

1.3.2.4 (c): $R_0 > 1$

Notice that $z(B^0) = (B^0/K)(K - B^0)(R_0 - 1) > 0$, $z(K) = -Q(K - B^0) < 0$, and $z(0) = B^0(Q - 1) < 0$. By Bolzano's theorem, there exist a root $B^* \in]0, B^0[$ and other root $\bar{B}^* \in]B^0, K[$. Thus, as $z(B^*)$ is a second-degree polynomial, we conclude that there is only one root in $[B^0, K[$.

Figure 1.6 shows a diagram with the behavior of B^* according to the value of Q. We can see that B^* approaches B^0 as we increase Q.

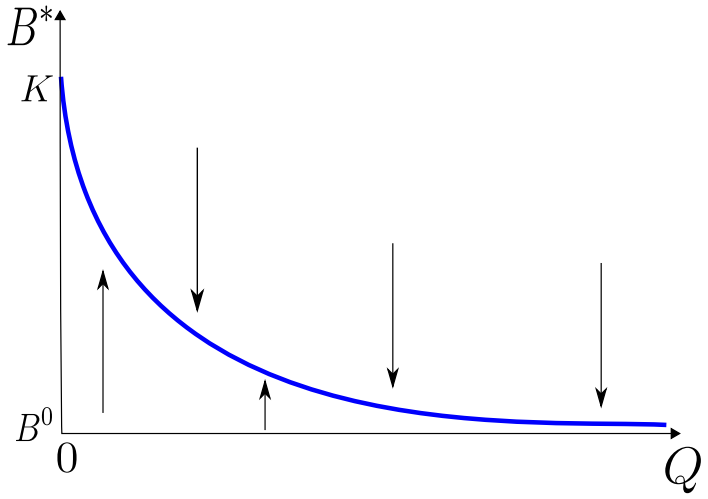

Figure 1.6 – Bifurcation diagram for B^* with respect to Q when $R_0 > 1$. The arrows indicate that B^* is the unique attractor.

According to the local stability, the VFE point P^0 is unstable, and the VPE point P^* is locally asymptotically stable. In fact, through numerical simulations, it was verified that Routh-Hurwitz criteria are satisfied. Figure 1.7 shows a bifurcation diagram with the steady state belonging to $[B^0, K[$, with $R_0 = 1.2$, $B^0 = 2000$, and $K = 8000$. Again, the blue color represents when VPE point P^* is locally asymptotically stable, and the red color represents when VPE point P^* is unstable.

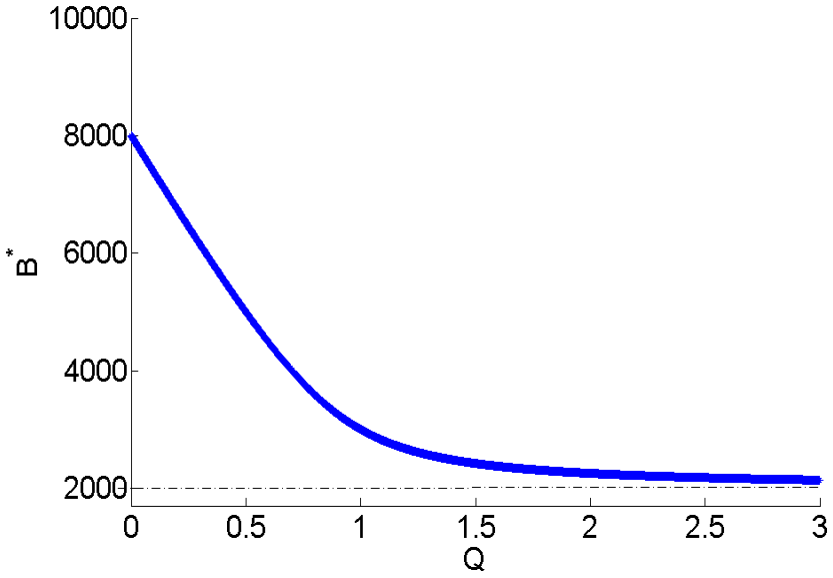

Figure 1.7 – Bifurcation diagram for B^* with respect to Q when $R_0 = 1.2$, $K = 8000$, and $B^0 = 2000$.

Therefore, if $R_0 > 1$, there is a unique VPE point. For $0 < R_0 < 1$, we have two cases: if $R_0 < (B^0/K) < 1$ then there is only the VFE point; and when $(B^0/K) < R_0 < 1$, we may have two VPE points or only the VFE point, according to the value of Q. Figure 1.8 shows existence regions for all steady states according to the values of R_0 and Q.

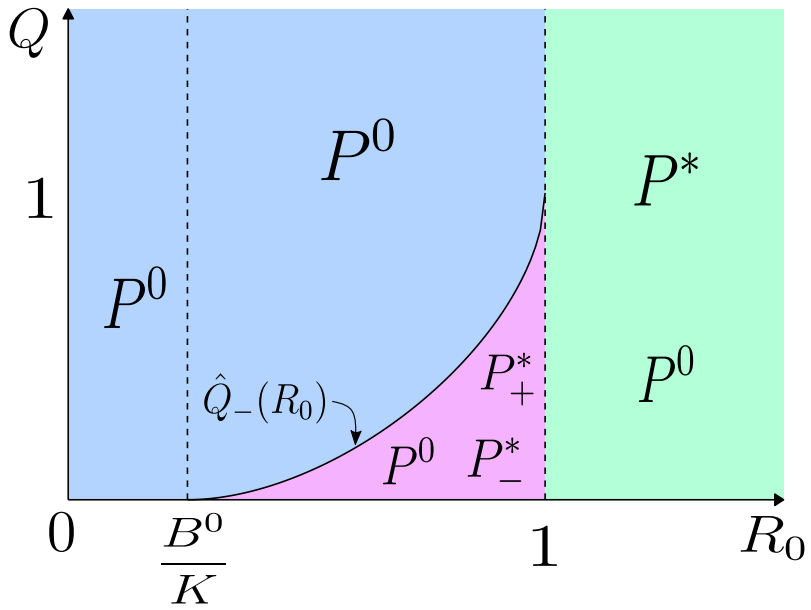

Figure 1.8 – Existence region diagram for all steady states of the model (1.1), according to parameters R_0 and Q.

1.4 Numerical simulations

In this section, we show some numerical results. For instance, we verified the dynamical trajectories for all populations according to the initial virus inoculation and the value of R_0. Also, we analyze the effect of plasma cell carrying capacity and the stable viral load value (V_+^*) when $R_0 < 1$.

In the previous section, we presented that the existence of positive steady states for all populations is related to the value of $\hat{Q}_-$, which depends on the value of R_0 and some other parameters, among them the parameter K. To evaluate the effect of the carrying capacity K in the amount of load viral, we analyze case (b) (in section 1.3.2.3), in which the equilibrium P_+^* is locally asymptotically stable. For this, we used different values of K and all other parameters fixed. It was verified the viral load V_+^* and the time it takes for the system to stabilize, which is denoted by t^*. Table 1.3 shows these values which are the units of t.

K	Viral load - V_+^*	t^*
$4B^0$	$1,971 \times 10^8$	$331,1$
$8B^0$	$2,390 \times 10^8$	$110,4$
$10B^0$	$2,490 \times 10^8$	$104,6$
$20B^0$	$2,680 \times 10^8$	$78,3$
$40B^0$	$2,776 \times 10^8$	$78,2$
$80B^0$	$2,823 \times 10^8$	$74,3$

Table 1.3 – Stable viral load and time spent to reach the stability for different values of K.

For the case $K = \infty$, the viral load is $V^\infty = 2.8710 \times 10^8$, as presented in Gómez and Yang (2019). Notice that, as we increase the value of K, the value of viral load tends to V^∞ and the time spent decreases. Thus, the lower the carrying capacity K, the lower the stable viral load, and the time required will be much longer for the system to stabilize.

To illustrate the different VPE point existence cases, we use the values of parameters, which are given in Table 1.2, and we vary only ρ and α_B. This way, we are able to reach R_0 within the three cases ($(a) : 0 < R_0 < (B^0/K)$, (b): $(B^0/K) < R_0 < 1$, and (c): $R_0 > 1$) and Q greater than or less than one.

For the case $(B^0/K) < R_0 < 1$, we assumed $\rho = 3.5\times10^{-5}$ and $\alpha_B = 5.0\times10^{-10}$, so that $R_0 = 0.5797$ and $Q = 0.0836 < \hat{Q}_-(R_0) = 0.1124$. Thus, we have three equilibrium points, P^0 (LAS), P_-^* (unstable), and P_+^* (LAS). We consider as initial condition the point $P_-^* + \zeta\hat{1}$, which is given by $P_-^* = (B_-^*, S_-^*, I_-^*, V_-^*)$ with $B_-^* = 4.0482\times10^3$, $S_-^* = 2.9818\times10^5$, $I_-^* = 8.6548 \times 10^3$, $V_-^* = 4.0970 \times 10^7$, and $\hat{1}$ is a vector with all four entries equal to one. Assuming $\zeta = 1$, in Figure 1.9 all variables converge to their respective value of VPE point

P^*_+, but if $\zeta = -1$, all populations converge to their respective value of VFE point P^0. Figure 1.10 shows the case with $\zeta = -1$.

Considering $\alpha_B = 3.0 \times 10^{-11}$, we have $Q = 1.3937$. As $Q > \hat{Q}_-(R_0) = 0.1124$, there is only the VFE point, P^0. Simulating the dynamic system with an initial condition $(B(0) = B^0, S(0) = S^0, I(0) = 0, V(0) = 1.0 \times 10^{10})$, the system take around three hundred days to converge to VFE point P^0. As this case is analogous to the Figure 1.10 the graphs are not shown here. So, even with a high virus inoculation, the population dynamics converge to the VFE point P^0, controlling the ADE phenomenon.

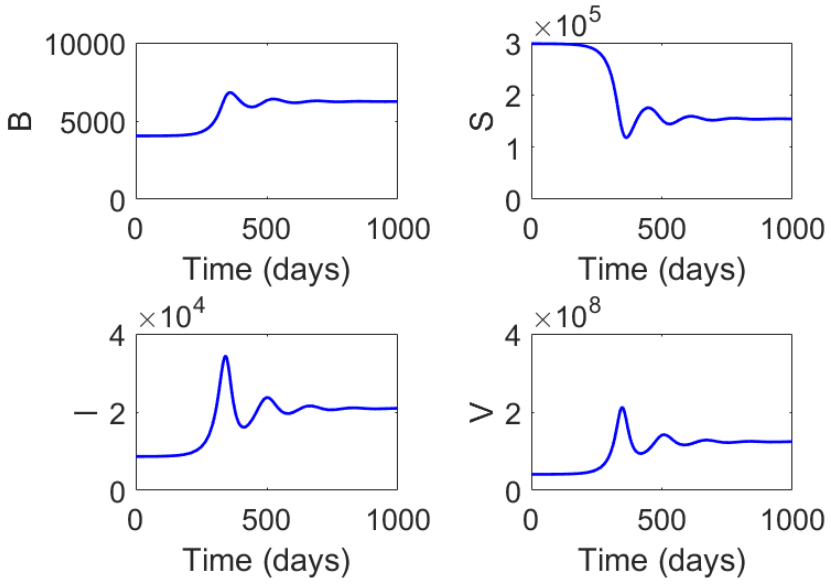

Figure 1.9 – Simulations of system (1.4) with $(B^0/K) < R_0 < 1$ and initial condition given by $(B^*_- + 1, S^*_- + 1, I^*_- + 1, V^*_- + 1)$.

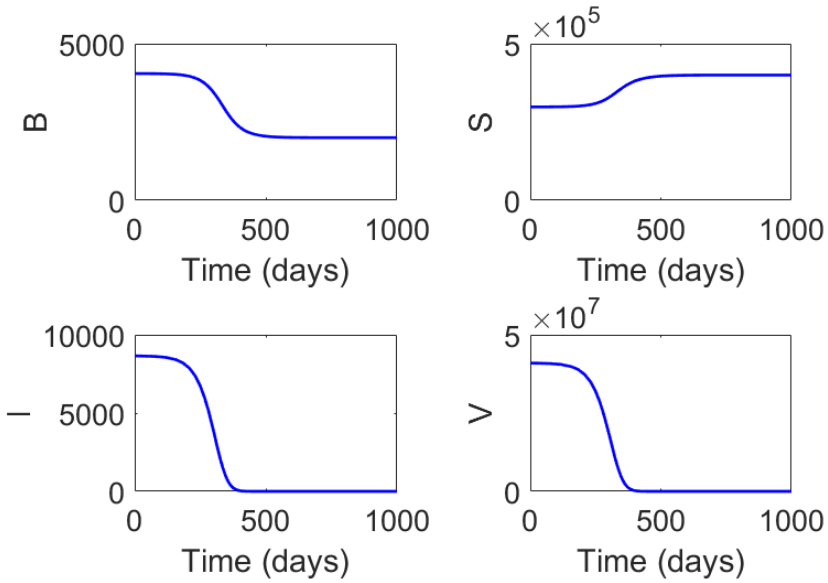

Figure 1.10 – Simulations of system (1.4) with $(B^0/K) < R_0 < 1$ and initial conditional given by $(B^*_- - 1, S^*_- - 1, I^*_- - 1, V^*_- - 1)$.

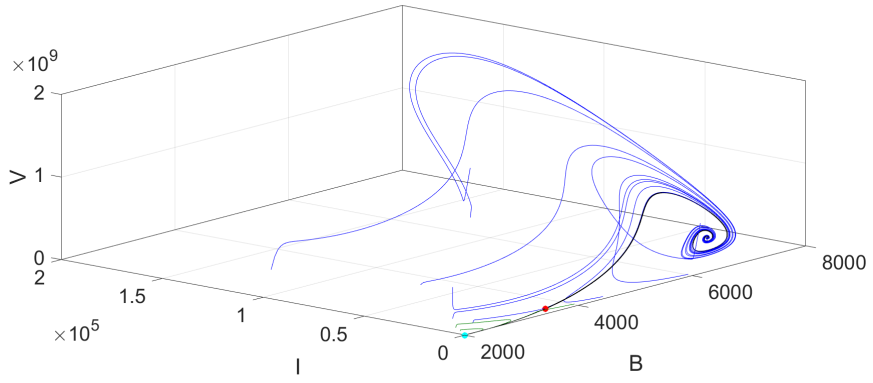

(a)

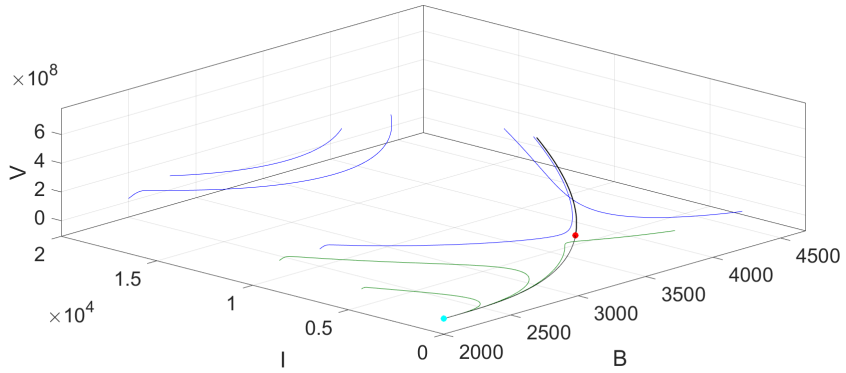

(b)

Figure 1.11 – (a) Convergence of dynamic trajectories $B(t)$, $I(t)$, and $V(t)$, for the case $B^0/K < R_0 < 1$. The blue and green colors represent that trajectories converge to the equilibrium point P_+^* and P^0, respectively. The red point represents the equilibrium P_-^* and the cyan color represents P^0. (b) Same graph as item (a) but restricted to a smaller region.

Figure 1.11 shows that the attraction region for the equilibrium point P^* is much larger than the attraction area to the free-equilibrium point P^0. We randomly chose the initial condition $B(0)$, $S(0)$, $I(0)$, and $V(0)$ inside Ω. The dynamical trajectories approach the curve in black and then converge to the respective steady-state; this occurs because the unstable equilibrium point (in red) has three negative real eigenvalues and only one positive real eigenvalue, which means that te he unstable manifold has dimension 1, and the stable one dimension 3.

In the case $R_0 < (B^0/K) < 1$, there is only the steady state P^0. We consider $\alpha_C = 7.0 \times 10^{-9}$, which leads us to $R_0 = 0.2161 < (B^0/K) = 0.25$. Indeed, even with a high DENV inoculation, the dynamic converges to VFE point P^0. The only difference lies in the time spent for the system to stabilize. With a low DENV inoculation, the dynamical trajectory reaches out to the VFE much faster (around two days) than when a high DENV inoculation (around one hundred days) is assumed. Again, the behavior is analogous to

the case presented in Figure 1.10, so we do not show the graphs here.

Last, assuming $\rho = 8.0 \times 10^{-5}$ and $\alpha_B = 3.0 \times 10^{-11}$, we have $R_0 = 2.2745$ and $Q = 3.1855$. In this situation, for any value of Q, we have only one VPE point P^* and the steady state P^0. If the initial condition is $(B(0), S(0), I(0), V(0)) = (B^0, S^0, 0, 1)$, with $B^0 = 2000$ and $S^0 = 4.0 \times 10^5$, the trajectory of the dynamic system (1.1) converges to the VPE point P^*. Figure 1.12 shows that even a lower viremia the ADE is established.

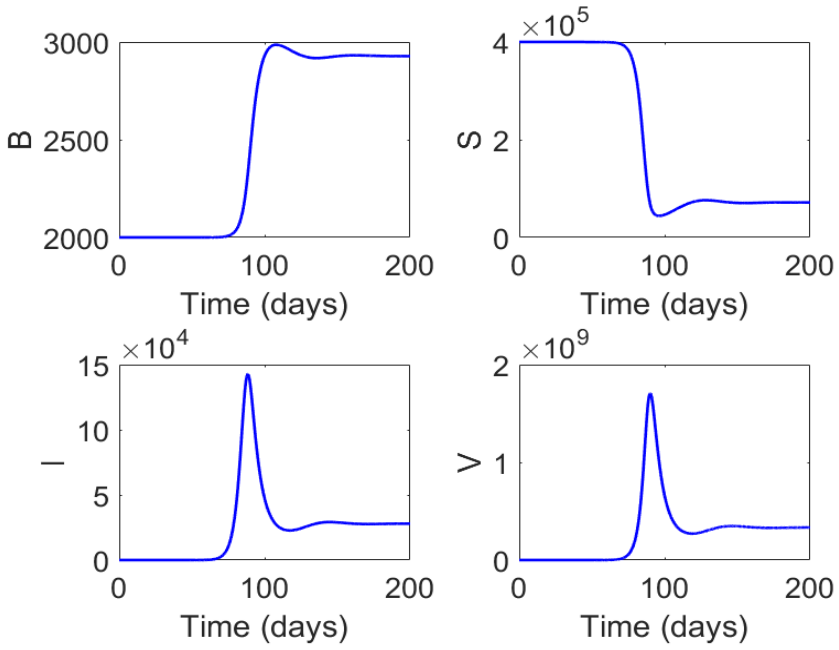

Figure 1.12 – Simulation of system (1.4) with $R_0 > 1$ and as initial condition the VFE point P^0, except for V, which we assumed $V(0) = 1$.

1.5 Sensitivity analysis

Sensitivity analysis (SA) is a method for quantifying uncertainty in any model. The goal of SA is to identify inputs of a model and quantifying how the input uncertainty impacts the model outcome (23). Here, we analyzed two different approaches: Global and Local sensitivity analysis.

In order to perform the global sensitivity analysis, we use the Latin Hypercube Sampling (LHS), which belongs to the Monte Carlo class of sampling methods, and the Partial Rank Correlation Coefficient (PRCC) to evaluate the strength of a linear association between the input and output. To implement the LHS scheme, firstly, we identify the uncertain parameters that we would like to analyze. Secondly, we specify the probability density or distribution function (pdf) for each LHS parameter and the baseline values or the range of values for the parameters. After that, we choose the sample size for our analysis, for instance, N_s, which we define as the number of simulations. The choice of N_s value is not

arbitrary; it depends on the size N_p of uncertain parameters (24, 25). After that, we divided the sample for each parameter into N_s non-overlapping equiprobable intervals. Thus, the sampling distribution of all values for each LHS parameter reproduces the respective pdf shape. Each equiprobable interval of each parameter is randomly sampled once. Moreover, each parameter is sampled independently, so the parameters are uncorrelated (26).

Therefore, we obtain a LHS matrix, which size is $N_s \times N_p$. Note that the values of this matrix are random. There is no order for the values. After N_s simulations, this matrix produce an N_s outcome measure. To perform PRCC, we rank the LHS matrix and the outcome measure (for more details see (23, 26)). The PRCC value belongs to the interval [-1, 1]. The closer the PRCC value to the edges of this range is, the more strongly the LHS parameter influences the outcome measure. A negative sign of the PRCC value indicates that the parameter is inversely proportional to the outcome measure. A positive sign indicates that the LHS parameter is directly proportional to the outcome measure. To perform the LHS/PRCC method, we consider the package "pcc" implemented in the R language, which is a free and open-source language (27). We assess the influence of each parameter that composes the parameters R_0 and Q, so we carry out a sensitivity analysis.

Here, we consider that the production and mortality parameters of plasma cells, macrophages, and the dengue virus follow a normal distribution with a mean equal to the value available in Table 1.2 and a standard deviation of 10% of the mean value of each parameter. For the other parameters, we adopted a uniform distribution in the interval [0, 1]. Besides that, we divide the range of each parameter into 1.0×10^4 parts, so we have $N_s = 1.0 \times 10^4$, $N_p = 10$ for the parameter Q, and $N_p = 12$ for the parameter R_0, in order to construct the $N_s \times N_p$ LHS matrix. Table 1.4 summarizes the distribution of each parameter considered. All histograms of each sampled parameter are presented in Appendix 1.C.

Parameter	Distribution
α_C	$\mathcal{U}(0, 10^{-5})$
K_B	$\mathcal{N}(40, 4)$
μ_B	$\mathcal{N}(0.02, 0.002)$
K_S	$\mathcal{N}(6.8 \times 10^3, 680)$
μ_S	$\mathcal{N}(0.017, 0.0017)$
γ	$\mathcal{N}(6.12 \times 10^4, 6120)$
ρ	$\mathcal{U}(0, 1)$
σ	$\mathcal{U}(0.2, 1)$
μ_I	$\mathcal{U}(\eta, 1)$
N	$\mathcal{U}(1, 10)$
α_V	$\mathcal{U}(10^{-5}, 1)$
μ_V	$\mathcal{N}(3.3, 0.33)$
α_B	$\mathcal{U}(10^{-10}, 1)$

Table 1.4 – Probability distribution assumed for each parameter that compose R_0 and Q. $\mathcal{N}(m, v)$ means Normal distribution, where m is the mean and v the variance of the distribution. $\mathcal{U}(a, b)$ stands for Continuous Uniform distribution on the interval $[a, b]$. To guarantee that always $\mu_I > \mu_S$, we assumed $\eta = \max \mu_S$, where μ_S has the distribution $\mathcal{N}(0.017, 0.0017)$.

Parameter	Range	Mean	Error
α_C	$[0, 10^{-5}]$	0.5×10^{-5}	0.5×10^{-5}
K_B	$[23, 57]$	40	17
μ_B (d)	$[0.01, 0.03]$	0.02	0.01
K_S	$[3600, 10000]$	6800	3200
μ_S (d)	$[0.009, 0.025]$	0.017	0.008
γ	$[31900, 90500]$	61200	29300
ρ	$[0, 1]$	0.5	0.5
σ (d)	$[0.2, 1]$	0.6	0.4
μ_I (d)	$[0.025, 1]$	0.5125	0.4875
N	$[1, 10]$	5.5	4.5
α_V	$[10^{-5}, 1]$	0.5	0.5
μ_V (d)	$[2, 4.6]$	3.3	1.3
α_B	$[10^{-10}, 1]$	0.5	0.5

Table 1.5 – Parameter values considered to the local sensitivity analysis. Here, we assumed as "Error" the distance between the mean value and the limits of the respective interval.

To perform the Local Sensitivity Analysis (LSA), we based on the work of Yang (2001). Considering H_i as the derivative of R_0 with respect to parameter i and L_j as the derivative of Q concerning parameter j, we have

$$H_i = \frac{\partial R_0}{\partial i}, \quad i \in \Theta. \quad \text{and} \quad L_j = \frac{\partial Q}{\partial j}, \quad j \in \Gamma, \tag{1.8}$$

where $\Theta = \{\alpha_C, K_B, K_S, \mu_B, \mu_S, \gamma, \rho, N, \sigma, \mu_I, \alpha_V, \mu_V\}$ and $\Gamma = \{\alpha_C, K_B, K_S, \mu_B, \mu_S, \rho, \sigma, \mu_I, \alpha_V, \mu_V, \alpha_B\}$.

We evaluated the matrices L and H considering the mean values presented in the third column of the Table 1.5, this values are given in the second column of Table 1.6 and Table 1.7, respectively. We denoted that as "Derivative". We call "Error" the distance between the edge and the mean value of the parameter interval. The Error values are presented in the fourth column of Table 1.5. In order to assess the local sensitivity analysis of the parameter R_0, we multiply $H|_\Theta$ and the respective Error. Also, we weight these values with the highest absolute value of $H|_\Theta \times$ Error. We denote these values as "sensitivity". After that, we scaled these sensitivity values, so the maximum value of LHS/PRCC analysis was the maximum sensitivity value. We denoted that as "scaled sensitivity" in order to compare both methods.

The procedure is analogous in order to assess the local sensitivity analysis of the parameter Q. Figures 1.13 and 1.14 show the results of the sensitivity analysis of both methods.

Parameter	Derivative	Sensitivity	Scaled Sensitivity
K_B	2.23559×10^{-9}	3.8005×10^{-8}	0.2906912
μ_V	2.70976×10^{-8}	3.52269×10^{-8}	0.2694422
σ	-8.03807×10^{-8}	-3.21523×10^{-8}	-0.2459253
ρ	1.78847×10^{-7}	8.94235×10^{-8}	0.6839792
α_C	1.78847×10^{-2}	8.94235×10^{-8}	0.6839792
α_B	-1.78847×10^{-7}	-8.94235×10^{-8}	-0.6839792
α_V	-1.78844×10^{-7}	-8.9422×10^{-8}	-0.6839677
K_S	-1.31503×10^{-11}	-4.2081×10^{-8}	-0.3218676
μ_S	-8.6792×10^{-11}	-6.94336×10^{-13}	-5.310039×10^{-6}
μ_I	9.41042×10^{-8}	4.58758×10^{-8}	0.3508931

Table 1.6 – Local sensitivity analysis of the parameter Q.

Parameter	Derivative	Sensitivity	Scaled Sensitivity
α_C	1.09999×10^{8}	549.933	0.7797121
K_B	13.7498	233.747	0.3314138
μ_B	-2.74997×10^{5}	-274.997	-0.3898993
K_S	1.33452×10^{-6}	4.27047×10^{-3}	6.054805×10^{-6}
μ_S	-0.533808	-4.27047×10^{-3}	-6.054805×10^{-6}
γ	8.98862×10^{-3}	263.366	0.3734085
ρ	1.10021×10^{3}	550.103	0.7799531
σ	-494.475	-197.79	-0.2804328
μ_I	-494.475	-241.056	-0.3417767
N	-1.99997×10^{-2}	-8.99985×10^{-2}	-0.0001276027
α_V	-1.09997×10^{3}	-549.984	-0.7797844
μ_V	-2.74992×10^{-3}	-3.5749×10^{-3}	-5.068604×10^{-6}

Table 1.7 – Local sensitivity analysis of the parameter R_0.

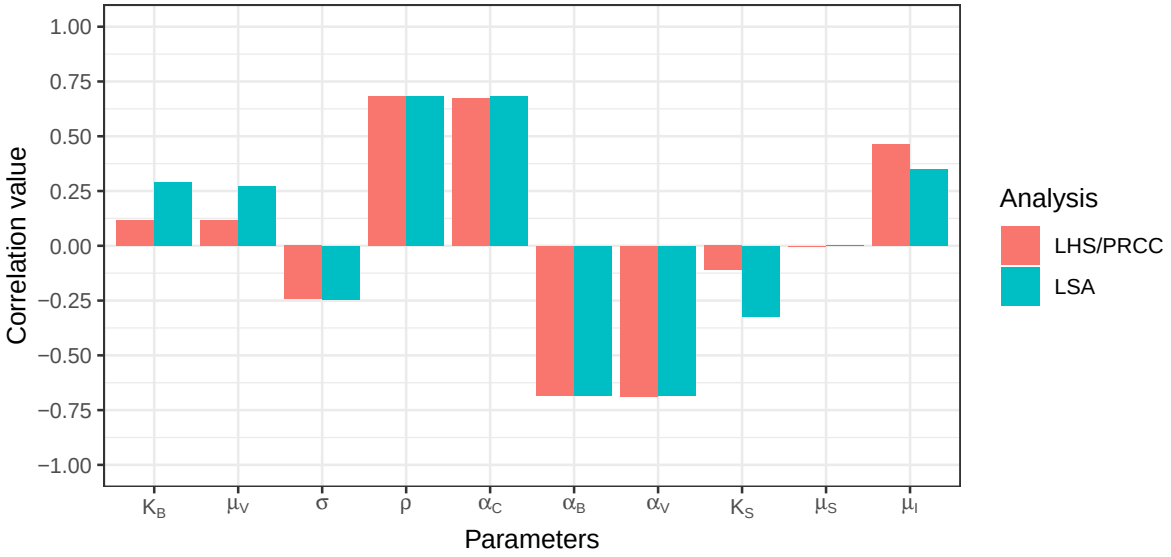

Figure 1.13 – Comparison between LHS/PRCC and LSA to the parameter Q.

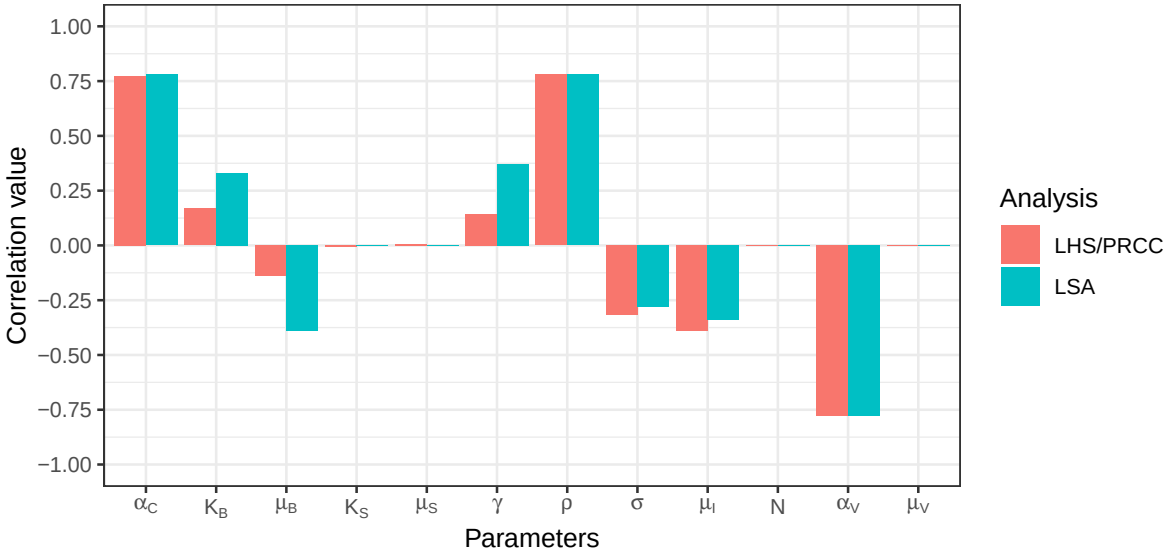

Figure 1.14 – Comparison between LHS/PRCC and LSA to the parameter R_0.

From Figure 1.14, we observe that α_C (0.77971), ρ (0.78000), and α_V (-0.77978) have higher PRCC absolute values than the other parameters. So, α_c and ρ are the most influential parameters in the threshold R_0 with a direct correlation and α_V with an inverse correlation. Similarly, ρ (0.6839792), α_C (0.6839792), α_B (-0.6839792), and α_V (-0.6839677) have higher PRCC absolute values in Figure 1.13.

Furthermore, it can be seen that some parameters in both Figures 1.13 and 1.14 have correlation values that are not similar between the LHS/PRCC and LSA methods. This difference occurs because we consider these parameters to have normal distributions, and we also consider a standard deviation of 10% of the mean value. Thus, we have a low variation of these parameters. The sampled values are more concentrated around the mean value when applying the LHS/PRCC method, while with the uniform distribution, we can capture a greater variation in the considered interval. It can be seen that for some parameters with a normal distribution, the LHS/PRCC method has lower correlation values compared to the LSA method. Thus, the correlation values in both methods were not close for parameters that have a normal distribution.

About the basic reproduction number, the rate of engulfment of the immune complex by naive macrophages, α_C, has a little bit higher influence than the fraction ρ of naive macrophages that will become infected. Also, the process of phagocytosis of naive macrophages is the most influential parameter in an inverse correlation with R_0. For ADE weakening factor, Q, we conclude that α_C, ρ, and α_B are the most influential parameters. The per-capita rate of phagocytosis by naive macrophages has a similar but slightly lower value than the ones mentioned before.

Therefore, considering the specific parameter range presented in Table 1.4 we conclude that α_C, ρ, and α_V are the parameters with the most significant influence on

both R_0 and Q parameters, as well α_B in the parameter Q.

1.6 Discussion

We proposed a mathematical model to describe the ADE phenomenon in secondary dengue infections, considering that plasma cells have a limited proliferation. A constant introduction of a carrying capacity K to plasma cell proliferation limited the possible regions VFE points existence, compared to the model considering $K = \infty$ presented by Gomez and Yang (2019). Their work showed that according to the value of Q and R_0, they could have an attractor point, a VFE point, and a unique VPE point. If $0 < R_0 < 1$ and $Q < R_0$, they observed that the model had only the VFE (unstable) and one attractor point, but if $0 < R_0 < 1$ and $Q > R_0$, then there only was the VFE point (stable). In fact, from the equation (1.7), if $K \to \infty$ then $\hat{Q}_- \to R_0$, in that case, the upper root B^*_+ is no longer an equilibrium point, and we had a unique VPE point B^*_-, which is unstable when $R_0 < 1$, as presented by Gómez and Yang (2019).

Also, increasing the carrying capacity of plasma cell proliferation, then the value (B^0/K) decreased, consequently more significant was the existence region for the three steady states (P^*_+, P^*_-, and P^0). The threshold Q determined the existence region of these three equilibrium points. The higher the value of $\hat{Q}_-$, the larger the existence region for P^*_+ and P^*_-. This variation in $\hat{Q}_-$ is analyzed in Figure 1.15.

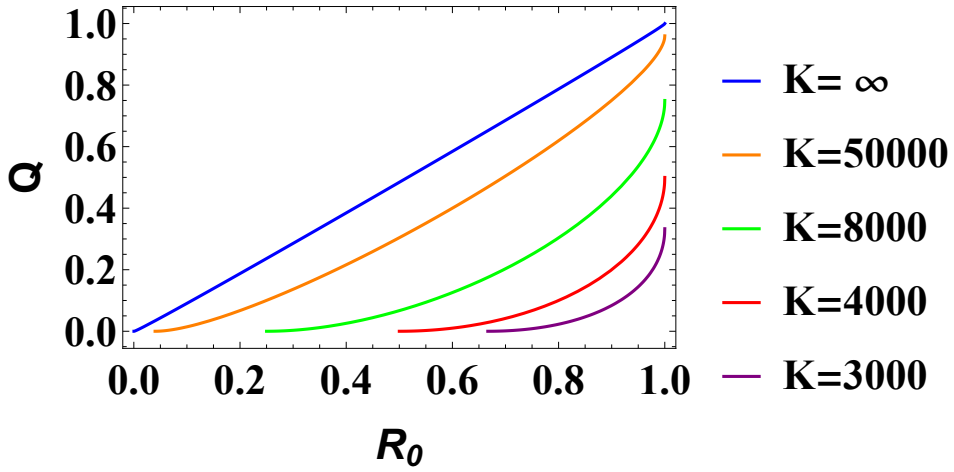

Figure 1.15 – Graphic of parameter $\hat{Q}_-$ by varying R_0 for different values of carrying capacity of plasma cell cloning. The value of K top to bottom is decreasing.

A constant limitation of the plasma cell proliferation carrying capacity suggests that the possibility of the ADE phenomenon is slighter than the case with an unlimited increase of plasma cells. Thus, if the carrying capacity of plasma cell proliferation is a finite value, then the existence region for a positive VPE point is less than when the plasma cells have an unlimited carrying capacity of proliferation.

Therefore, if R_0 is less than one, then VFE point P^0 is locally asymptotically stable; and it is unstable if $R_0 > 1$. However, suppose the value of R_0 is located between the values (B^0/K) and 1. In that case, we have the possibility of the existence of two positive steady states, that is, with positive values for all populations, which are denoted by P^*_+ and P^*_-.

To make it clear, consider the value of R_0 fixed and less than (B^0/K). Regardless of initial DENV inoculation and the value of Q, the ADE failed to progress in heterologous secondary dengue infection. In that case, the immune system was capable of eliminating the DENV. On the other hand, if $(B^0/K) < R_0 < 1$, then initial DENV inoculation was determinant for the ADE occurrence. So, even if the number of virions produced by only one DENV introduced in a population composed only of uninfected macrophages (that is, there are no infected macrophages) is less than one, but higher than the proportion B^0/K, the ADE phenomenon could occur. As said before, this occurrence is directly related to the initial DENV inoculation. Figure 1.11 showed that if the initial DENV inoculation was relatively low, the dynamical trajectories could converge to the VFE point so that the host was able to eliminate DENV. However, assuming that the initial DENV inoculation was too high, the dynamical trajectory had a huge possibility of converging to the VPE point since its region of attraction is much larger than the VFE attraction region. Therefore, the possibility of reinforcement was much higher than the elimination of the DENV.

However, for the case $R_0 > 1$, unlike what occurred in Gómez and Yang (2019), the ADE is inevitable. The system (1.1) always had a unique positive steady state, which was stable and denoted by P^*, independently of the value of Q. Thus, in that case, the ADE weakening factor did not influence the occurrence of the ADE phenomenon.

In the sensitivity analysis, it is important to note that the LSA method proved to be an excellent approach to analyze the influence of the parameters present in R_0 and Q. The computational effort by the LSA method is minimal, in contrast to the LHS/PRCC method, whose computational cost is hours of simulation. Also, considering the LHS/PRCC method, we obtain the output provided by this method, but a positive or negative correlation is not easy to understand. However, with the LSA method, we can clearly understand why we get a positive or negative correlation. For instance, with the LSA method, it is possible to see that the parameter α_V has a negative correlation with the threshold R_0 since the first-order approximation gives a negative value. However, using the LHS/PRCC method, the reason of a negative relationship is not easily seen.

Therefore, as pointed out, the LSA method is an excellent approach since provides a better understanding of the results obtained by the sensitivity analysis.

1.7 Conclusion

In conclusion, this model, in a simplified way, explained the dynamic of the ADE phenomenon in secondary DENV infections. It showed that if the basic reproduction number was less than the quotient between the number of plasma cells to their cloning support capacity, the infection was controlled. However, it was possible to occur DENV infection when the basic reproduction number is greater than the quotient between the number of plasma cells to their cloning support capacity and less than one. In that case, the DENV inoculation had an essential role in the ADE progress or elimination. Also, the parameters related to the engulfment of the immune complex by naive macrophages, the fraction of naive macrophages that will become infected, and the process of phagocytosis are the most influential in the variation of both R_0 and Q. The model has some limitations. We emphasize that the main goal here was to study the dynamic behavior of the ADE phenomenon and do not make predictions. Stochastic and more predictive models that consider other variables, as the specific antibodies of the primary DENV infection and the cytotoxic cells, merit further investigations.

Appendix

This Appendix presents proofs of the positive invariance set and coefficients of the characteristic polynomial evaluated at the VPE point.

1.A Proof of Proposition 1.1

From the first equation of (1.1), considering $V = 0$, we have

$$\begin{cases} \dfrac{dB}{dt} = K_B - \mu_B B > 0, & \text{if } B \leqslant 0, \quad (1.9) \\ \dfrac{dB}{dt} = K_B - \mu_B B = 0, & \text{if } B = \dfrac{K_B}{\mu_B}, \quad (1.10) \end{cases}$$

However, for $V > 0$, we have

$$\frac{dB}{dt} = K_B + \alpha_B \left(1 - \frac{B}{K}\right) VB - \mu_B B > 0, \quad \text{if } B = \frac{K_B}{\mu_B},$$

since $K > (K_B/\mu_B)$. Thus, $\dfrac{dB}{dt} \geqslant 0$ at the boundary $B = K_B/\mu_B$, and there is no flow that crosses this boundary towards values smaller than $B = K_B/\mu_B$, once within of Ω, the flow remains inside this region. If we consider the lower limit as $B = K_B/\mu_B$, we have $B \geqslant 0$.

For naive and infected macrophages, observe that

$$\frac{d(S+I)}{dt} = K_S - \mu_S S - \mu_I I$$

and as per hypothesis, $\mu_I > \mu_S$, so $\dfrac{d(S+I)}{dt} = K_S - \mu_S S - \mu_I I \leqslant 0$ if $S + I \leqslant K_S/\mu_S$.

For V, its maximum production occurs when all macrophages are infected, that is, $S = 0$, and so

$$\begin{cases} \dfrac{dV}{dt} = \gamma I > 0, & \text{if } V = 0, \quad (1.11) \\ \dfrac{dV}{dt} = \gamma I - \mu_V V \leqslant 0, & \text{if } V \geqslant \dfrac{\gamma I}{\mu_V}, \quad (1.12) \end{cases}$$

as the maximum value of I can be K_S/μ_S, so the value for maximum production of V is given by $V^{\max} = \gamma K_S/(\mu_V \mu_S)$.

Thus, we consider all initial conditions $(B(0), S(0), I(0), V(0))$ inside Ω, which assures us that the flow will remain inside Ω. □

1.B Coefficients of the polynomial (1.6)

$$
\begin{aligned}
q_3 &= \left(\frac{2}{K}B^* - 1\right)\alpha_B V^* + B^*S^*N\alpha_C + B^* * V^*\alpha_C\rho + S^*\alpha_V + \sigma + \mu_B + \mu_I + \mu_S + \mu_V,\\
q_2 &= \frac{\alpha_C\alpha_B N S^*V^*(B^*)^2}{K} + \frac{2B^*S^*V^*\alpha_B\alpha_V}{K} - S^*V^*\alpha_B\alpha_V + B^*S^*N\alpha_C\mu_B + S^*\alpha_V\mu_B\\
&\quad + \frac{2B^*V^*\alpha_B\mu_I}{K} - V^*\alpha_B\mu_I + B^*S^*N\alpha_C\mu_I + S^*\alpha_V\mu_I + \mu_B\mu_I + \frac{2B^*V^*\alpha_B\mu_S}{K}\\
&\quad - V^*\alpha_B\mu_S + B^*S^*N\alpha_C\mu_S + S^*\alpha_V\mu_S + \mu_B\mu_S + \mu_I\mu_S + \frac{2B^*V^*\alpha_B\mu_V}{K} - V^*\alpha_B\mu_V\\
&\quad + \mu_B\mu_V + \mu_I\mu_V + \mu_S\mu_V + \frac{2\alpha_B\alpha_C\rho(B^*V^*)^2}{K} - \alpha_B\alpha_C\rho B^*(V^*)^2 + B^*S^*V^*\alpha_C\alpha_V\rho\\
&\quad - B^*S^*\alpha_C\gamma\rho + B^*V^*\alpha_C\mu_B\rho + B^*V^*\alpha_C\mu_I\rho + B^*V^*\alpha_C\mu_V\rho + \frac{2B^*V^*\alpha_B\sigma}{K}\\
&\quad - V^*\alpha_B\sigma + B^*S^*N\alpha_C\sigma + S^*\alpha_V\sigma + \mu_B\sigma + \mu_S\sigma + \mu_V\sigma,\\
q_1 &= \frac{N\alpha_C\alpha_B\mu_I S^*V^*(B^*)^2}{K} + \frac{2\alpha_B\alpha_V\mu_I B^*S^*V^*}{K} - \alpha_B\alpha_V\mu_I S^*V^* + N\alpha_C\mu_B\mu_I B^*S^*\\
&\quad + \alpha_V\mu_B\mu_I S^*\frac{N\alpha_C\alpha_B\mu_S S^*V^*(B^*)^2}{K} + \frac{2\alpha_B\alpha_V\mu_S B^*S^*V^*}{K} - \alpha_B\alpha_V\mu_S S^*V^*\\
&\quad + N\alpha_C\mu_B\mu_S S^*B^* + \alpha_V\mu_B\mu_S S^* + \frac{2\alpha_B\mu_I\mu_S B^*V^*}{K} - \alpha_B\mu_I\mu_S V^* + N\alpha_C\mu_I\mu_S S^*B^*\\
&\quad \alpha_V\mu_I\mu_S S^* + \mu_B\mu_I\mu_S + \frac{2\alpha_B\mu_I\mu_V B^*V^*}{K} - \alpha_B\mu_I\mu_V V^*\mu_B\mu_I\mu_V + \frac{\alpha_B\mu_S\mu_V B^*V^*}{K}\\
&\quad - \alpha_B\mu_S\mu_V V^* + \mu_B\mu_S\mu_V + \mu_I\mu_S\mu_V + \frac{\alpha_B\alpha_C\alpha_V\rho S^*(B^*V^*)^2}{K} - \alpha_B\alpha_C\mu_I\rho S^*B^*(V^*)^2\\
&\quad - \frac{\alpha_B\alpha_C\gamma\rho S^*V^*(B^*)^2}{K} - \alpha_C\mu_B\mu_I\rho B^*S^* + \frac{2\alpha_B\alpha_C\mu_I\rho(B^*V^*)^2}{K} - \alpha_B\alpha_C\mu_I\rho B^*(V^*)^2\\
&\quad + \alpha_C\mu_B\mu_I\rho B^*V^* - \alpha_C\mu_S\gamma\rho B^*S^*\frac{2\alpha_B\alpha_C\mu_V\rho(B^*V^*)^2}{K} - \alpha_B\alpha_C\mu_V\rho B^*(V^*)^2\\
&\quad + \alpha_C\mu_B\mu_V\rho B^*V^* + \alpha_C\mu_I\mu_V\rho B^*V^* + \frac{N\alpha_C\alpha_B\sigma S^*V^*(B^*)^2}{K} + \frac{2\alpha_B\alpha_V\sigma B^*S^*V^*}{K}\\
&\quad - \alpha_B\alpha_V\sigma S^*V^* + N\alpha_C\mu_B\sigma B^*S^* + \alpha_V\mu_B\sigma S^* + \frac{2\alpha_B\mu_S\sigma B^*V^*}{K} - \alpha_B\mu_S\sigma V^*\\
&\quad + N\alpha_C\mu_S\sigma B^*S^* + \alpha_V\mu_S\sigma S^* + \mu_B\mu_S\sigma + \frac{2\alpha_B\mu_V\sigma B^*V^*}{K} - \alpha_B\mu_V\sigma V^* + \mu_B\mu_V\sigma\\
&\quad + \mu_S\mu_V\sigma,
\end{aligned}
$$

$$
\begin{aligned}
q_0 \;=\; & \frac{N\alpha_C\alpha_B\mu_I\mu_S S^*V^*(B^*)^2}{K} + \frac{2\alpha_B\alpha_V\mu_I\mu_S B^*V^*S^*}{K} - \alpha_B\alpha_V\mu_I\mu_S S^*V^* \\
& + N\alpha_C\mu_B\mu_I\mu_S B^*S^* + \alpha_V\mu_B\mu_I\mu_S S^* + \frac{2\alpha_B\mu_I\mu_S\mu_V B^*}{K} - \alpha_B\mu_I\mu_S\mu_V V^* \\
& + \mu_B\mu_I\mu_S\mu_V + \frac{2\alpha_B\alpha_C\alpha_V\mu_I\rho S^*(B^*V^*)^2}{K} - \alpha_B\alpha_C\mu_I\rho B^*S^*(V^*)^2 \\
& + \alpha_C\alpha_V\mu_B\mu_I\rho B^*S^*V^* - \frac{\alpha_B\alpha_C\mu_S\gamma\rho S^*V^*(B^*)^2}{K} - \alpha_C\mu_B\mu_S\gamma\rho B^*S^* \\
& + \frac{2\alpha_B\alpha_C\mu_I\mu_V\rho(B^*V^*)^2}{K} - \alpha_B\alpha_C\mu_I\mu_V\rho B^*(V^*)^2 + \alpha_C\mu_B\mu_I\mu_V\rho B^*V^* \\
& + \frac{N\alpha_B\alpha_C\mu_S\sigma S^*V^*(B^*)^2}{K} + \frac{2\alpha_B\alpha_C\mu_I\mu_V\rho B^*S^*V^*}{K} - \alpha_B\alpha_V\mu_S\sigma S^*V^* \\
& + N\alpha_C\mu_B\mu_S\sigma B^*S^* + \alpha_V\mu_B\mu_S\sigma S^* + \frac{2\alpha_B\mu_S\mu_V\sigma B^*V^*}{K} - \alpha_B\mu_S\mu_V\sigma V^* \\
& + \mu_B\mu_S\mu_V\sigma.
\end{aligned}
$$

1.C Histogram of each sampled parameter

This section presents the histogram of each sampled parameter with Normal or Uniform distribution. Figures 1.16 and 1.17 show histograms with Uniform distribution, while Figures 1.18, 1.19, and 1.20 show the histograms with Normal distribution.

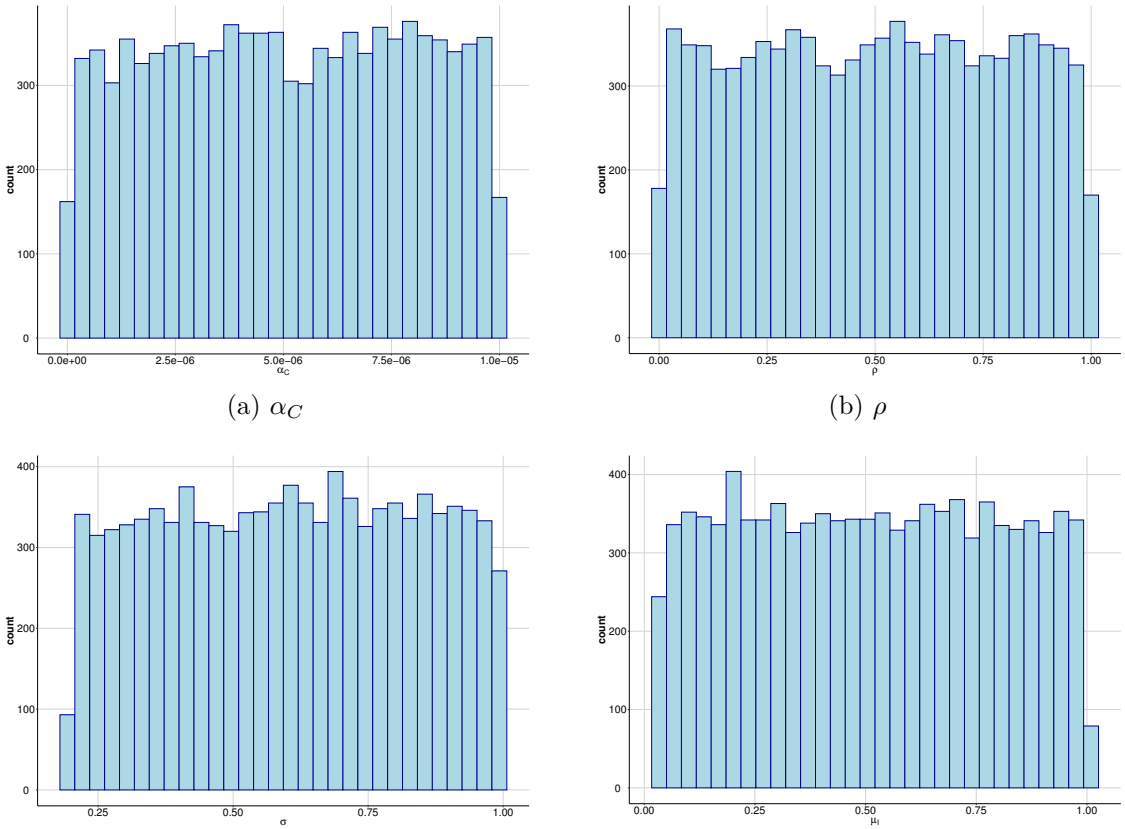

(a) α_C (b) ρ

(c) σ (d) μ_I

Figure 1.16 – Histograms of all parameters with Uniform distribution related to macrophage dynamics.

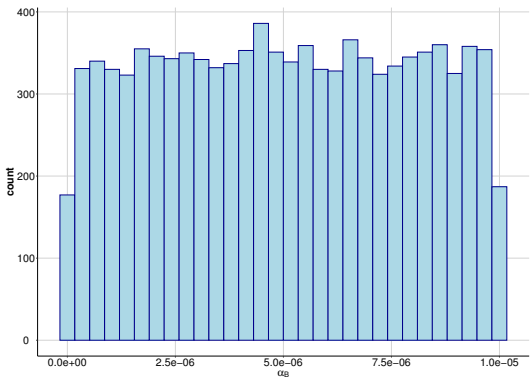

(a) α_B

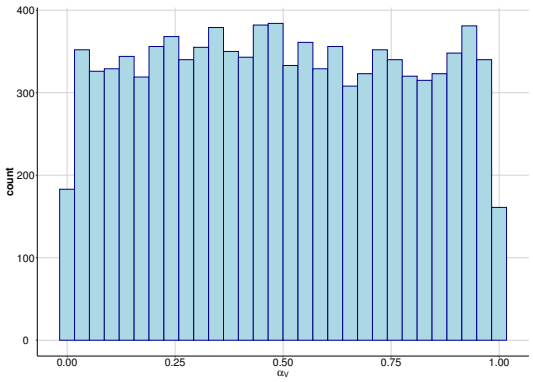

(b) α_V

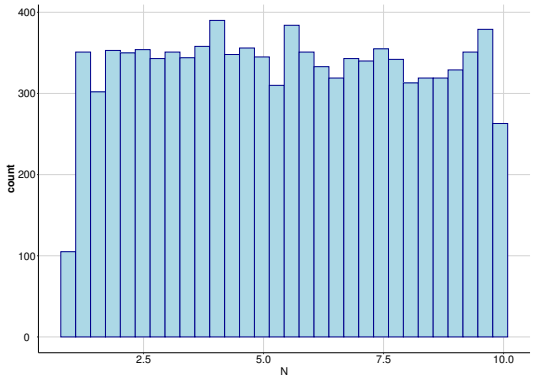

(c) N

Figure 1.17 – Histograms of all parameters with Uniform distribution related to plasma cell and DENV dynamics.

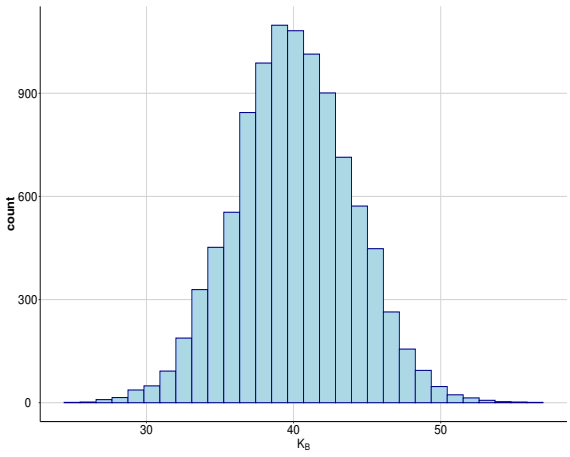

(a) K_B

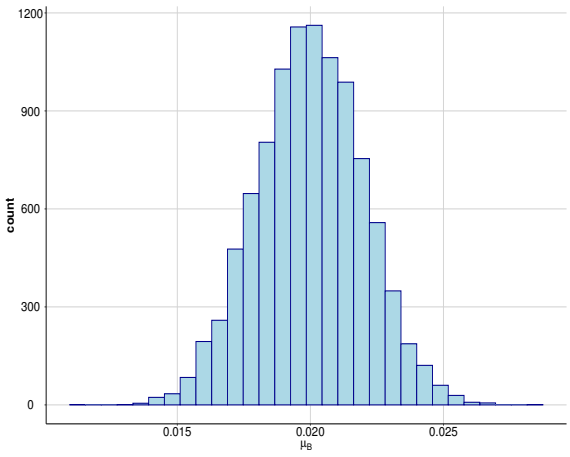

(b) μ_B

Figure 1.18 – Histograms of all parameters with a Normal distribution related to plasma cell dynamics.

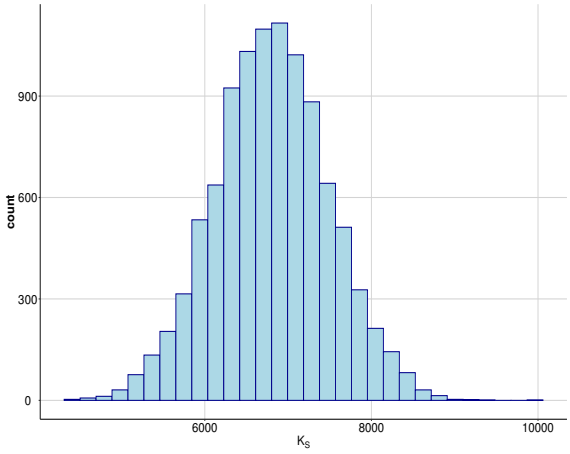

(a) K_S

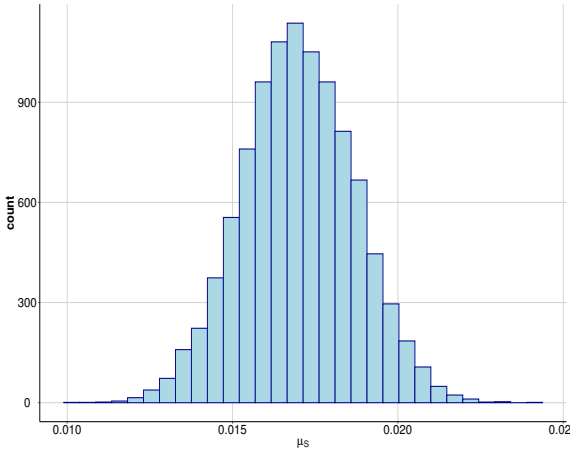

(b) μ_S

Figure 1.19 – Histograms of all parameters with a Normal distribution related to macrophage dynamics.

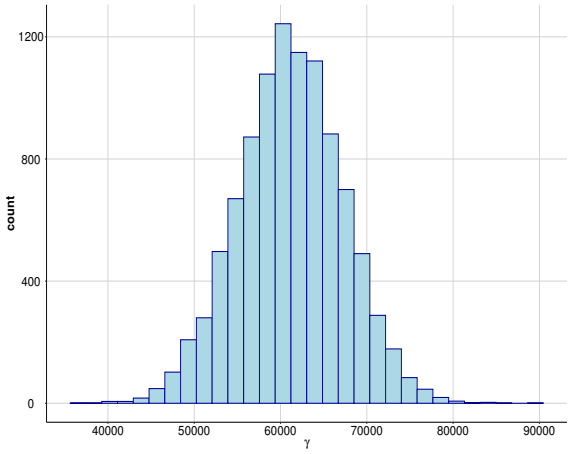

(a) γ

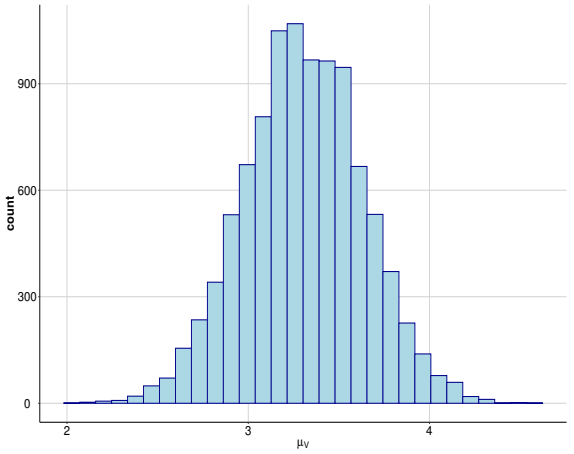

(b) μ_V

Figure 1.20 – Histograms of all parameters with a Normal distribution related to DENV dynamics.

2 Modeling Antibody-Dependent Enhancement Phenomenon - comparing the deterministic and stochastic approaches

Abstract. We propose a mathematical model to study the antibody-dependent enhancement (ADE) phenomenon. We investigate the interaction between plasma cells, macrophages, and dengue virus in heterologous dengue infection. Here we compare two mathematical modeling approaches: a deterministic one and a stochastic one. To make this comparison, we considered a mathematical model composed of four ordinary differential equations and applied the Gillespie Stochastic Simulation Algorithm to perform the stochastic approach. We explore the influence of population size on the outcomes. The size of the population showed an essential role in the convergence for the stochastic approach to obtain the same results as the deterministic model.

Keywords: Mathematical modeling. Antibody-dependent enhancement. Stochastic Simulation. Gillespie algorithm.

2.1 Introduction

Virus-specific antibodies have a fundamental play in controlling the virus infection. However, sometimes these antibodies can be beneficial to enhance the virus concentration in the host (29). This phenomenon is called Antibody-Dependent Enhancement (ADE). Hawkes first described it in 1964 (8), and in 1977, the ADE phenomenon had scientific relevance with the association between the concept of reinforcement and severe dengue detailed by Halstead and O'rourke (1977). The mechanisms involved in the dengue severity process are barely understood. One of these mechanisms is the ADE phenomenon in heterologous dengue infection. There are four serotypes of dengue virus (DENV), DENV1 - DENV4, which have 60%-80% homology to each other (4, 5). The cross-reactive immune response contributes to increased disease severity following heterologous infections (30, 15, 31). Thus, the specific antibodies of primary dengue infection start acting on the secondary virus because they suppose it is the same primary dengue virus. This false recognition induces a reinforcement of the new virus. More severe dengue cases have been reported in secondary infections, such as dengue hemorrhagic fever (DHF) and dengue shock syndrome (DSS), some cases leading the patient to death (4).

Mathematical modeling has been an important tool to investigate biological systems. It is possible with computational and analytical approaches to assess different

scenarios with low cost. Deterministic and stochastic models are two possible approaches in order to investigate the dynamics of biological systems. Several deterministic models have been proposed to simulate dengue disease considering ordinary or partial differential equations (15, 32, 33, 34), and stochastic models have been used as well (35, 36, 37). The main difference of these approaches lies in considering individual probabilities to event occurrence in the stochastic framework, which does not occur with the deterministic one. Also, in a deterministic model, all events occur simultaneously, but this may not be the case when we consider a stochastic model.

Here, we compare a deterministic and stochastic approach analyzing the ADE phenomenon in heterologous secondary infection. To make this comparison, we consider the deterministic model presented by Rubio and Yang (2020); and we applied the Stochastic Simulation Algorithm (SSA) proposed by Gillespie to simulate chemical reactions (2).

2.2 Materials and methods

In this section, we present the deterministic model considered and the existence and stability conditions of the equilibrium points. Also, the procedures for stochastic simulation are presented.

2.2.1 Deterministic model

We based on the mathematical model formulated by Rubio and Yang (2020). They considered a compartmental model composed of four variables to describe the ADE phenomenon: plasma cell, naive and infected macrophages, and the dengue viruses. In that case, the authors assumed that the production rate of dengue viruses was γI. So, the amount of new virions released is proportional to the infected macrophage concentration. Here, in order to consider that each infected macrophage releases θ new virions in the bloodstream after dies, we admit $\theta\mu_I I$ as the production rate to the virus dynamics.

Therefore, we have the following system adapted from Rubio and Yang (2020),

$$\begin{aligned}
\frac{dB}{dt} &= K_B + \alpha_B \left(1 - \frac{B}{K}\right) BV - \mu_B B \\
\frac{dS}{dt} &= K_S + \sigma I - \rho\alpha_C BVS - \mu_S S \\
\frac{dI}{dt} &= \rho\alpha_C BVS - (\sigma + \mu_I) I \\
\frac{dV}{dt} &= \theta\mu_I I - N\alpha_C BVS - \alpha_V SV - \mu_V V.
\end{aligned} \tag{2.1}$$

Table 2.1 summarizes the variables and Table 2.2 describes the meaning of each parameter considered in the system (2.1).

Variable	Meaning	Unit
B	Plasma cells	$[B]/vol$
S	Naive macrophages	$[M]/vol$
I	Infected macrophages	$[M]/vol$
V	Virions	$[V]/vol$
t	Time	T

Table 2.1 – Variables of the model (2.1) and their meanings.

Parameter	Meaning	Value	Unit	Reference
K_B	Production rate at rest of plasma cells	40.0	$[B]\,vol^{-1}T^{-1}$	(15)
μ_B	Per-capita mortality rate of plasma cells	0.02	T^{-1}	(16)
α_B	Per-capita proliferation rate of plasma cells	3.0×10^{-5}	$[V]^{-1}\,volT^{-1}$	Assumed
K	Carrying capacity for proliferation of plasma cells	$^*8.0 \times 10^3$	$[B]\,vol^{-1}$	Assumed
K_S	Production rate of naive macrophages	6.8×10^3	$[M]\,vol^{-1}T^{-1}$	(17, 18)
μ_s	Per-capita mortality rate of naive macrophages	0.017	T^{-1}	(17)
α_c	Per-capita engulfment rate of antigen-antibody complex	$^*2.0 \times 10^{-9}$	$[B]^{-1}\,[V]^{-1}\,vol^2T^{-1}$	Assumed
ρ	Fraction of infected macrophages	1.0×10^{-1}	-	Assumed
σ	Per-capita recovery rate of infected macrophages	0.2	T^{-1}	(15)
μ_I	Per-capita rate mortality of infected macrophages	0.2	T^{-1}	(19)
θ	Number of virions released by one infected macrophage	70	$[M]^{-1}\,[V]\,T^{-1}$	Assumed
α_v	Per-capita phagocytosis rate by naive macrophages	8.0×10^{-6}	$[M]^{-1}\,volT^{-1}$	(15)
μ_v	Per-capita inactivation of virions	3.3	T^{-1}	(21)
N	Number of antigen-antibody complex engulfed by macrophages	3.0	$[M]^{-1}\,[V]$	(15)

Table 2.2 – Parameter description and values adopted in simulations of the model (2.1). (We used $vol = mm^3$ and $T = day$. *Value allowed to vary.)

Using a deterministic approach, Rubio and Yang (2020) determined the existence and stability of the equilibrium points of the system (2.1) concerning the parameters R_0 and Q, which are the basic reproduction number and the ADE weakening factor,

respectively. Figure 2.1 shows the existence conditions and stability for all equilibrium points with respect to the value of R_0 and Q, where

$$R_0 = \alpha_C \frac{K_B}{\mu_B}\frac{K_S}{\mu_S}\left[\frac{\frac{\gamma\rho}{\sigma+\mu_I} - N}{\alpha_V\frac{K_S}{\mu_S} + \mu_V}\right] \qquad \text{and} \qquad Q = \frac{K_B\mu_V\mu_I\rho\alpha_C}{\alpha_B(\alpha_V K_S + \mu_V\mu_S)(\sigma+\mu_I)}.$$

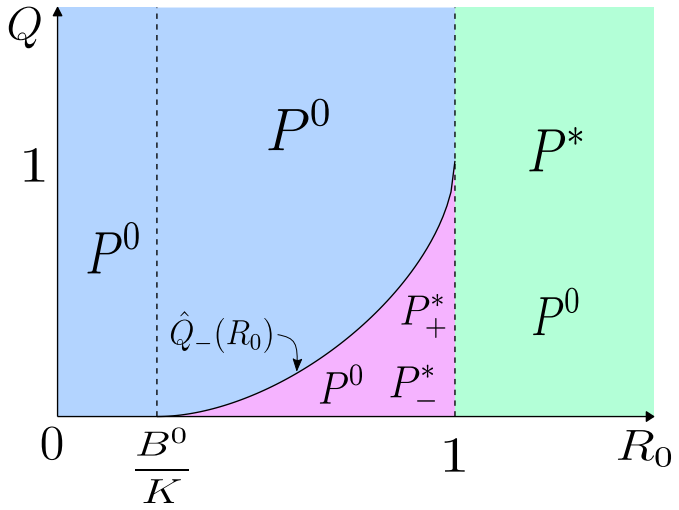

Figure 2.1 – Existence region diagram for all steady states of the model (2.1), according to parameters R_0 and Q. Extracted from (1).

Therefore, they obtained three scenarios for the equilibrium point existence. The deterministic model showed that if $R_0 < B^0/K$, the unique equilibrium point that exists is the free-virus equilibrium (VFE) point, P^0, which is locally asymptotically stable (LAS). Also, if $B^0/K < R_0 < 1$ and $Q > \hat{Q}_-$, where

$$\hat{Q}_- = R_0 + \frac{B^0}{K} - 2R_0\frac{B^0}{K} - 2\frac{\sqrt{\phi}}{K},$$

with $\phi = B^0R_0(R_0-1)(B^0-K)$ and $B^0 = K_B/\mu_B$, only the VFE point exists (LAS); but in that case, if $Q < \hat{Q}_-$, there are three equilibrium points, which are P^0 (LAS), and two virus-presence equilibrium (VPE) points: P^*_- (unstable) and P^*_+ (LAS). It is important to note, the coordinate of P^*_+ for the dengue virus (V^*_+) is higher than the coordinate of P^*_- for the dengue virus (V^*_-). It shows that the unstable coordinate is located between the two stable coordinates. Last, if $R_0 > 1$ there is only the VPE point, P^* (LAS), and the VFE point, P^0 (unstable).

2.2.2 Procedures for stochastic simulation

We considered Monte Carlo simulations (a thousand trajectories were simulated) and the stochastic simulation algorithm (SSA) proposed by Gillespie to simulate chemical reactions (2). In that work, he considered that the molecules P could change their shape, at certain reaction rates (that could depend on the P value). Here, we consider the P variable as the vector (B, S, I, V) and the reaction rates based on $N = 8$ possible events $e_v, i = 1, 2, \ldots, N$: plasma cell proliferation, infected macrophage recovery, engulfment process, phagocytosis process, and the natural mortality of the dengue virus, both naive and infected macrophage, and the plasma cell. For more details about the events, see Appendix 2.A.

We can divide the SSA execution into four steps: (i) initialization, (ii) calculating the reaction rates, (iii) calculating the reaction time and choosing the event that happens, and (iv) updating the values of the time and population. In the initialization step, we set the population P at the zero time as the initial condition $P(0) = (B(0), S(0), I(0), V(0))$. In the second step, we calculate all reaction rates associated with the events e_v and the value E_T, which corresponds to the sum of all reaction rates. In the third step, we generate two random values τ and ρ with uniform distribution in the interval $[0, 1]$. This part is responsible for calculating the reaction time and what event will happen. The time reaction is given by $\Delta_t = \dfrac{1}{E_T} \ln\left(\dfrac{1}{\tau}\right)$. Once we calculated the reaction time, we choose the μ-th event, verifying

$$\sum_{i=1}^{\mu-1} e_i < \rho \sum_{i=1}^{N} e_i < \sum_{i=1}^{\mu} e_i.$$

The population is updated according to the μ-th event, which is given by the vector $X_\mu = (\Delta B, \Delta S, \Delta I, \Delta V)$.

Afterward, in the last step, we update the time t, adding the increment Δ_t and the population (B, S, I, V) according to the vector X_μ chosen. For instance, suppose that the event selected is the mortality rate of the dengue virus, then the vector X_μ is given by $(0, 0, 0, -1)$. In that case, the population is updated as $P \to P + X_\mu$, that is,

$$(B, S, I, V) \to (B, S, I, V) + (0, 0, 0, -1).$$

The steps 2 to 4 presented in the flowchart described in Figure 2.2 repeat until a stop criterion. Here, we adopted as stop criterion a specific time or the extinction scenario (Both infected macrophage and dengue virus null) in the case it occurs before the time specified. Also, we separate the algorithm into three cases: (i) $I > 0$ and $V > 0$, (ii) $V = 0$ and $I > 0$, and (iii) $V > 0$ and $I = 0$, in order to properly define the events. The algorithm was implemented in Python, which is a free and open-source language (38).

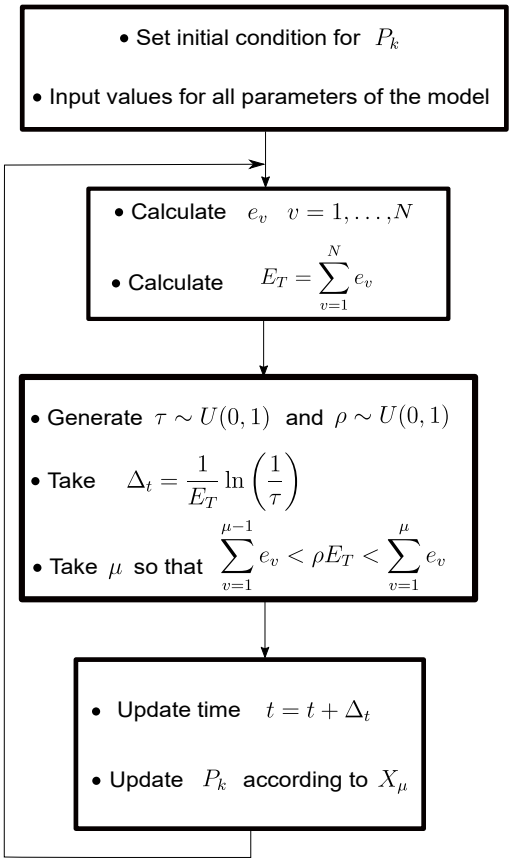

Figure 2.2 – Flowchart of the stochastic simulation algorithm proposed by Gillespie (1977) (2).

2.3 Results

In this section, we present the results applying the Gillespie SSA in order to explore all regions of the equilibrium points existence stochastically, that is, the cases: $R_0 < 1$ and $Q > \hat{Q}_-$, $R_0 < 1$ and $Q < \hat{Q}_-$, and $R_0 > 1$. Also, we analyze the influence of the initial condition and the varying value of R_0 in the Gillespie SSA convergence.

2.3.1 Case $R_0 < 1$ and $Q > \hat{Q}_-$

To analyze the region where there is only the VFE point, we consider $R_0 = 0.8$ and $\alpha_B = 1.0 \times 10^{-6}$ such that $Q > \hat{Q}_-$. In that case, we found that all stochastic simulations converge to the VFE point, regardless the initial condition. Figure 2.3 shows the dengue virus dynamics considering the initial condition $(B(0), S(0), I(0), V(0)) = (B^0, S^0 - I(0), 5.0 \times 10^2, 5.0 \times 10^2)$, where $B^0 = K_B/\mu_B$ and $S^0 = K_S/\mu_S$.

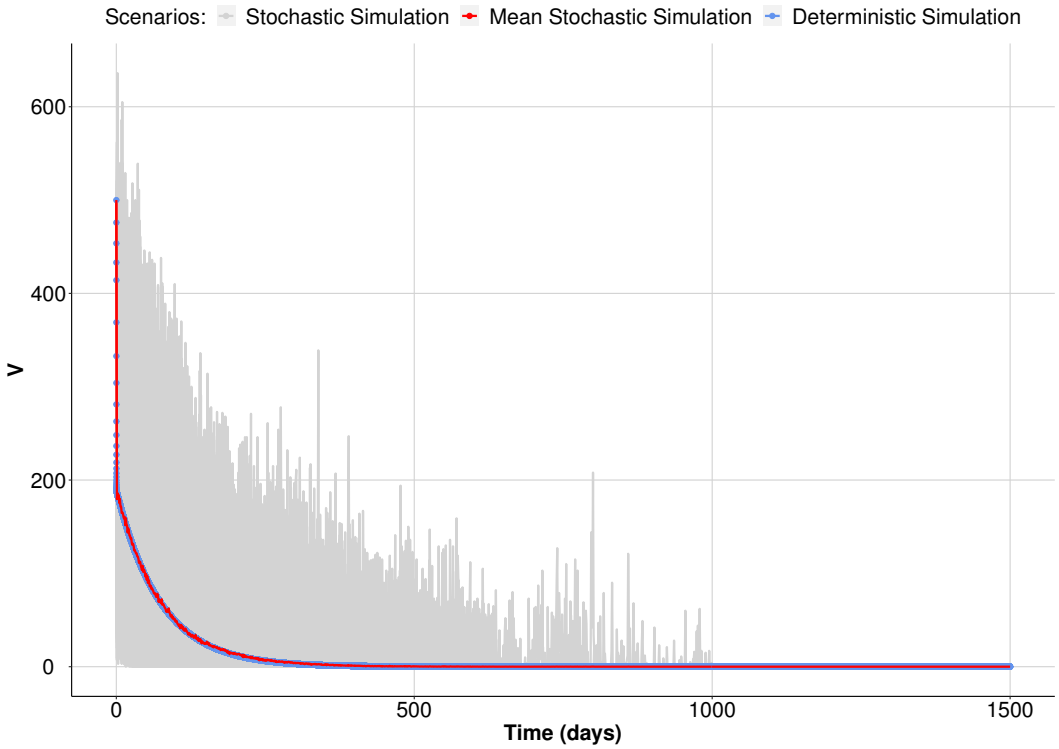

Figure 2.3 – Dengue virus dynamics with initial condition $(B(0), S(0), I(0), V(0)) = (B^0, S^0 - I(0), 5.0 \times 10^2, 5.0 \times 10^2)$ converging to the extinction.

The extinction time was set as t_{ext}. Table 2.3 shows the time to reach the infection extinction for different initial condition, which was considered as $(B(0), S(0), I(0), V(0)) = (B^0, S^0 - I(0), V(0))$. To compare to the deterministic approach, we assumed if $V(t) < \nu$ then $t^1_{\text{ext}} = t$, and if $I(t) < \nu$ then $t^2_{\text{ext}} = t$, considering $\nu = 0.1$ and $\nu = 1$. These extinction times are shown in Table 2.4.

V(0) and I(0)	Median	Mean	Min	Max	CI - 90%
100	149.35	167.57	40.61	658.23	[67.55, 348.55]
500	261.19	278.33	99.94	1024.66	[151.66, 456.98]
1000	309.1057	325.54	137.14	1113.95	[201.61, 506.44]

Table 2.3 – Extinction time to the stochastic simulations varying the initial condition.

V(0) and I(0)	t^1_{ext} $(\nu = 1)$	t^1_{ext} $(\nu = 0.1)$	t^2_{ext} $(\nu = 1)$	t^2_{ext} $(\nu = 0.1)$
100	265.99	434.68	338.52	507.17
500	383.72	552.34	456.27	624.91
1000	434.37	602.96	506.86	675.50

Table 2.4 – Extinction time of the deterministic model varying the initial condition and the value of ν.

Through Tables 2.3 and 2.4, we can see that the extinction time in the deterministic model increase as we decrease the value of ν. It occurs in both cases, considering the dengue virus or the infected macrophage less than the value of ν. Also, the extinction time when $V < \nu$ (t^1_{ext}) always occurs before $I < \nu$ (t^2_{ext}). It happens because the dengue virus is eliminated before the infected macrophage. Also, the asymptotic behavior for the dynamics convergence to the equilibrium point contributes to a higher extinction time. Besides that, the higher the initial condition is, the higher the extinction time is.

2.3.2 Case $R_0 < 1$ and $Q < \hat{Q}_-$

For the region with three equilibrium points, we consider $R_0 = 0.5$ and $\alpha_B = 3.0 \times 10^{-5}$, such that $Q < \hat{Q}_-$. Also, we set as initial condition the coordinates of the unstable virus-presence equilibrium point, P^*_-. These initial condition coordinates were approximated as an integer value closer to the respective coordinate of the stable virus-presence equilibrium point. For instance, if $V^*_- = 152.7$ and $V^*_+ = 10540.6$, we considered $V(0) = 153$. On the other hand, if $S^*_- = 354050.8$ and $S^*_+ = 154761.3$, we assumed $S(0) = 354050$. Figure 2.4 shows that the stochastic trajectories can converge to a stable VPE point or a stable VFE point. Due to the initial condition assumed and the existence of two stable equilibrium points, the mean curve (in red) lies in the middle of them. Here, we present only the graphs to the dengue virus dynamics; graphs of the other variables can be found in Appendix 2.B.

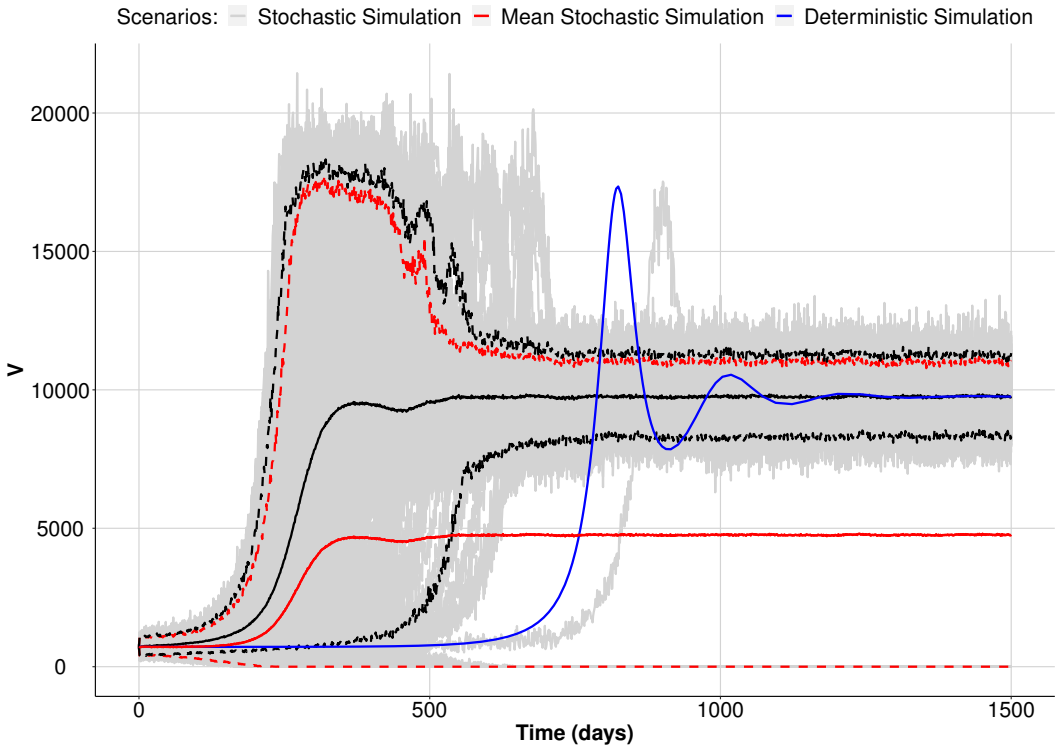

Figure 2.4 – Dengue virus dynamics with initial condition $(B(0), S(0), I(0), V(0)) = (B^*_-, S^*_-, I^*_-, V^*_-)$, with perturbed initial condition in the direction of the stable point VPE. The colors red and black are assumed to all trajectories and only those going to V^*_+, respectively. Region between the dashed lines represents the stochastic simulations with a confidence interval of 95%.

2.3.3 Case $R_0 > 1$

Now, supposing $R_0 > 1$, for any perturbation in the non-negative initial condition, the deterministic model shows that the dynamical trajectory converges to the virus-presence equilibrium point since the VPE point is the only one stable equilibrium point. However, for the stochastic simulation, this behavior does not replicate. Even if the viral inoculation is not low, some simulations converge to extinction. Figure 2.5 shows the dynamical behavior for DENV, considering $R_0 = 1.5$ and the initial condition $(B(0), S(0), I(0), V(0)) = (2.0 \times 1^3, 5.0 \times 10^4, 1.0 \times 10^3, 1.0 \times 10^3)$. Also, in that case, all trajectories converge to V^*, so we suppressed the dashed red lines from Figure 2.5.

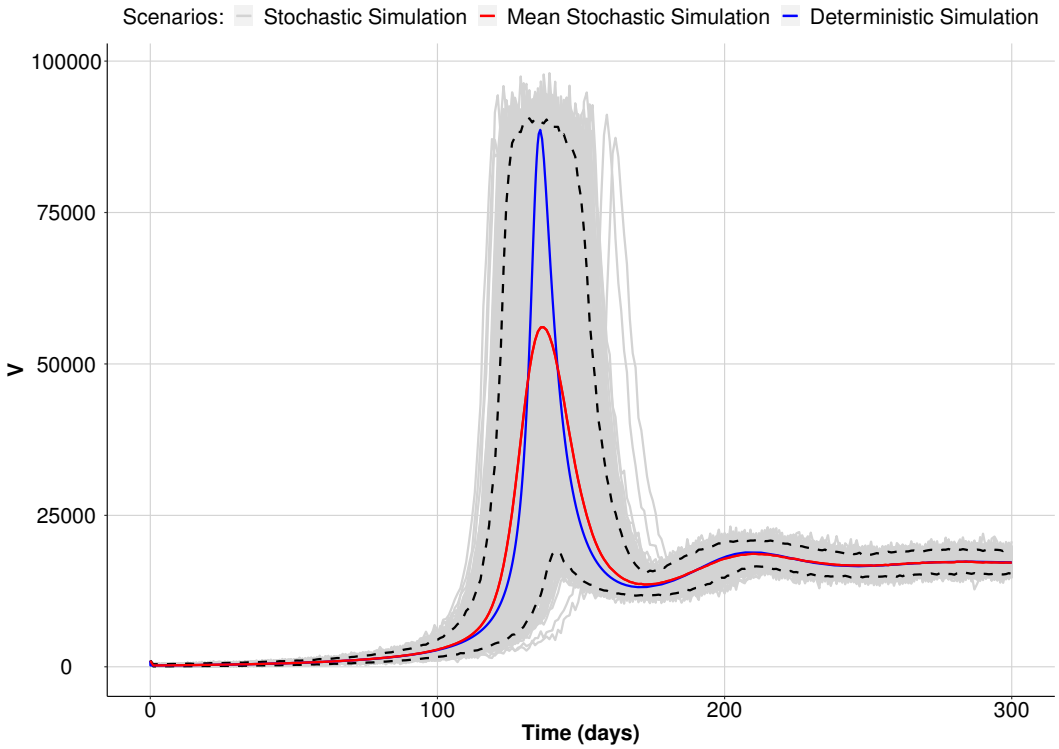

Figure 2.5 – Dengue virus dynamics with convergence for V^*, $R_0 = 1.5$, and initial condition $(B(0), S(0), I(0), V(0)) = (2.0 \times 10^3, 5.0 \times 10^4, 1.0 \times 10^3, 1.0 \times 10^3)$. Region between the dashed lines represents the stochastic simulations with a confidence interval of 95%.

In order to explore the influence of varying R_0 or the initial condition, we consider two scenarios. First, we fixed the initial condition and varied the basic reproduction number R_0, and second we fixed the value of R_0 and varied the initial condition. For the first scenario, as initial condition, we considered $(B(0), S(0), I(0), V(0)) = (B^0, S^0 - I(0), 100, 100)$. In order to study the influence of varying the basic reproduction number, we consider the following range for R_0: $[0.7, 2.5]$ with step by 0.1.

Figure 2.6 shows that the higher the basic reproduction number is, the fewer the proportion of simulations going to extinction is. Also, values greater than $R_0 = 1.3$ showed less than 1% of simulations going to extinction; and starting at $R_0 = 2$, all simulations converged to the virus-presence equilibrium point.

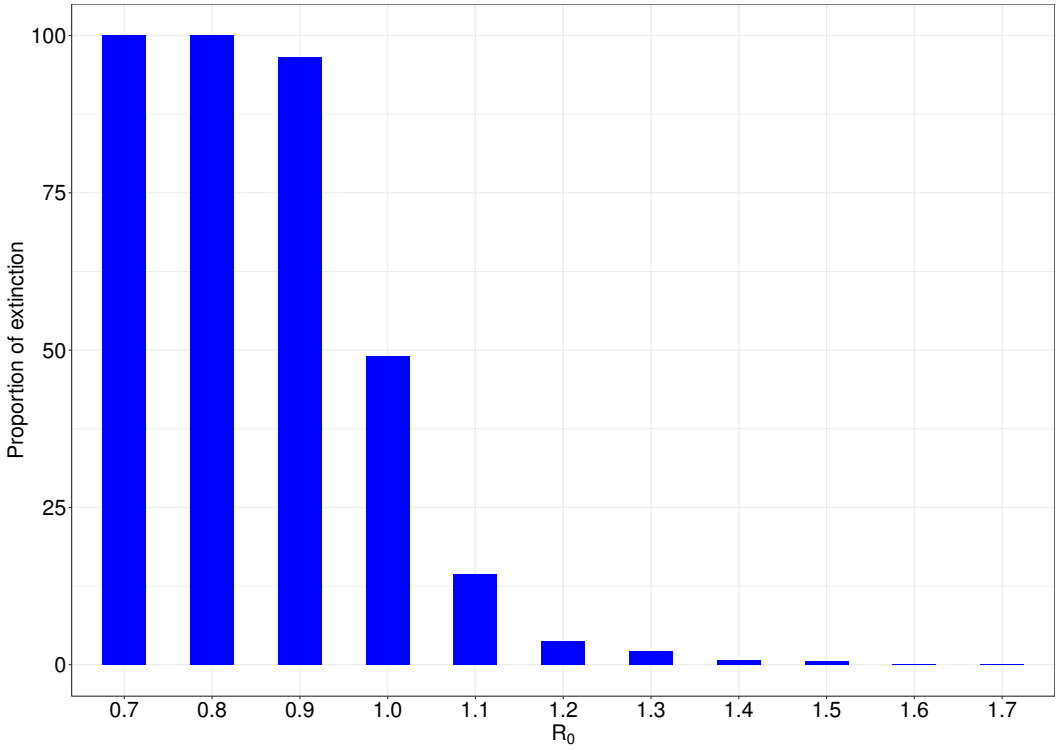

Figure 2.6 – Percentage of simulations going to extinction with respect to R_0 with $V(0) = 100$ and $I(0) = 100$.

In the second scenario, to investigate the influence of the initial condition in the convergence of the stochastic simulations, we fixed the value of R_0 and varied the initial condition. Also, we fixed the values of $B(0)$ and $S(0)$ as equal to the correspondent values of the VFE point. To evaluate the influence of increasing the initial condition in the number of simulations that converge to the dengue virus extinction, we vary the viral inoculation and the initial concentration of infected macrophages. Also we consider that $V(0) = I(0)$, and as in the previous section, we consider the initial condition $(B(0), S(0), I(0), V(0)) = (B^0, S^0 - I(0), I(0), V(0))$. To perform it, we consider $R_0 = 1$ and the following values for $V(0)$ and $I(0)$: 5, 10, 50, 100, 250, 500, 750, and 1000.

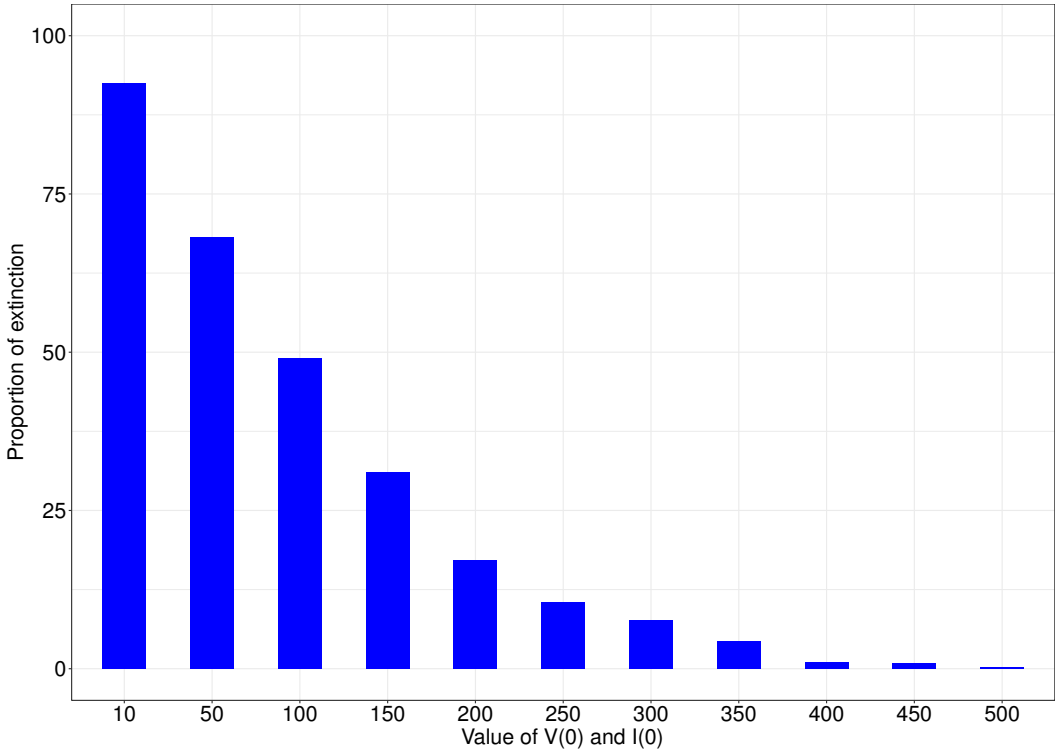

Figure 2.7 – Percentage of simulations going to extinction with respect to the initial condition of dengue virus and infected macrophage with $R_0 = 1$.

Figure 2.6 shows that as the value of DENV and infected macrophages increase, the stochastic simulations tend to converge to the VPE point. Infected macrophage and dengue virus initial condition higher than 500 made the all trajectories converged to the VFE point, P^*.

2.4 Discussion

This work presented a mathematical model to simulate the ADE phenomenon in heterologous secondary dengue infection. The model was implemented considering two approaches: a deterministic one and a stochastic one. Figure 2.6 showed a considerable decrease in the number of simulations that go to extinction when we surpass $R_0 = 1$; this phenomenon occurs due to the deterministic threshold. Since for $R_0 > 1$, with the same parameter set and initial condition, the simulation is expected to converge to the VPE point. However, in stochastic simulation, this may not be the case.

In general, if $R_0 < 1$ in deterministic models, then any positive initial condition of DENV drives the dynamics to an extinction-level, while the virus presence leads to an endemic level of the dengue infection if $R_0 > 1$. However, for stochastic models, around $R_0 = 1$, that behavior could not be replicated. It is necessary higher values of the basic reproduction number to obtain the same deterministic model convergence results. Nåsell (2011) showed that in an SIS model exists a certain population level necessary

to the stochastic model replicates the deterministic behavior (39). In some cases, the basic reproduction number is sufficient to rule deterministic model convergence, but a two-dimensional space is necessary for the stochastic framework. The stochastic model convergence depends on the values of R_0 and the population size.

Using Gillespie SSA, we obtained that the stochastic model results were similar to the deterministic system, depending on the basic reproduction number value and the size population as expected. It is important to note that for the case $R_0 < 1$ when we analyzed a deterministic model with bistability, we detected that the results of these two approaches could differ greatly. That difference lies in the stochasticity present in the simulations and the possibility of convergence to two stable equilibrium points. In Figure 2.4, we observed that a simple shift in the initial condition toward the equilibrium point in the presence of a stable virus; the deterministic model converges to the point P_+^*. Also, as the initial condition is close to the unstable equilibrium point, P_-^*, the dynamics system takes time to reach convergence to the equilibrium point P_+^*. However, in stochastic simulations, the convergence of the mean curve (solid red line) for DENV fluctuated between stable equilibrium values. If we take away all simulations (in gray) that have gone to extinction, then the mean curve (solid black line) increases and reaches the same convergence of the deterministic model. Also, for initial conditions with the dengue coordinate above the value of V_-^*, many simulations converged to the virus extinction, which did not occur for the deterministic model.

We also simulated the case with initial condition values closer to the VPE point P_+^* for the case $R_0 = 0.5$. In that case, the mean curve (in red) approached the deterministic curve (in blue) since fewer simulations (in gray) converged to the VFE point P^0. For $R_0 > 1$, the deterministic model (2.1) showed us that the VFE point is unstable and the VPE is LAS; that is, a slight perturbation in the initial condition given by P^0 will make the dynamics to converge to P^*. However, using Gillespie SSA, we notice that a simple perturbation in the initial condition is not enough to drive the dynamics to the point P^*. By increasing the virus injection and the number of infected macrophages, we decrease the proportion of simulations that go to infection extinction.

Moreover, in our model, we obtained that for a large population and $R_0 > 1$, stochastic simulations approximate the behavior of the deterministic model. However, the results may differ for small samples since each value of the population directly influences the probability of the determined events, and it can lead the dynamics to extinction. For a low population and $R_0 < 1$, the stochastic model approaches the behavior of the deterministic model when there is only a stable equilibrium point (the VFE point). A higher population is necessary to obtain similar deterministic model convergence results in a scenario with two stable equilibrium points.

Therefore, the deterministic model is crucial to understand the general idea

of the dynamics considered, gathering the equilibrium points and essentials thresholds to determine the existence and stability of the equilibrium points. On the other hand, the stochastic simulation does not provide results of thresholds or stability equilibrium points. For instance, suppose the value of R_0 is around one. Without previous knowledge about the expression of the basic reproduction number, it is impossible to determine if the model was supposed to converge to a virus-presence equilibrium point or lead to extinction through stochastic simulation. Besides, only with the stochastic simulation is it impossible to determine if the value of R_0 is less or greater than one. Considering the scenario shown in Figure 2.4, if we increase the dengue virus and infected macrophage values in the initial condition, we obtain a similar qualitative result of Figure 2.5, that is, all trajectories converge to a virus-presence equilibrium point. Looking at the two scenarios, we could presume that both portraits a case with $R_0 > 1$. Also, if we decrease the initial condition in the case shown in Figure 2.5, we obtain a scenario similar to the case shown in Figure 2.4. Again, we could suppose that both cases portrait the scenario with $R_0 > 1$, with some trajectories converging to the extinction. In fact, Figure 2.7 showed that for $R_0 = 1$, considering $V(0) = I(0) = 100$ only half of the trajectories converged to the VPE point P^*. However, we noticed that Figures 2.4 and 2.5 presented a case with $R_0 < 1$ and $R_0 > 1$, respectively. Also, using stochastic simulation, we cannot determine the expression of the threshold R_0. Only with the deterministic model, we obtained the threshold Q, which is essential to determine the existence and stability of the virus-presence equilibrium points of the model. Thus, we cannot infer anything through stochastic simulations about the thresholds that appear in the model.

2.5 Conclusion

Here, we explored the deterministic and stochastic approaches in the context of an ADE phenomenon mathematical model. We found that the initial condition has a vital role in the stochastic simulation. Also, we concluded that considering stochastic simulation is always possible to simulate the dynamic system and analyze different scenarios, such as investigating the extinction time of a given infection, investigating the probability of a given event occurring, obtaining confidence intervals for dynamic trajectories, among other aspects. However, suppose the idea is to understand the model dynamics, infer the attraction basin, or find the critical thresholds of the model. In that case, a study of the corresponding deterministic model is necessary. It is advisable to consider the stochastic simulation approach coupled with the respective deterministic model in order to get a complete understanding of the model dynamics since stochastic models do not allow you to determine threshold expressions, for instance R_0.

Appendix

2.A Events of the model

In this section, we present all events of the model and their respective population updating.

Event 1 - Plasma cell proliferation:

The event associated with the plasma cell proliferation, e_1, is given by the term $\alpha_B(1-(B/K))VB$, if $B \leqslant K$, otherwise the event does not occur. Here, we do not consider the possibility of B surpass K because that deterministic model showed that this value could not surpass the carrying capacity of plasma cell proliferation. So, we admit this simplification in event 1.

The population updating is given by

$$(B, S, I, V) \rightarrow (B+1, S, I, V).$$

Event 2 - Plasma cell natural mortality:

The term $\mu_B B$ gives the event associated with the natural mortality of plasma cells. Here, we considered that one cell is consumed when the event occurs. The population updating is given by

$$(B, S, I, V) \rightarrow (B-1, S, I, V).$$

Event 3 - Infected macrophage recovery:

The event associated with the infected macrophage recovery is σI. The population updating is given by

$$(B, S, I, V) \rightarrow (B, S+1, I-1, V).$$

Event 4 - Engulfing the dengue virus by the naive macrophage:

The event associated with the engulfment of the dengue virus by naive macrophages is $\alpha_C BVS$. The population updating occurs in two processes:

(1) If $V > N$ then

$$(B, S, I, V) \rightarrow (B, S, I, V-N),$$

else

$$(B, S, I, V) \to (B, S, I, 0).$$

(2) If $\rho_b < \rho$ then

$$(B, S, I, V) \to (B, S - 1, I + 1, V),$$

else there is no updating.

Event 5 - Natural mortality of naive macrophages:

The event associated with the natural mortality of naive macrophages is $\mu_S S$, the population updating is given by

$$(B, S, I, V) \to (B, S - 1, I, V).$$

Event 6 - Mortality of infected macrophages:

The event associated with the mortality of infected macrophages is $\mu_I I$. In the model, we consider that the cell at death releases an r amount of virions. So, the population updating is given by,

$$(B, S, I, V) \to (B, S, I - 1, V + r).$$

Event 7 - Phagocytosis of the virus via macrophage action:

The event associated with the process of phagocytosis is $\alpha_V SV$. The population updating is given by

$$(B, S, I, V) \to (B, S, I, V - 1).$$

Event 8 - Natural mortality of the dengue virus:

The term $\mu_V V$ gives the event associated with the dengue virus natural mortality. So, the population updating is

$$(B, S, I, V) \to (B, S, I, V - 1).$$

Moreover, we do not consider that plasma cell and naive macrophage production are random events. The deterministic model has an invariance region that needs to be respected. Biologically, it means that it has strong homeostasis. Although migration is an event that exists, proliferation is much more intense than the migration process. Thus, we do not consider the migration process in both plasma and macrophage cells for simplicity.

We admit a Poisson process for naive macrophage and plasma cell reproduction, with the Poisson parameter being, $\lambda_B = \Delta_t K_B$ and $\lambda_S = \Delta_t K_S$, respectively, in order to maintaining the homeostasis from a biological point of view and because we do not consider the migration process.

Besides, we split the algorithm into three parts in order to consider only the events that could occur. We consider the cases (i) $V > 0$ and $I > 0$, (ii) $V = 0$ and $I > 0$, and (iii) $V > 0$ and $I = 0$. Therefore, we consider the following events in each case

i All events: 1 - 8;

ii Events: 2, 3, 5, and 6;

iii Events: 1, 2, 4, 5, 7, and 8.

2.B Stochastic simulations for plasma cell and both naive and infected macrophage populations

This section presents the stochastic simulation graphs for the plasma cell and both naive and infected macrophage populations, considering the cases $R_0 < 1$ and $Q < \hat{Q}_-$, and $R_0 > 1$.

2.B.1 Case $R_0 < 1$ and $Q < \hat{Q}_-$

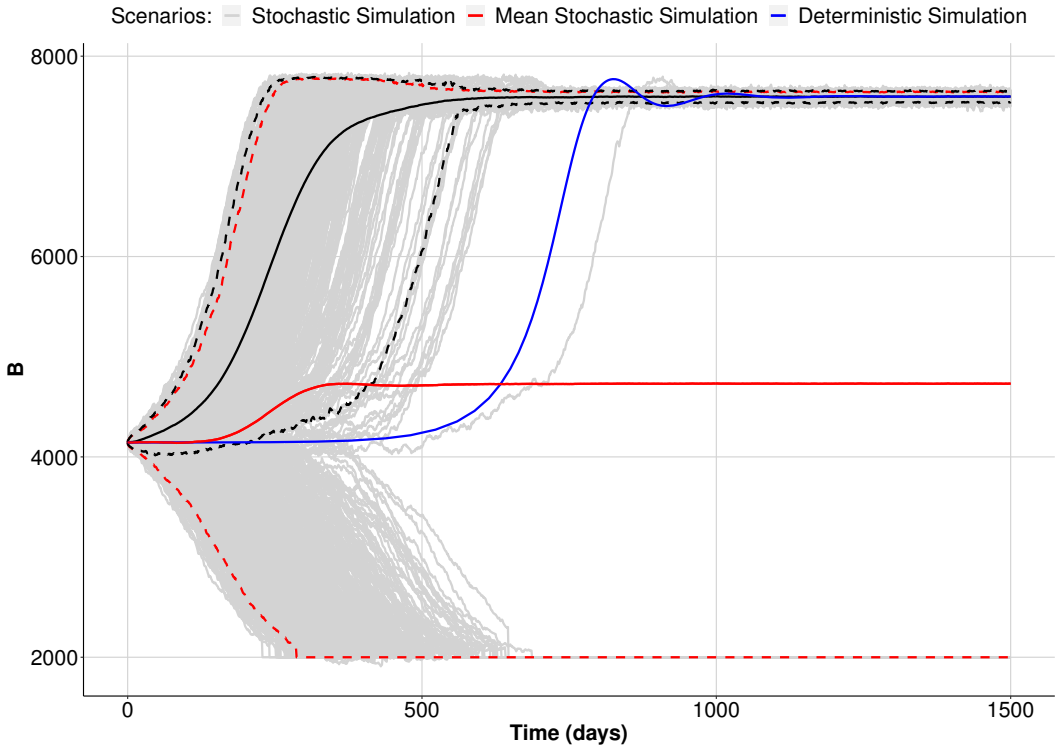

Figure 2.8 – Plasma cell dynamics with initial condition $(B(0), S(0), I(0), V(0)) = (B^*_-, S^*_-, I^*_-, V^*_-)$, with perturbed initial condition in the direction of the stable point VPE. Region between the dashed lines represents the stochastic simulations with a confidence interval of 95%.

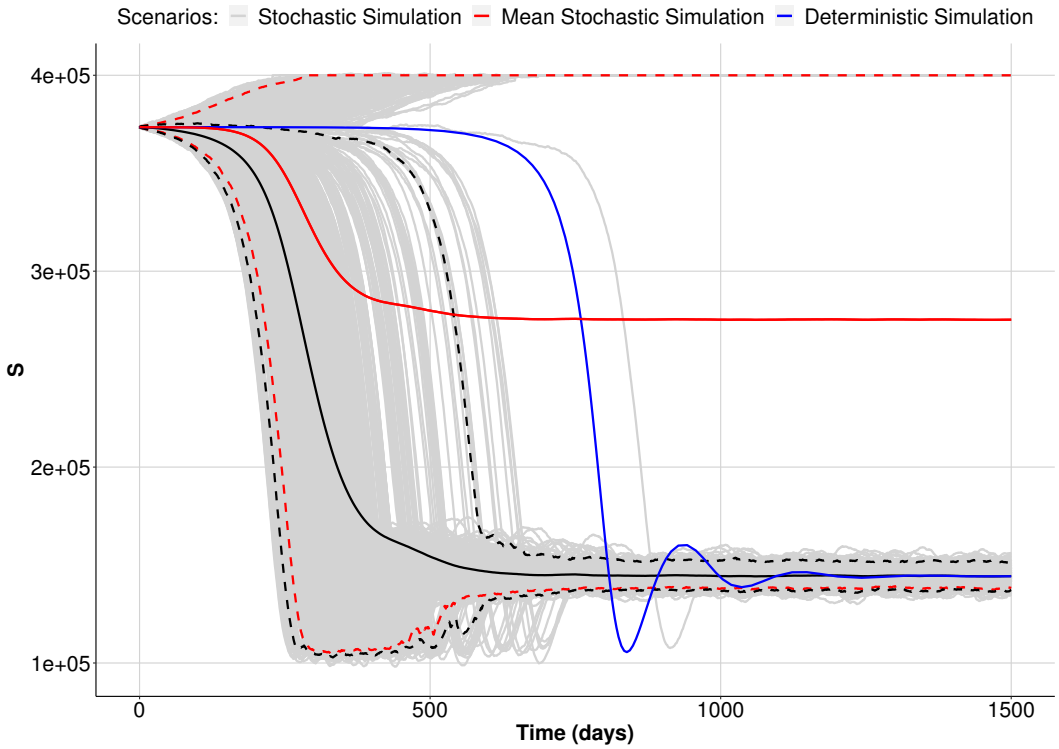

Figure 2.9 – Naive macrophage dynamics with initial condition $(B(0), S(0), I(0), V(0)) = (B^*_-, S^*_-, I^*_-, V^*_-)$, with perturbed initial condition in the direction of the stable point VPE. Region between the dashed lines represents the stochastic simulations with a confidence interval of 95%.

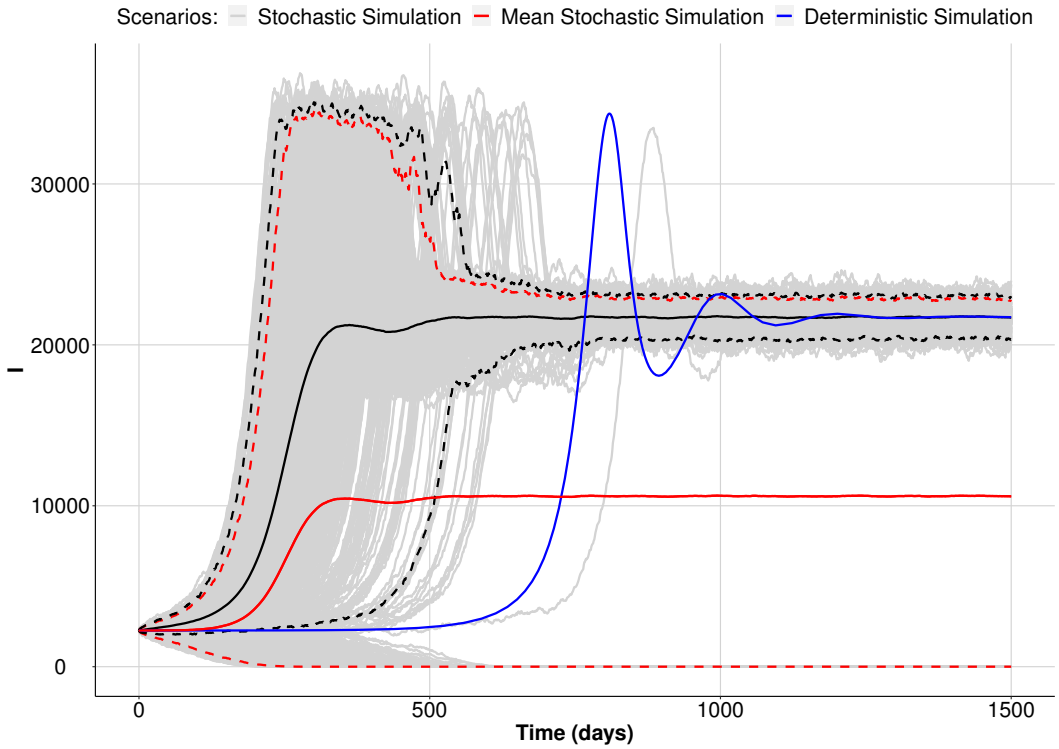

Figure 2.10 – Infected macrophage dynamics with initial condition $(B(0), S(0), I(0), V(0)) = (B^*_-, S^*_-, I^*_-, V^*_-)$, with perturbed initial condition in the direction of the stable point VPE. Region between the dashed lines represents the stochastic simulations with a confidence interval of 95%.

2.B.2 Case $R_0 > 1$

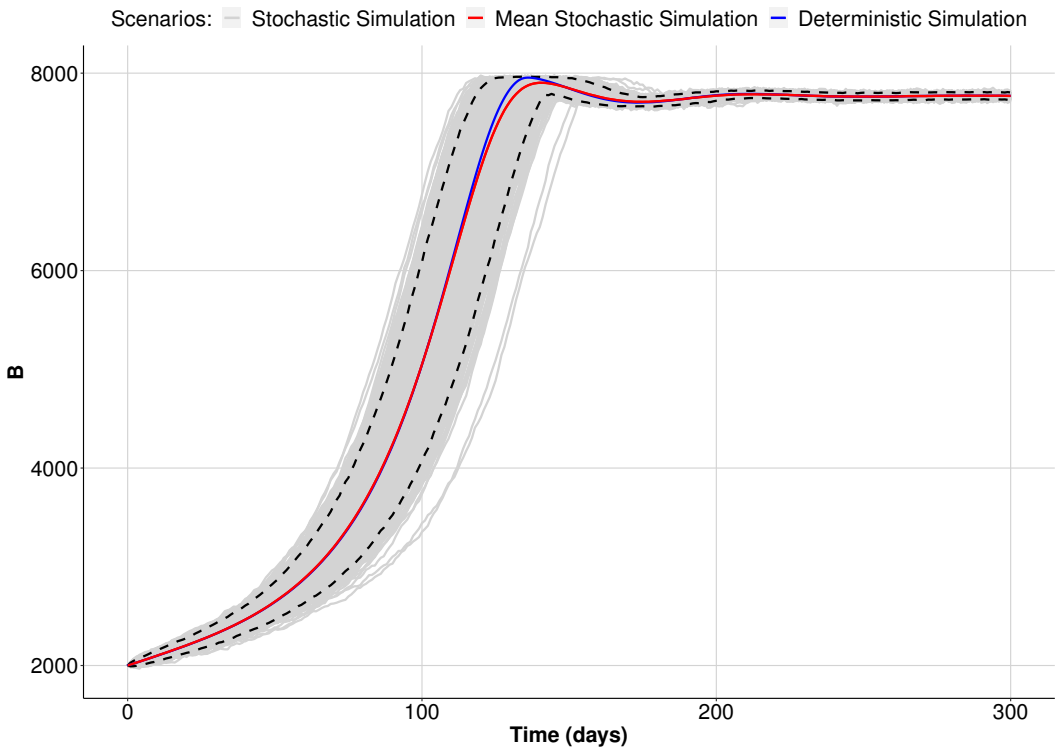

Figure 2.11 – Plasma cell dynamics with convergence for B^*, $R_0 = 1.5$, and initial condition $(B(0), S(0), I(0), V(0)) = (2.0 \times 1^3, 5.0 \times 10^4, 1.0 \times 10^3, 1.0 \times 10^3)$. Region between the dashed lines represents the stochastic simulations with a confidence interval of 95%.

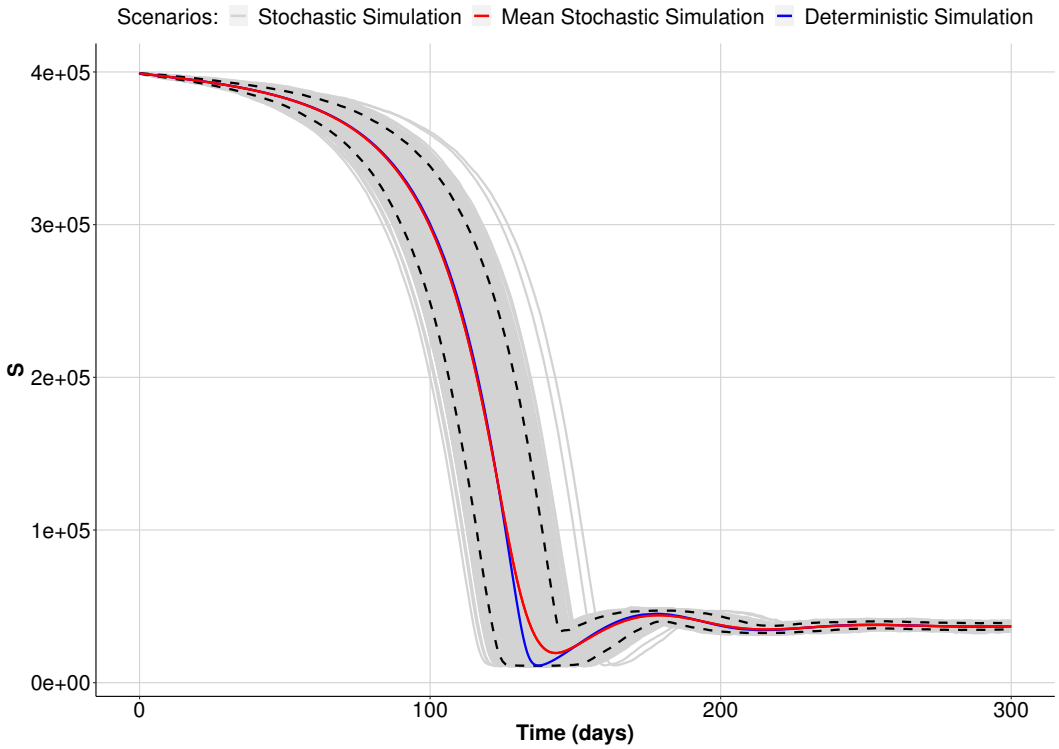

Figure 2.12 – Naive macrophage dynamics with convergence for S^*, $R_0 = 1.5$, and initial condition $(B(0), S(0), I(0), V(0)) = (2.0 \times 1^3, 5.0 \times 10^4, 1.0 \times 10^3, 1.0 \times 10^3)$. Region between the dashed lines represents the stochastic simulations with a confidence interval of 95%.

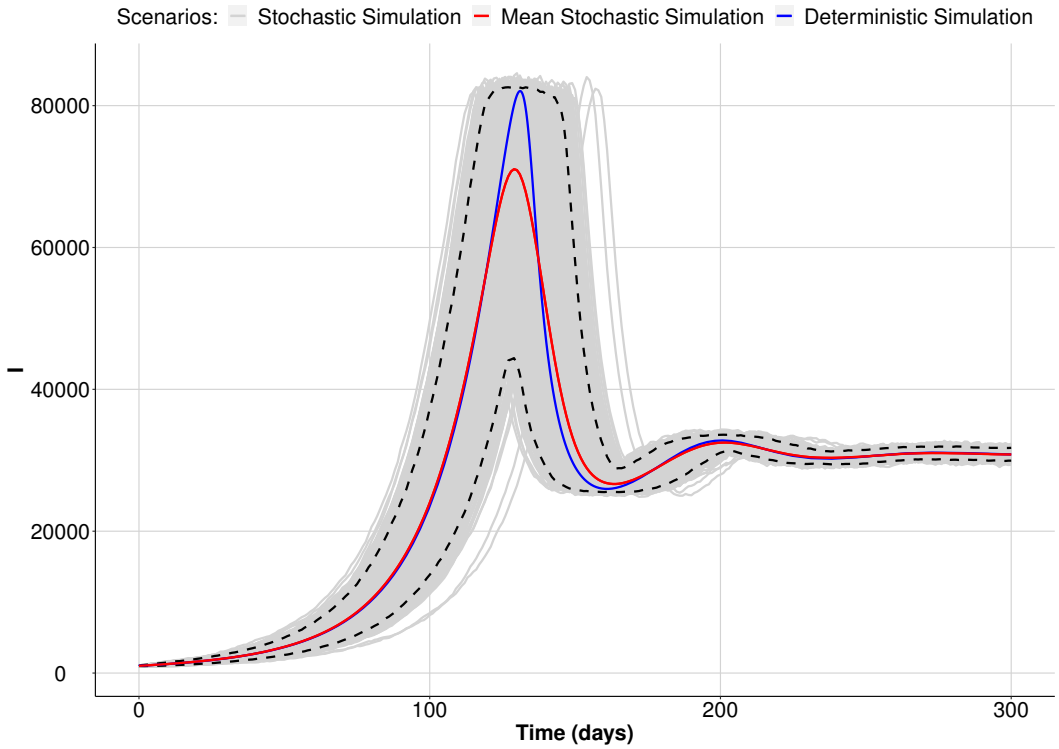

Figure 2.13 – Infected macrophage dynamics with convergence for I^*, $R_0 = 1.5$, and initial condition $(B(0), S(0), I(0), V(0)) = (2.0 \times 1^3, 5.0 \times 10^4, 1.0 \times 10^3, 1.0 \times 10^3)$. Region between the dashed lines represents the stochastic simulations with a confidence interval of 95%.

3 A mathematical model to evaluate the role of memory B and T cells in heterologous secondary dengue infection

Abstract. *We propose a mathematical model to investigate the antibody-dependent enhancement (ADE) phenomenon during secondary dengue infection. The model consists of an ODE system that describes the interaction of the dengue virus with macrophages and memory B and T cell role during the infection. The model qualitative analysis is done in terms of memory B and T cell cloning parameters and the basic reproduction number R_0. In the absence of memory B and T cell cloning, if $R_0 < 1$ the virus population extinguishes, while for $R_0 > 1$, it tends asymptotically to a positive equilibrium. However, when we consider the B cell cloning, it is possible to occur dengue infection even when $R_0 < 1$. Memory T cells have an essential role in eliminating the possibility of ADE occurrence when $R_0 < 1$.*

Keywords: Mathematical model. Antibody-dependent enhancement. Memory B cells. Memory T cells. Dengue virus.

3.1 Introduction

Dengue viruses (DENV) are transmitted by *Aedes* mosquito bite that causes mild dengue fever (DF) or dengue severe (DS). There are more than 50 million DF cases each year (30). There are four dengue virus serotypes, DENV-1, DENV-2, DENV-3, and DENV-4, which have only 20%-35% divergence (31). The cross-reactive immune response contributes to increased disease severity following heterologous infections (30, 15, 31). In general, primary infections result in either asymptomatic or mild DF disease. Secondary infections with different serotypes are either cleared or can induce severe dengue. Mechanisms responsible for the severity of secondary dengue infections are not entirely understood. One of them is the cross-reactive antibodies can enhance the disease, which is called antibody-dependent enhancement (ADE) (9, 8). ADE is explained as follows. When a person is first infected with one dengue strain, the humoral immune response of the host produces neutralizing antibodies specific against this strain. After the primary infection is eliminated, plasma cells produce specific antibodies for the first dengue strain, which persist in the body due to the immunological memory. If this person is secondly infected with a different dengue strain, antibodies from the primary infection bind the second virus but do not neutralize it. Besides that, macrophages are recruited to clear the immune

complex; they internalize this non-neutralized virus and become infected in the process of clearance. There is evidence that Fc receptors, which are proteins on the surface of some cells like macrophages and monocytes that bind to the antigen-antibody complex, might facilitate viral entry in cells and increase dengue viral replication (15, 40, 41).

This article proposes a mathematical model to describe the ADE phenomenon in secondary dengue infection, considering that partial cross-immunity occurs due to primary dengue infection. We consider that the immune system has not yet performed a complete response against the secondary infection. During this time, the circulating antibodies against the primary virus can facilitate heterologous secondary infection.

Mathematical models were formulated to describe the ADE phenomenon in secondary dengue infection. For instance, Gómez and Yang propose a model with only some variables, such as B memory cell, macrophages, and the dengue virus. In order to study the effect of B memory cell cloning during a heterologous secondary dengue infection (15). Nikin-Beers and Ciupe investigate the role of antibodies in enhancing dengue virus infection. They consider monocytes as target cells, B lymphocytes, plasma cells, and the two dengue strains (primary and secondary, which is different from the first one) (30). Here we consider few agents as macrophages, a specific antibody against the primary infection, memory B cells, memory T cells, the formation of immune complex, and dengue virus. We focus on the role of B and T cells during the secondary dengue infection. It is possible to determine the basic reproduction number parameter, which is given by R_0 and the effect of B and T cell cloning during the secondary dengue infection.

The paper is structured as follows. In section 2.2, a mathematical model is presented to describe the ADE phenomenon. In section 2.3, the model is analyzed, determining the existence region of the equilibrium points and their stability. In Section 2.4, a discussion about the role of memory B and T cell cloning in secondary dengue infection is presented. Section 2.5 gives the conclusion.

3.2 Mathematical modeling

We consider that memory B cells turn into plasma cells quickly in contact with the dengue virus. These cells, denoted by B, are releasing specific antibodies against the primary dengue virus, which are indicated by A. The memory B cells are kept in homeostasis, through production rate k_B and death μ_B. During secondary dengue infection, through acquired memory of the first infection, these cells are stimulated to increase at a per capita rate α_B, to release more antibodies to neutralize the antigen.

Antibodies are produced at a per capita rate r_A and have a rate of degradation μ_A. We considered that n of these antibodies would contact the circulating virus of the second infection, thus forming the antigen-antibody complex, which is denoted by C. This

binding forms only one immune complex, so in the dynamic equation of C, δ represents a correction factor whose value is $1/n$.

These immune complexes remain interconnected during a time μ_C^{-1}, where μ_C is the dissociation rate. We also assumed that the average number of immune complexes engulfed by a macrophage is $N \geqslant 1$. Uninfected macrophages die at a per capita rate μ_M, and they are produced in the bone marrow at a constant per capita rate k_M in order to maintain system homeostasis.

Naive macrophages can interact with the free virus in two ways: by phagocytosis of the virus, resulting in a phagosome that fuses the lysosome to destroy the virus, and by opsonization and internalization of the antigen-antibody complex in cells. Virus phagocytosis is described by the phagocytosis per capita rate α_M, and we also assume that the virus will always be destroyed. The FcγR receptors facilitate the engulfment process on the macrophage membrane and other immune cells, which is described by the engulfment per-capita rate α_C.

Due to the heterologous antibodies against different cross-reactive viruses, some naive macrophages become infected by releasing new viruses. We describe this imperfect cross-reactive immune response in heterologous viruses by the parameter ρ, with $0 \leqslant \rho \leqslant 1$, it means, macrophages harboring the immune complex can become infected with probability ρ. Infected macrophages have a death rate μ_I, where $\mu_I \geqslant \mu_M$, which can be increased by cell apoptosis. These infected macrophages release new virions at a per capita production rate r_V, and they are eliminated through the cellular immune response by the effector T cells at a per capita rate γ_T. The circulating virus has a death rate μ_V and binds to $n \geqslant 1$ antibodies to result in the antigen-antibody complex. The process of this formation of complex is described by the term $n\beta AV$.

Macrophages that engulf the immune complex and destroy the virus by the action of enzymes return to their natural state at a per capita rate $\sigma_{\hat{M}}$. This process has been assumed to be very rapid, and there is no associated mortality for this cell. It is also possible that some macrophages may kill the virus and return to the natural class, which occurs at a σ per capita recovery rate. Memory T cells are produced at a per capita rate k_T and have a mortality rate of μ_T. In the presence of infected macrophages, these cells are stimulated, at a per capita rate α_T, to produce new memory T cells to help eliminate infected macrophages. We considered that memory T cells turn into effector T cells quickly in contact with the infected macrophage.

Thus, based on the hypothesis above, we have the following nonlinear ordinary differential equations system,

$$\begin{aligned}
\frac{dB}{dt} &= k_B + \alpha_B VB - \mu_B B \\
\frac{dA}{dt} &= r_A B - \mu_A A - n\beta VA \\
\frac{dV}{dt} &= r_V I - \mu_V V - \alpha_M MV - \beta AV \\
\frac{dC}{dt} &= \delta n\beta VA - N\alpha_C MC - \mu_C C \\
\frac{dM}{dt} &= k_m + \sigma I - \alpha_C CM - \mu_M M + \sigma_{\hat{M}}\hat{M} \\
\frac{d\hat{M}}{dt} &= (1-\rho)\alpha_C CM - \sigma_{\hat{M}}\hat{M} \\
\frac{dI}{dt} &= \rho\alpha_C CM - (\mu_I + \sigma)I - \gamma TI \\
\frac{dT}{dt} &= k_T + \alpha_T IT - \mu_T T.
\end{aligned} \tag{3.1}$$

Assuming macrophages spend a swift time in class $\hat{M}$, that is, assuming $\sigma_{\hat{M}} \gg \alpha_C$, the sixth equation of the system (3.1) can be considered at the steady state. So, we have $\sigma_{\hat{M}}\hat{M} = (1-\rho)\alpha CM$ and substituting this term in the fifth equation (naive macrophages) we get the following simplified system,

$$\begin{aligned}
\frac{dB}{dt} &= k_B + \alpha_B VB - \mu_B B \\
\frac{dA}{dt} &= r_A B - \mu_A A - n\beta VA \\
\frac{dV}{dt} &= r_V I - \mu_V V - \alpha_M MV - \beta AV \\
\frac{dC}{dt} &= \delta n\beta VA - N\alpha_C MC - \mu_C C \\
\frac{dM}{dt} &= k_m + \sigma I - \mu_M M - \rho\alpha_C CM \\
\frac{dI}{dt} &= \rho\alpha_C CM - (\mu_I + \sigma)I - \gamma TI \\
\frac{dT}{dt} &= k_T + \alpha_T IT - \mu_T T.
\end{aligned} \tag{3.2}$$

Table 3.1 shows the model variables described by the system of equations (3.1) and Table 3.2 describes the parameters of the model (3.1).

Variable	Definition	Unit
B	Memory B cell	[B]/vol
A	Antibodies released by Plasma cell	[A]/vol
V	Dengue virus	[V]/vol
C	Antigen-antibody complex	[A][V]/vol
M	Naive macrophages	[M]/vol
$\hat{M}$	Macrophages effectively eliminating virus	$[\hat{M}]$/vol
I	Infected macrophages	[I]/vol
T	Memory T lymphocyte	[T]/vol

Table 3.1 – Description of the variables of the model (3.1).

Parameter	Meaning	Value	Unit	Reference
k_B	Production rate at rest of memory B cells	40.0	$[B]\, vol^{-1} T^{-1}$	(15)
μ_B	Per-capita mortality rate of memory B cells	0.02	T^{-1}	(16)
α_B	Per-capita proliferation rate of memory B cells	-	$[V]^{-1}\, vol T^{-1}$	-
k_M	Production rate of naive macrophages	6.8×10^3	$[M]\, vol^{-1} T^{-1}$	(17, 18)
μ_M	Per-capita mortality rate of naive macrophages	0.017	T^{-1}	(17)
α_c	Per-capita engulfment rate of antigen-antibody complex	-	$[B]^{-1}\,[V]^{-1}\, vol^2 T^{-1}$	-
ρ	Fraction of infected macrophages	3.6×10^{-5}	-	(15)
σ	Per-capita recovery rate of infected macrophages	0.2	T^{-1}	(15)
$\sigma_{\hat{M}}$	Per-capita recovery rate of effective macrophages	-	T^{-1}	-
μ_I	Per-capita rate mortality of infected macrophages	0.2	T^{-1}	(19)
r_V	Per-capita releasing rate of virions by infected macrophages	6.12×10^4	$[M]^{-1}\,[V]\, T^{-1}$	(20, 17)
α_M	Per-capita phagocytosis rate by naive macrophages	8.0×10^{-6}	$[M]^{-1}\, vol T^{-1}$	(15)
μ_v	Per-capita death rate of virus	3.3	T^{-1}	(21)
N	Number of antigen-antibody complex engulfed by macrophages	3.0	$[M]^{-1}\,[V]$	(15)
β	Per-capita immune complex formation rate	-	$[A]^{-1}\,\text{vol}\,\tau^{-1}$	-
r_A	Antibody production rate by a plasma cell	1.728×10^8	$[A]\,[B]^{-1}\,\tau^{-1}$	(18, 30)
μ_A	Per-capita degradation rate of antibody	0.07	τ^{-1}	(30)
n	Number of antibodies that bind to a virus to form an immune complex	15	$[A]\,[V]^{-1}$	(42)
δ	Dimension correction factor	1/15	$[V]$	Assumed
μ_C	Per-capita mortality rate of immune complex	1.0×10^{-3}	τ^{-1}	Assumed
k_T	Production rate at rest of memory T lymphocytes T	30	$[T]\,\text{vol}^{-1}\,\tau^{-1}$	(43, 44)
μ_T	Per-capita mortality rate of memory T cells T	0.5	τ^{-1}	(43)
γ	Per-capita effector T cell killing rate	2.77×10^{-6}	$[T]^{-1}\,\text{vol}\,\tau^{-1}$	(44)
α_T	Per-capita proliferation rate of memory T lymphocytes	-	$[M]^{-1}\,\text{vol}\,\tau^{-1}$	-

Table 3.2 – Parameters description of the model (3.1) and values used in simulations of the model (3.2). (We used $vol = mm^3$ and $\tau = day$.)

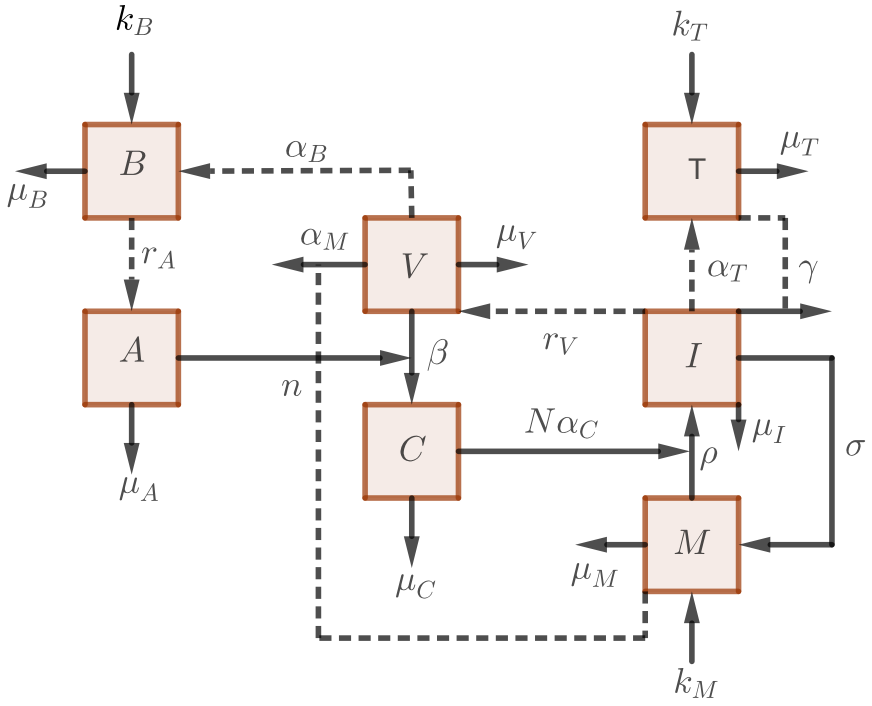

Figure 3.1 – Flow chart for model (3.2). The solid arrows mean a change of state, while dashed arrows represent only interference between the cells.

The solutions of the system (3.2) with an initial condition in Ω, which is given by

$$\Omega = \left\{ P = (B, A, V, C, M, I, T) \in \mathbb{R}^7_+ : B \geqslant \frac{k_B}{\mu_B}, V \leqslant V^{\max}, \right.$$
$$\left. C \leqslant C^{\max}, M + I \leqslant \frac{k_M}{\mu_M}, T \geqslant \frac{k_T}{\mu_T} \right\},$$

with $V^{\max} = r_V k_M/(\mu_V \mu_M)$ and $C^{\max} = (\delta\beta/\mu_C)[n r_V k_M/(\mu_V \mu_M)]^2$, they are always positively limited.

Proposition 3.1. *The set Ω is positively invariant with respect to the system (3.2), considering $\mu_I > \mu_M$.*

Proof: See appendix 3.A. □

3.3 Model Analysis

The virus-free equilibrium point is $W^0 = (B^0, A^0, 0, 0, M^0, 0, T^0)$, where $B^0 = k_B/\mu_B$, $A^0 = r_A k_B/(\mu_A \mu_B)$, $M^0 = k_M/\mu_M$, and $T^0 = k_T/\mu_T$.

The steady state stability is determined by analyzing the signal of the real part of the eigenvalues of the Jacobian matrix, J, evaluated at steady state. The Jacobian matrix is given by

$$J(P) = \begin{bmatrix} J_{11} & 0 & \alpha_B B & 0 & 0 & 0 & 0 \\ r_A & J_{22} & -\beta n A & 0 & 0 & 0 & 0 \\ 0 & -\beta V & J_{33} & 0 & -\alpha_M V & r_V & 0 \\ 0 & \beta\delta n V & \beta\delta n A & J_{44} & -N\alpha_C C & 0 & 0 \\ 0 & 0 & 0 & -\rho\alpha_C M & J_{55} & \sigma & 0 \\ 0 & 0 & 0 & \rho\alpha_C M & \rho\alpha_C C & J_{66} & -\gamma I \\ 0 & 0 & 0 & 0 & 0 & \alpha_T T & J_{77} \end{bmatrix}$$

where $J_{11} = \alpha_B V - \mu_B$, $J_{22} = -\beta n V - \mu_A$, $J_{33} = -\mu_V - \alpha_M M - \beta A$, $J_{44} = -\mu_C - N\alpha_C M$, $J_{55} = -\rho\alpha_C C - \mu_M$, $J_{66} = -\mu_I - \sigma - \gamma T$, and $J_{77} = -\mu_T - \alpha_T I$. The characteristic polynomial associated to W^0 is given by

$$s(\lambda) = (\lambda + \mu_M)(\lambda + \mu_A)(\lambda + \mu_B)(-\lambda - \mu_T)z(\lambda), \tag{3.3}$$

where $z(\lambda) = \lambda^3 + z_2\lambda^2 + z_1\lambda + z_0$, wherein the coefficients are

$$\begin{aligned}
z_2 &= \frac{r_A k_B \beta}{\mu_A \mu_B} + \frac{k_M}{\mu_M}(N\alpha_c + \alpha_M) + \frac{\gamma k_T}{\mu_T} + \mu_V + \sigma + \mu_I + \mu_C \\
z_1 &= \left(\frac{1}{\mu_A \mu_B \mu_T {\mu_M}^2}\right) \mu_A \mu_B \mu_T (k_M \alpha_M + \mu_M \mu_V)(k_M N \alpha_C + \mu_C \mu_M) \\
&\quad + \left(\frac{1}{\mu_A \mu_B \mu_T {\mu_M}^2}\right) [k_M \mu_M k_T \gamma \mu_A \mu_B \mu_T (N\alpha_C + \alpha_M) + k_M \mu_M k_B N \alpha_C r_A \beta \mu_T] \\
&\quad + \left(\frac{1}{\mu_A \mu_B \mu_T {\mu_M}^2}\right) [\mu_A \mu_B \mu_T k_M \mu_M (\alpha_M + N\alpha_C)(\mu_I + \sigma) + {\mu_M}^2 k_B r_A \beta k_T \gamma] \\
&\quad + \left(\frac{1}{\mu_A \mu_B \mu_T {\mu_M}^2}\right) [{\mu_M}^2 k_B r_A \beta \mu_T (\mu_C + \mu_I + \sigma) + {\mu_M}^2 \mu_A \mu_B k_T \gamma (\mu_C + \mu_V)] \\
&\quad \left(\frac{1}{\mu_A \mu_B \mu_T {\mu_M}^2}\right) {\mu_M}^2 \mu_A \mu_B [(\mu_T \mu_V + \mu_C \mu_T)(\mu_I + \sigma) + \mu_C \mu_T \mu_V] \\
z_0 &= \frac{1}{{\mu_M}^2 \mu_T}(k_M \alpha_M + \mu_M \mu_V)(k_M N \alpha_C + \mu_C \mu_M)[k_T \gamma + \mu_T(\mu_I + \sigma)](1 - R_0),
\end{aligned}$$

where R_0 is given by

$$R_0 = \left(\frac{k_B r_A \mu_M \beta}{\mu_A \mu_B}\right) \left[\frac{k_M \alpha_C r_V \mu_T \delta n \rho - (k_M N \alpha_C + \mu_C \mu_M)[\gamma k_T + \mu_T(\mu_I + \sigma)]}{(k_M \alpha_M + \mu_M \mu_V)(k_M N \alpha_C + \mu_C \mu_M)[\gamma k_T + \mu_T(\mu_I + \sigma)]}\right]. \tag{3.4}$$

To guarantee the local stability of W^0, we need that all roots of $s(\lambda)$ have a negative real part. Using the Routh-Hurwitz criteria, we prove the local stability of this point, which is stated in Theorem 3.1.

Theorem 3.1. *If $R_0 < 1$ then the virus-free equilibrium point, W^0, is locally asymptotically stable and unstable if $R_0 > 1$.*

Proof: *The characteristic polynomial $s(\lambda)$ has four negative real roots $-\mu_M$,, $-\mu_A$, $-\mu_B$, and $-\mu_T$. To ensure the local stability of W^0, it is necessary that the roots of $z(\lambda)$ must also*

have a negative real part. We use the Routh-Hurwitz criteria to complete the demonstration. The Routh-Hurwitz criteria of a third-degree polynomial are $z_2 > 0$, $z_0 > 0$, and $z_2 z_1 > z_0$. We have z_2 and z_1 as positive values because all parameters of the model (3.2) are non-negative. The coefficient z_0 is positive when $R_0 < 1$ and negative when $R_0 > 1$. The last condition $z_2 z_1 > z_0$ is easily checked. Therefore, if $R_0 < 1$, the local stability of equilibrium point W^0 is guaranteed. □

3.3.1 Biological meaning of the parameter R_0

We can rewrite the parameter R_0 as $R_0 = R_0^e - R_0^s$ where

$$R_0^e = \frac{A^0 \beta M^0 n r_V \alpha_C \delta \rho}{(\mu_C + N\alpha_C M^0)(\mu_V + \alpha_M M^0)(\mu_I + \sigma + \gamma T^0)} \quad \text{and} \quad R_0^s = \frac{A^0 \beta}{\mu_V + \alpha_M M^0}.$$

Biologically, the first term R_0^e represents that one virus in its lifespan $(\mu_V + \alpha_M M^0)^{-1}$, which is decreased by phagocytosis via macrophages, binds with a rate $\beta\ nA^0$ antibodies in circulation. This process forms δ antigen-antibody complex. These complexes, during their lifespan $(\mu_C + N\alpha_C M^0)^{-1}$ are engulfed with a rate α_C by a macrophage population M^0. Note that the macrophage lifespan is decreased due to engulfment of N immune complexes during the process of infection.

However, only a fraction ρ of naive macrophages will become infected macrophages. During their lifespan $(\mu_I + \sigma + \gamma T^0)^{-1}$, which is decreased due to T lymphocyte cytotoxic action and the possibility of macrophage recovery to the naive stage, these infected macrophages will produce r_V virions. So, R_0^e is the number of new viruses that only one virus will produce when introduced into a population composed of uninfected macrophages.

$$R_0^e = \frac{1}{\mu_V + \alpha_M M^0} \times \beta n A^0 \times \delta \times \frac{1}{\mu_C + N\alpha_C M^0} \times \alpha_C \times \rho M^0 \times \frac{1}{\mu_I + \sigma + \gamma T^0} \times r_V$$

On the other hand, R_0^s can be interpreted as the amount of virus consumed to form the antigen-antibody complex. Therefore, the parameter R_0 represents the net number of viruses generated by a single virus by forming the immune complex and subsequent macrophage infection when the single virus is inserted in an organism completely susceptible.

$$R_0^s = \frac{1}{\mu_V + \alpha_M M^0} \times \beta n A^0.$$

The virus-presence equilibrium point is $W^* = (B^*, A^*, V^*, C^*, M^*, I^*, T^*)$, where

$$
\begin{aligned}
B^* &= \frac{k_B}{(\mu_B - \alpha_B V^*)} \\
A^* &= \frac{r_A k_B}{(\mu_B - \alpha_B V^*)(\mu_A + n\beta V^*)} \\
M^* &= \frac{k_M(\mu_T - \alpha_T I^*) - [\mu_I(\mu_T - \alpha_T I^*) + \gamma k_T]I^*}{\mu_M(\mu_T - \alpha_T I^*)} \\
C^* &= \frac{[(\sigma + \mu_I)(\mu_T - \alpha_T I^*) + \gamma k_T]\mu_M I^*}{\rho\alpha_C\{k_M(\mu_T - \alpha_T I^*) - [\mu_I(\mu_T - \alpha_T I^*) + \gamma k_T]I^*\}} \\
T^* &= \frac{k_T}{\mu_T - \alpha_T I^*},
\end{aligned}
\tag{3.5}
$$

with I^* and V^* being the positive solutions of the system,

$$0 = r_V I^* - \mu_V V^* - \alpha_M M^* V^* - \beta A^* V^* \tag{3.6}$$

$$0 = \delta n\beta V^* A^* - N\alpha_C M^* C^* - \mu_C C^*. \tag{3.7}$$

Replacing all expressions obtained by I^* and V^* in equation (3.6), we obtain an equation of second-degree to I^* or third-degree to V^*. Considering the equation (3.7) we have a second-degree to V^* or third-degree to I^*. Thus, it is not possible to obtain a linear relationship between V^* and I^*. In this way, we will analyse the model into three parts. Firstly, we will analyse the case without the two cloning parameters α_B and α_T. Secondly, a numerical study will be done to evaluate the effect of each cloning, that is, $\alpha_B \neq 0$ and $\alpha_T = 0$ and after $\alpha_B = 0$ and $\alpha_T \neq 0$. Finally, the analysis of the joint effect of cloning ($\alpha_B \neq 0$ and $\alpha_T \neq 0$) will be done.

3.3.2 Case study of no-cloning of both memory B and T cells

To analyze this case, we consider the model (3.2) with both parameters α_B and α_T null. This absence will change only the virus presence equilibrium point W^*, which now is given by

$$
\begin{aligned}
B^* &= \frac{k_B}{\mu_B} \\
A^* &= \frac{r_A k_B}{\mu_B(\mu_A + n\beta V^*)} \\
M^* &= \frac{k_M\mu_T - (\mu_I\mu_T + \gamma k_T)I^*}{\mu_M\mu_T} \\
I^* &= \frac{[\mu_T\mu_B(\mu_V\mu_M + \alpha_M k_M)(\mu_A + n\beta V^*) + \mu_M\mu_T\beta r_A k_B]V^*}{\mu_B(\mu_A + n\beta V^*)[r_V\mu_M\mu_T + \alpha_M(\mu_I\mu_T + \gamma k_T)V^*]} \\
C^* &= \frac{[(\sigma + \mu_I)\mu_T + \gamma k_T]\mu_M I^*}{\rho\alpha_C[k_M\mu_T - (\mu_I\mu_T + \gamma k_T)I^*]} \\
T^* &= \frac{k_T}{\mu_T},
\end{aligned}
\tag{3.8}
$$

and V^* is solution of the equation below,

$$\delta n \beta A^* V^* = (N \alpha_C M^* + \mu_C) C^*. \tag{3.9}$$

Substituting the population values, which are given by (3.8), in the equation (3.9); we obtain a third-degree equation $\Lambda(V^*) = 0$ where $\Lambda(V^*) = \varphi(V^*) - \psi(V^*)$, $\varphi = c_3 V^{*3} + c_2 V^{*2}$, and $\psi = -c_1 V^* - c_0$. The coefficients $c_i,\ i = 0, \ldots, 3$ are given by appendix 3.B.

Through the Descartes sign rule, we have the possibility of up to 3 positive roots for $\Lambda(V^*)$, regardless of the value of R_0. However, if we impose the restriction $I^* < k_M \mu_T / (\mu_I \mu_T + \gamma k_T)$ required for all population values to be non-negative in (3.8) only one is feasible when $R_0 > 1$ and there is no root feasible if $R_0 < 1$.

Therefore, if $0 < R_0 < 1$, there is only the virus-free equilibrium point W^0, and if $R_0 > 1$, there is only one positive virus-presence equilibrium point W^*. Indeed, when $0 < R_0 < 1$, it is possible to show the global stability of the equilibrium point W^0 for the case without cloning of plasma cells and T cells. Theorem 3.2 asserts this result.

Theorem 3.2. *The virus-free equilibrium point W^0 for the case without cloning for plasma cells and T cells is globally asymptotically stable if $R_0 < 1$.*

Proof: *See Appendix 3.C.* □

Figure 3.2 shows the forward bifurcation for V^* in the absence of cloning in the model (3.2).

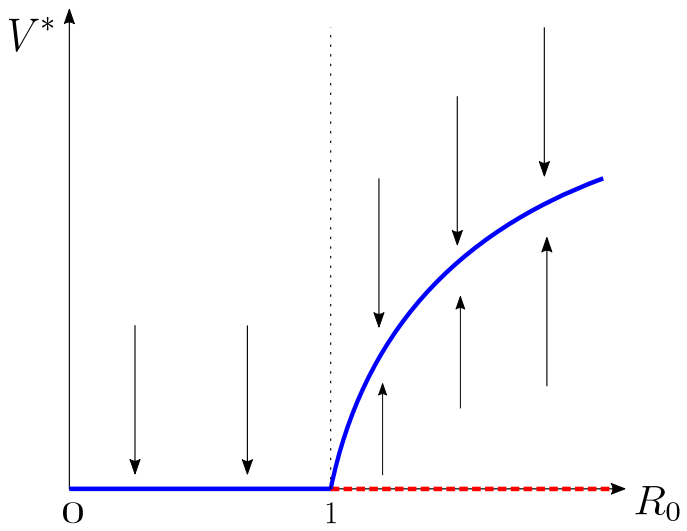

Figure 3.2 – Bifurcation diagram for V^* with respect to R_0.

3.3.3 Cloning only memory B cells

We consider only the parameter α_T equal to zero in the model (3.2). The components of equilibrium point W^* are given by

$$\begin{aligned}
B^* &= \frac{k_B}{\mu_B - \alpha_B V^*} \\
A^* &= \frac{r_A k_B}{(\mu_B - \alpha_B V^*)(\mu_A + n\beta V^*)} \\
M^* &= \frac{k_M \mu_T - (\mu_I \mu_T + \gamma k_T) I^*}{\mu_M \mu_T} \\
I^* &= \frac{[(\mu_B - \alpha_B V^*)(\mu_V \mu_M + \alpha_M k_M)(\mu_A + n\beta V^*) + \mu_M r_A k_B \beta]\mu_T V^*}{(\mu_B - \alpha_B V^*)(\mu_A + n\beta V^*)[r_V \mu_M \mu_T + \alpha_M(\mu_I \mu_T + \gamma k_T)V^*]} \\
C^* &= \frac{[(\sigma + \mu_I)\mu_T + \gamma k_T]\mu_M I^*}{\rho \alpha_C [k_M \mu_T - (\mu_I \mu_T + \gamma k_T) I^*]} \\
T^* &= \frac{k_T}{\mu_T},
\end{aligned} \tag{3.10}$$

and V^* is the root of $p(V^*) = \zeta(V^*) - \chi(V^*)$, where

$$\begin{aligned}
\zeta(V^*) &= \delta n \beta r_A k_B \mu_M \mu_T \rho \alpha_C \{k_M \mu_T (\mu_B - \alpha_B V^*)(\mu_A + n\beta V^*)[r_V \mu_M \mu_T \\
&\quad + \alpha_M(\mu_I \mu_T + \gamma k_T)V^*] - (\mu_I \mu_T + \gamma k_T)[\mu_T(\mu_B - \alpha_B V^*)(\mu_v \mu_M + \alpha_M k_M)(\mu_A \\
&\quad + n\beta V^*) + \mu_M \mu_T r_A k_B \beta]V^*\}[r_V \mu_M \mu_T + \alpha_M(\mu_I \mu_T + \gamma k_T)V^*] \\
\chi(V^*) &= \mu_M[(\sigma + \mu_I)\mu_T + \gamma k_T][\mu_T(\mu_B - \alpha_B V^*)(\mu_V \mu_M + \alpha_M k_M)(\mu_A + n\beta V^*) \\
&\quad + \mu_M \mu_T r_A k_B \beta]\{\mu_T(\mu_B - \alpha_B V^*)(N\alpha_C k_M + \mu_C \mu_M)(\mu_A + n\beta V^*)[r_V \mu_M \mu_T \\
&\quad + \alpha_M(\mu_I \mu_T + \gamma k_T)V^*] - N\alpha_C(\mu_I \mu_T + \gamma k_T)[\mu_T(\mu_B - \alpha_B V^*)(\mu_V \mu_M + \alpha_M k_M)(\mu_A \\
&\quad + n\beta V^*) + \mu_M \mu_T r_A k_B \beta]V^*\}.
\end{aligned}$$

Notice that ζ is a fourth-degree polynomial, and χ is a fifth-degree polynomial. In order to analyze the amount of positive virus-presence equilibrium points, we construct bifurcation diagrams with respect to the parameter α_B and according to the value of R_0.

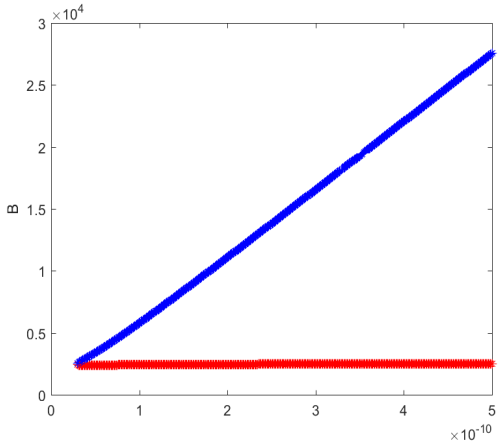

(a) Plasma cell

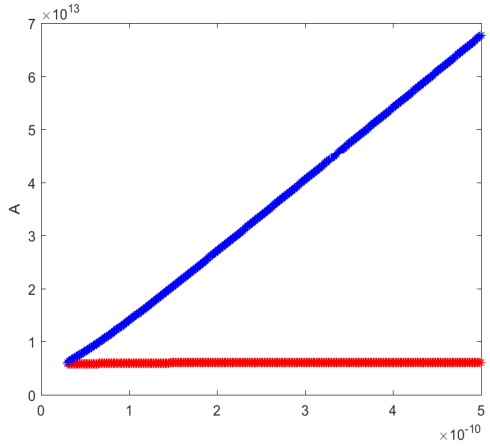

(b) Antibody

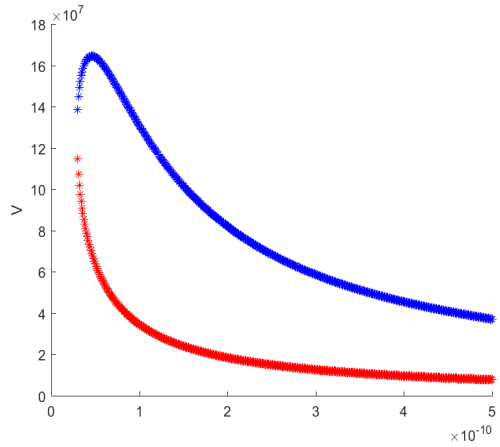

(c) Dengue virus

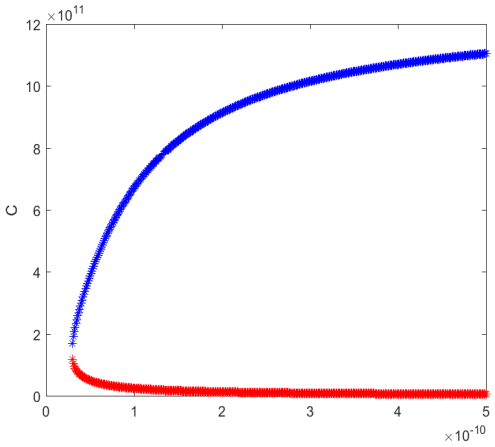

(d) Antigen-antibody complex

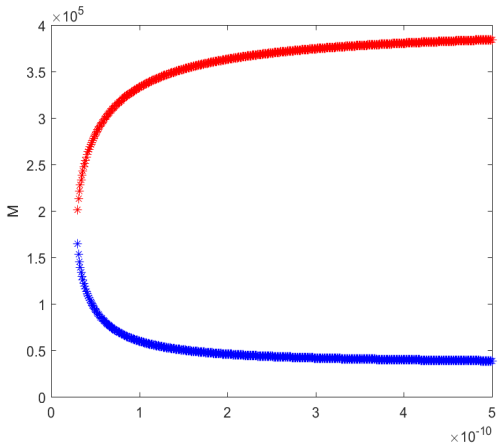

(e) Naive macrophage

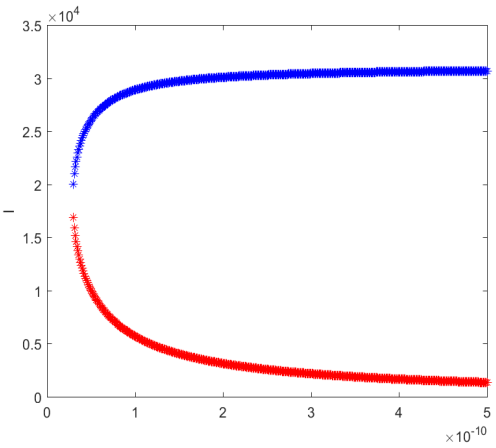

(f) Infected macrophage

Figure 3.3 – Bifurcation diagrams for B^*, A^*, V^*, M^*, I^*, and C^* with respect to the parameter α_B and $R_0 = 0.8$. The blue color indicates the stability of the equilibrium point and the red color indicates instability.

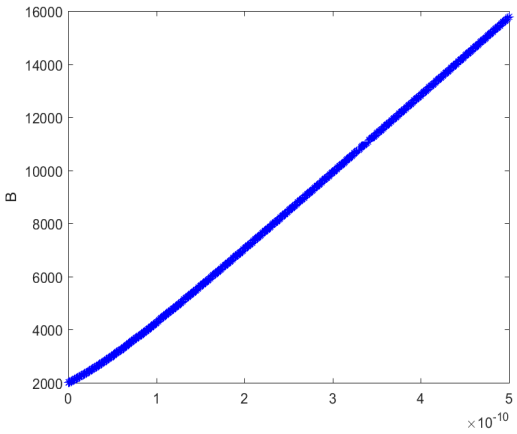

(a) Plasma cell

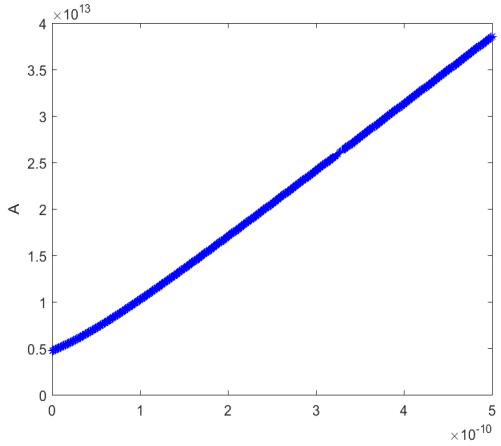

(b) Antibody

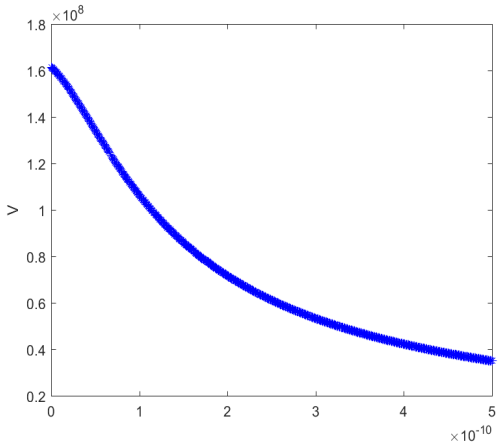

(c) Dengue virus

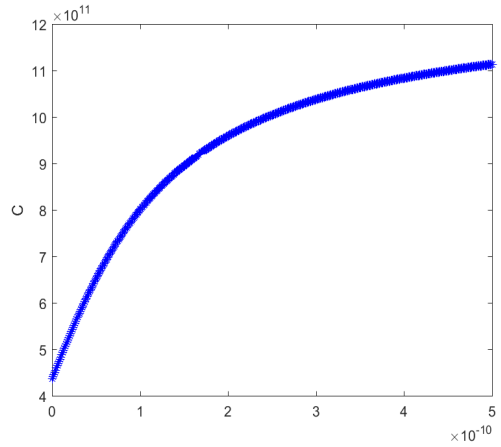

(d) Antigen-antibody complex

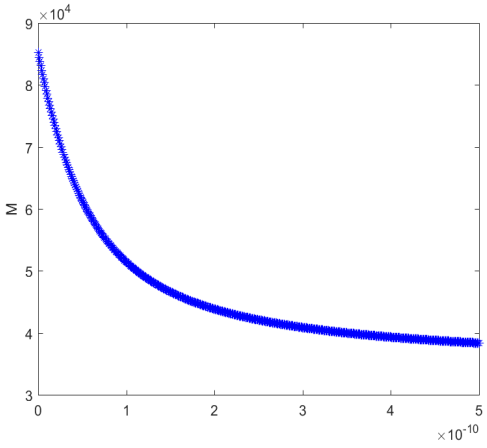

(e) Naive macrophage

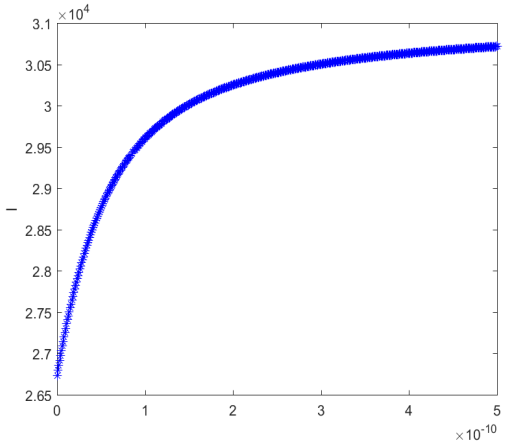

(f) Infected macrophage

Figure 3.4 – Bifurcation diagrams for B^*, A^*, V^*, M^*, I^*, and C^* with respect to the parameter α_B and $R_0 = 1.5$. The blue color indicates the stability of the equilibrium point, and the red color indicates instability.

When $R_0 < 1$, if α_B is greater than α_B^*, we found two positive virus-presence equilibrium points, and if $\alpha_B < \alpha_B^*$ then there is only the virus-free equilibrium point. It

means that if B cells have a low proliferation ($\alpha_B < \alpha_B^*$) then the virus will be eliminated, but if the proliferation rate is higher than α_B^* the virus can persist in the body. It depends on the initial inoculation of the virus. For the case $R_0 > 1$, we obtain only one positive virus-presence equilibrium point. In this case, the immune system will not be able to eliminate the virus.

3.3.4 Cloning only memory T cells

The absence of plasma cell cloning is evaluated by $\alpha_B = 0$ in the model (3.2). The components of the equilibrium point W^* are given by

$$\begin{aligned}
B^* &= \frac{k_B}{\mu_B} \\
A^* &= \frac{r_A k_B}{\mu_B(\mu_A + n\beta V^*)} \\
V^* &= \frac{\mu_B\mu_A(N\alpha_C M^* + \mu_C)C^*}{\delta n\beta r_A k_B - \mu_B n\beta(N\alpha_C M^* + \mu_C)C^*} \\
C^* &= \frac{[(\sigma+\mu_I)(\mu_T - \alpha_T I^*) + \gamma k_T]\mu_M I^*}{\rho\alpha_C[(k_M - \mu_I I^*)(\mu_T - \alpha_T I^*) - \gamma k_T I^*]} \\
M^* &= \frac{(k_M - \mu_I I^*)(\mu_T - \alpha_T I^*) - \gamma k_T I^*}{\mu_M(\mu_T - \alpha_T I^*)} \\
T^* &= \frac{k_T}{\mu_T - \alpha_T I^*},
\end{aligned} \tag{3.11}$$

and I^* is solution of $q(I^*) = \Psi(I^*) - \phi(I^*) = 0$, where

$$\begin{aligned}
\Psi(I^*) &= \{\{\mu_V\mu_M\mu_B(\mu_T - \alpha_T I^*) + \alpha_M\mu_B[(k_M - \mu_I I^*)(\mu_T - \alpha_T I^*) - \gamma k_T I^*]\}(\mu_A V^{den} \\
&\quad + n\beta V^{num}) + \beta r_A k_B \mu_M(\mu_T - \alpha_T I^*)V^{den}\}V^{num} \\
\phi(I^*) &= V^{den} r_V \mu_B\mu_M I^*(\mu_T - \alpha_T I^*)(\mu_A V^{den} + n\beta V^{num}),
\end{aligned}$$

and

$$\begin{aligned}
V^{den} &= \delta n\beta r_A k_B \mu_M \rho\alpha_C(\mu_T - \alpha_T I^*)[(k_M - \mu_I I^*)(\mu_T - \alpha_T I^*) - \gamma k_T I^*] \\
&\quad - \mu_B n\beta\{N\alpha_C[(k_M - \mu_I I^*)(\mu_T - \alpha_T I^*) - \gamma k_T I^*] + \mu_C\mu_M(\mu_T - \alpha_T I^*)\} \\
&\quad \times [(\sigma+\mu_I)(\mu_T - \alpha_T I^*) + \gamma k_T]\mu_M I^* \\
V^{num} &= \mu_M\mu_B\mu_A I^*[(\sigma+\mu_I)(\mu_T - \alpha_T I^*) + \gamma k_T]\{N\alpha_C[(k_M - \mu_I I^*)(\mu_T - \alpha_T I^*) - \gamma k_T I^*] \\
&\quad + \mu_C\mu_M(\mu_T - \alpha_T I^*)\}.
\end{aligned}$$

As $q(I^*)$ is a tenth-degree polynomial, we can obtain up to ten positive real values for I^*. However, for all population equilibrium values are positive, I^* must satisfy two conditions:

$$I^* < I_r \tag{3.12}$$

$$\frac{[(\sigma+\mu_I)(\mu_T-\alpha_T I^*)+\gamma k_T]\mu_M I^*}{\rho\alpha_C[(k_M-\mu_I I^*)(\mu_T-\alpha_T I^*)-\gamma k_T I^*]} < \frac{\delta r_A B^*}{\mu_C + N\alpha_C M^*} \tag{3.13}$$

where I_r is the lowest value solution of $(k_M-\mu_I I^*)(\mu_T-\alpha_T I^*)=\gamma k_T I^*$.

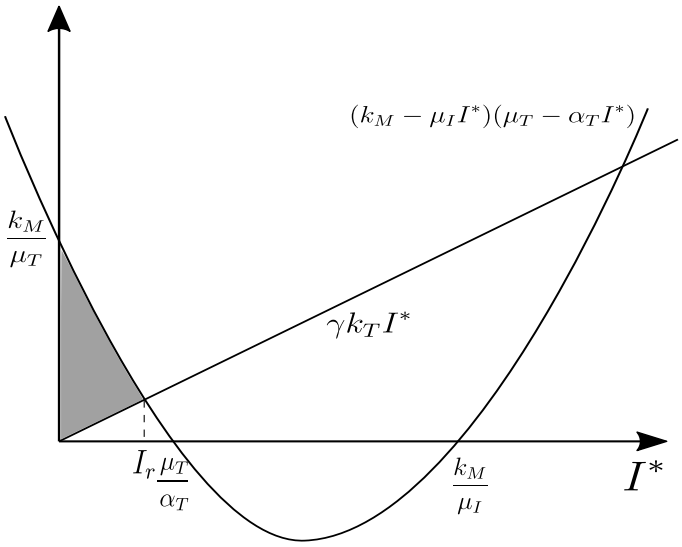

Figure 3.5 – Region (in Gray) biologically viable for the value of I^* satisfying the condition (3.12).

Numerically, if $R_0 > 1$ we obtain only one biologically viable root for I^* and if $R_0 < 1$ there is no biologically viable root for I^*. Thus, if $R_0 < 1$ there is only the VFE point W^0 and if $R_0 > 1$ there are the VPE point W^*, which is locally asymptotically stable and the VFE point W^0, which is unstable. Figure 3.6 shows that memory T cell cloning reduces the concentration of dengue virus, infected macrophages and the immune complex. The effect of T cell cloning does not collaborate to increase the infection, which occurs when we consider only the cloning of memory B cells.

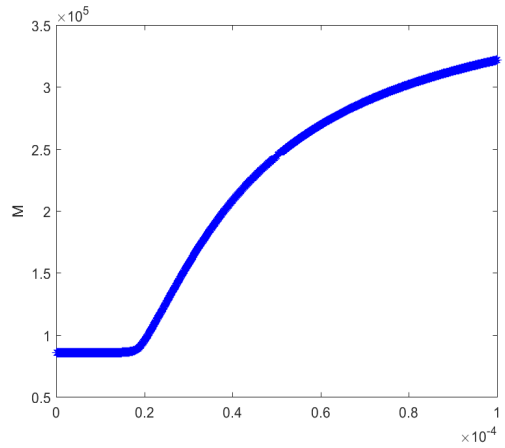

(a) Naive macrophage

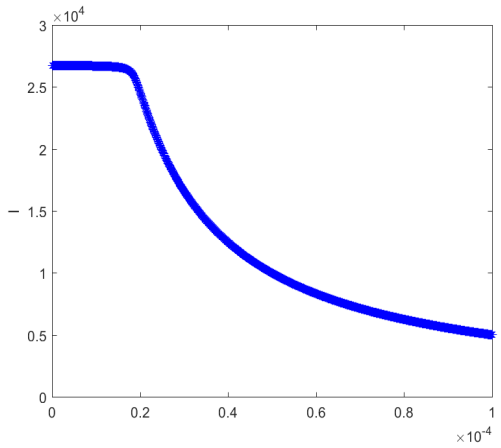

(b) Infected macrophage

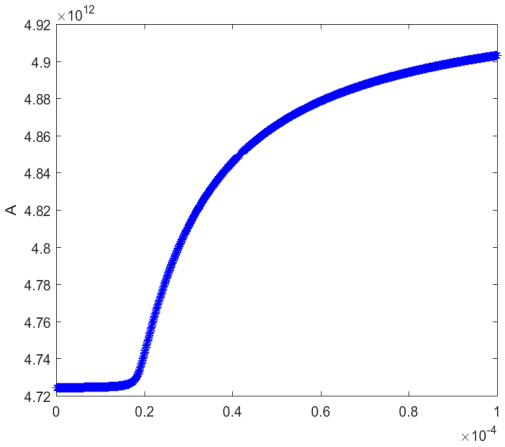

(c) Antibody

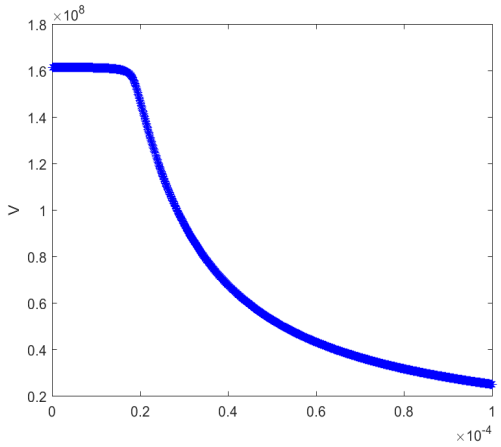

(d) Dengue virus

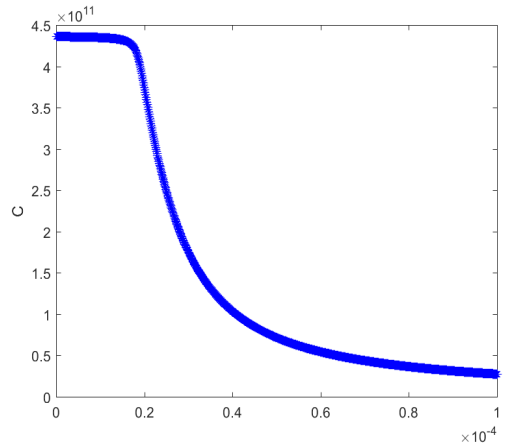

(e) Antigen-antibody complex

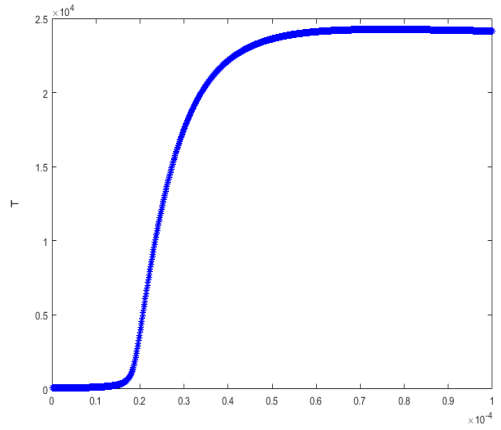

(f) Memory T cell

Figure 3.6 – Bifurcation diagrams for M^*, I^*, A^*, V^*, C^*, and T^* with respect to the parameter α_T and $R_0 = 1.5$. The blue color indicates the stability of the equilibrium point.

3.3.5 Cloning both memory B and T cells

In this case, both memory B and T cells are cloning. To evaluate this joint effect of cloning, we analyze for what values of α_B and α_T are possible the existence of one or three equilibrium points, which all components are non-negative. Concerning $R_0 > 1$, we find only two equilibrium points, which are W^0 (unstable) and W^* (LAS), regardless of the values of α_B and α_T. When $0 < R_0 < 1$, the amount of equilibrium points depends on the values of α_B and α_T.

Figure 3.7 shows that increasing the value of R_0 the value of α_B could be reduced to exist a region with three equilibrium points. Besides that, the value of α_T must increase to eliminate the other two equilibrium points.

3.4 Discussion

In this paper, a compartmental mathematical model was developed to obtain and analyze the steady states. We investigated the influence of memory B and T lymphocyte cloning action during secondary dengue infection.

In the absence of memory B and T cell cloning, there was a forward behavior: when $R_0 < 1$ only if the virus-free equilibrium point W^0 exists, which was locally and asymptotically stable, and for $R_0 > 1$ this same virus-free equilibrium point became unstable and appeared one virus-presence equilibrium point W^*, which was locally stable. When we considered only the possibility of memory T cell cloning, assumed by $\alpha_B = 0$ and $\alpha_T \neq 0$, memory T cells reduced the infected macrophage concentration, but qualitatively the dynamical behavior was not altered.

However, when we considered the possibility of only memory B cell cloning, through $\alpha_B \neq 0$ and $\alpha_T = 0$, this behavior changed. It was possible, even when the basic reproductive number was less than one, the appearance of two virus-presence equilibrium points, which depended on the value of α_B. In that case, there was a steady state with a colossal concentration for the virus, denoted by W^*_+, which was locally asymptotically stable, and another steady state (unstable) with a low density for the dengue virus, indicated by W^*_-. This behavior is showed in Figure 3.3. Therefore, the dynamical system behavior depended on the initial condition. For instance, for a high viral inoculation, the system converged to the equilibrium point W^*_+. A low viral inoculation for the virus was necessary for the virus to be eliminated.

For $R_0 > 1$, regardless of the effect of plasma cell cloning, we had only steady states W^*, which were locally asymptotically stable and W^0 (unstable). Thus, for any positive viral initial condition, the infection persisted.

When we considered the possibility of the joint cloning of memory B and T

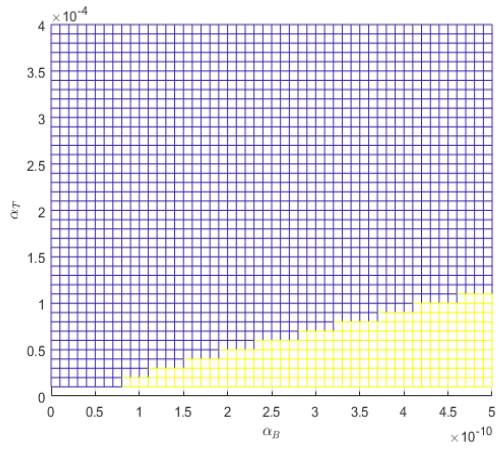

(a) $R_0 = 0.4$

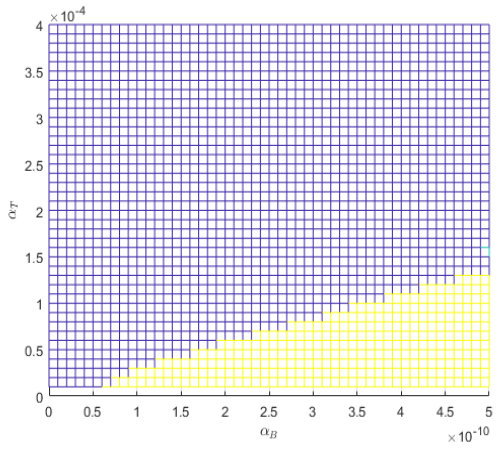

(b) $R_0 = 0.5$

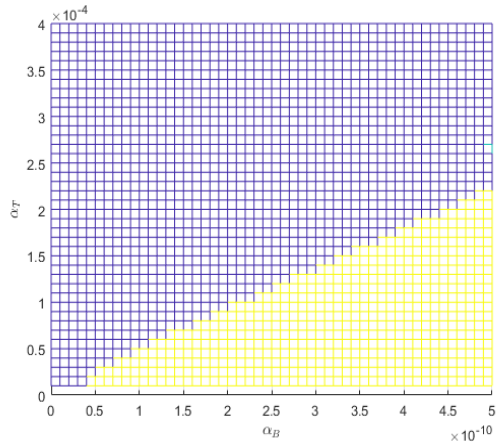

(c) $R_0 = 0.7$

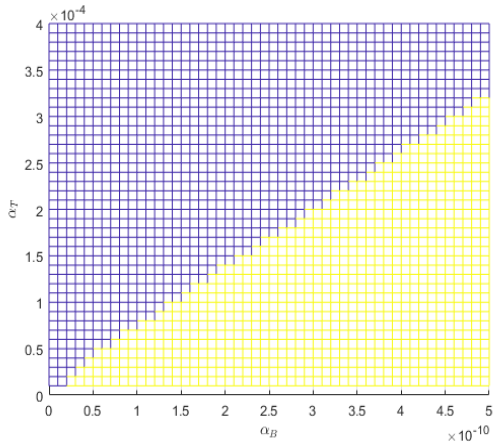

(d) $R_0 = 0.8$

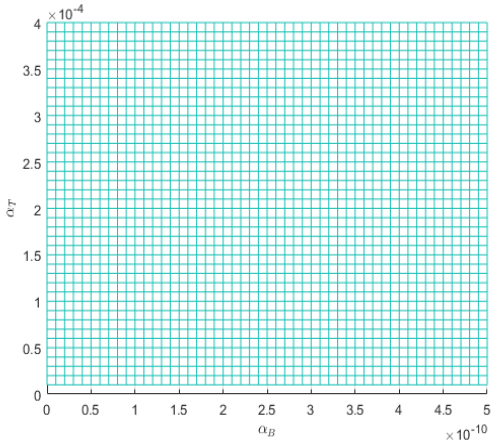

(e) $R_0 = 1.5$

Figure 3.7 – Existence regions for equilibrium points according to the value of R_0 and varying α_B and α_T. The colours indicate the region which equilibrium point exists, with blue (W^0), yellow (W^0, W^*_- and W^*_+), and green (W^0 and W^*).

cells, the values for the parameters of cloning α_B and α_T directly influenced the equilibrium points existence of the model, as presented in Figure 3.7.

Notice that, for $R_0 > 1$ the values of α_B and α_T did not influence the equilibrium points existence. In that case, there was only the virus-free equilibrium point W^0 (unstable) and the virus-presence equilibrium point W^* (stable). However, for values of R_0 in the range $[0, 1[$, there were two non-trivial stationary states when $\alpha_B > \alpha_B^*$ (the region in yellow in Figure 3.8).

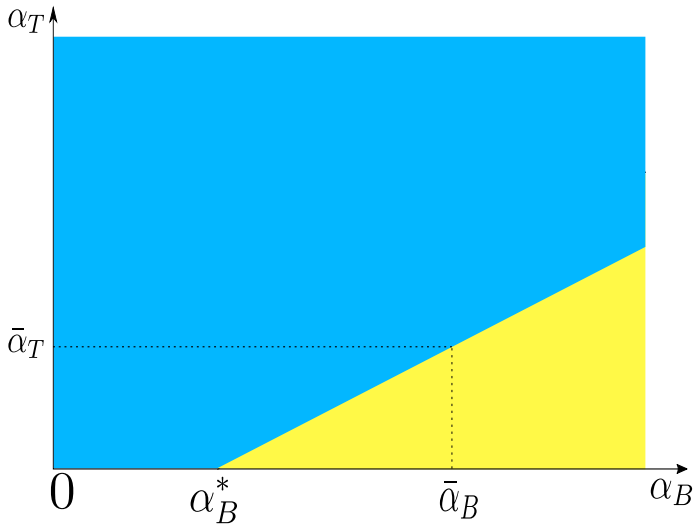

Figure 3.8 – Effect of the joint cloning of memory B and T cells for the region equilibrium points existence when $0 < R_0 < 1$.

Figure 3.8 shows the effect of the joint cloning of memory B and T cells for the region equilibrium points existence when $0 < R_0 < 1$. Consider $\overline{\alpha}_B \in [\alpha_B^*, +\infty[$, it was necessary for the elimination of this two non-trivial equilibrium points that $\alpha_T > \overline{\alpha}_T$, as we can see in the blue region in Figure 3.8. The higher the value of α_B, the greater α_T was necessary to eliminate the virus-presence equilibrium points. In other words, the higher memory B cell cloning capacity, the greater memory T lymphocyte proliferation was necessary to eliminate the possibility of ADE's occurrence.

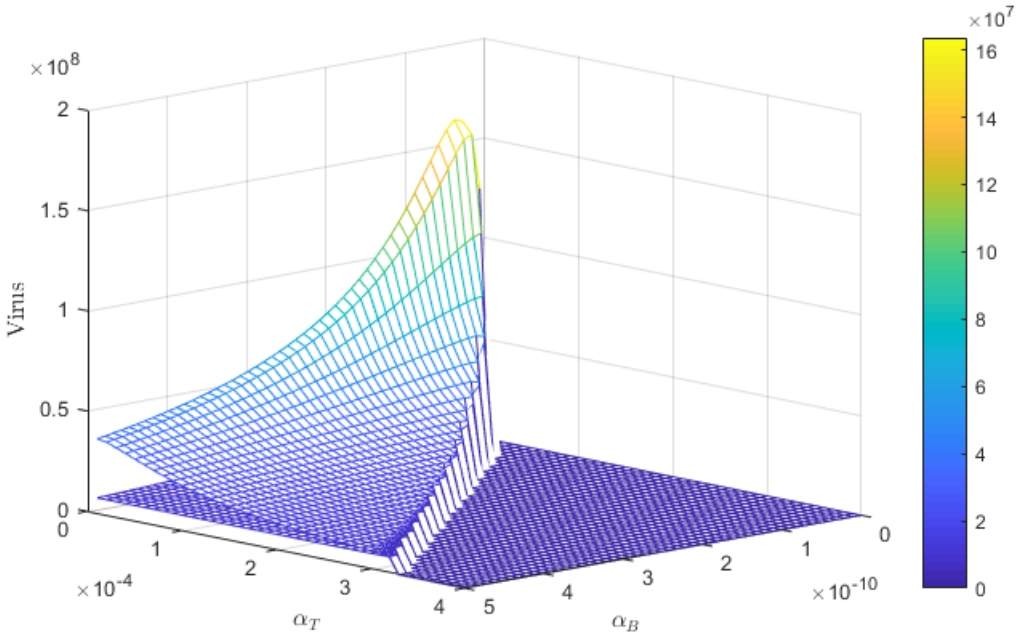

Figure 3.9 – Dengue virus coordinate in terms of the parameters α_B and α_T, considering $R_0 = 0.8$.

Figure 3.9 shows the dengue virus concentration, in terms of the parameters α_B and α_T, with $R_0 = 0.8$. As presented in Figure 3.3c, we showed that for low values of α_B, there was no positive value for the virus coordinate of the virus-presence equilibrium point, but as we increased this value, appeared two virus-presence equilibrium points, with positive values for V^*. Also, as we increased the value of α_B, the two values for the dengue virus coordinates approximated each other. Moreover, suppose the value of α_T was increased. In that case, the viral concentration decreased, eliminating the two surfaces with positive values for the dengue viral concentration, left only the virus-free equilibrium point, as presented in Figure 3.9.

Therefore, we found that the ADE phenomenon can occur in two cases: (i) the cellular memory response is too weak or (ii) both cellular and humoral memory responses are strong, but the cellular memory response decreased faster than the humoral memory response. Thus, the action of T cells collaborated to eliminate the possibility of ADE occurrence. However, an exaggerated concentration of T lymphocytes in the host may favor the appearance of worsening infections (41, 45). T cells release cytokines to act during the inflammatory process. The exacerbated releasing of cytokines, a phenomenon known as cytokine storm, has been related to development of the vascular leak characteristic of dengue severe (41, 46, 47). Thus, a balance of immune responses is necessary in order to control but without aggravating the infection. So, the organism can eliminate the ADE occurrence and at the same time not be aggravated by other factors, such as excessive production of inflammatory cytokines.

3.5 Conclusion

A mathematical model was proposed to analyze the effect of memory B and T cells during a secondary dengue infection by heterologous dengue virus. In the impossibility of cloning these cells, we found that if $R_0 < 1$ there was no possibility of the ADE appearance. However, when we introduced the memory B cell cloning, we observed that an infectious state could arise even when the basic reproduction number is less than one - suggesting that an increase in the production of antibodies may stimulate the formation of a more significant amount of antigen-antibody complexes leading to a higher infection of the target cells by the circulating virus. Analogously, when we analyzed only the effect of memory T cell cloning, we saw that ADE emergence is not possible. These cells acted only to reduce the viral concentration.

In order to portray a real circumstance, both B and T memory cells could clone in the presence of antigen and infected macrophages, respectively. In that scenario, we found that the main responsible for ADE appearance was the memory B cell, depending on the clonal intensity. If they did not have a low cloning capacity, memory T cells were responsible for eliminating this possibility of the ADE appearance.

This model adopted a limited number of variables and an unbounded cloning capacity for both memory T and B cells. B and T cell cloning carrying capacity could be incorporated in future work since they do not have an unbounded proliferation capacity. We can also include the cytokines to understand better the role of T lymphocytes during secondary dengue infection.

Appendix

In this Appendix, proofs of the positive invariance region and the global stability for virus-free equilibrium point without B and T cell cloning are presented. Also, the polynomial coefficients that determine the equilibrium point V^* (for the case without cloning of memory B and T cells) are shown.

3.A Proof of Proposition 3.1

For naive and infected macrophages, we have

$$\begin{aligned}\frac{d(M+I)}{dt} &= k_M - \mu_M M - \mu_I I - \gamma T I \\ &\leqslant k_M - \mu_M M - \mu_I I\end{aligned}$$

Since $\mu_I > \mu_M$, then $M + I \leqslant k_M/\mu_M$.

For V, the maximum production value occurs when all naive macrophages are infected. Thus, we have $M = 0$, $I = I^{\max} = \dfrac{k_M}{\mu_M}$, and the maximum production value of V is $V^{\max} = \dfrac{r_V k_M}{\mu_V \mu_M}$.

For B when $V = 0$, we have

$$\begin{cases}\dfrac{dB}{dt} = k_B - \mu_B B < 0, & \text{if } B > \dfrac{k_B}{\mu_B}, \\ \dfrac{dB}{dt} = k_B - \mu_B B = 0, & \text{if } B = \dfrac{k_B}{\mu_B},\end{cases}$$

However, if $V > 0$ then

$$\frac{dB}{dt} = k_B + \alpha_B V B - \mu_B B > 0, \quad \text{if } B = \frac{k_B}{\mu_B},$$

Thus, $\dfrac{dB}{dt} \geqslant 0$ at the boundary $B = \dfrac{k_B}{\mu_B}$, and no flow crosses this boundary towards values smaller than $B = \dfrac{k_B}{\mu_B}$. Once within of Ω, the flow remains inside this region. Consider the lower limit as $B = \dfrac{k_B}{\mu_B}$, we have $B \geqslant 0$. Analogous to the limitation of B region, we found $T \geqslant \dfrac{k_T}{\mu_T}$.

For the variable C, analogous to V limitation we found the maximum production value for C is when $V = V^{\max}$ and $A = A^{\max}$. Thus, we found $C \leqslant \dfrac{\delta n \beta V^{\max} A^{\max}}{\mu_C}$. Since n antibodies bind to one virus, then for $V = V^{\max}$ we have $nV^{\max}$ antibodies bidden. Therefore, we found the maximum production value for C is

$$C^{max} = \frac{\delta n \beta V^{\max} A^{\max}}{\mu_C} = \frac{\delta \beta}{\mu_C}\left(\frac{n r_V k_M}{\mu_V \mu_M}\right)^2.$$

3.B Coefficients of the φ and ψ polynomials

The coefficients of the polynomial $\varphi(V^*)$ are

$$\begin{aligned}
c_3 &= -n^2\beta^2\mu_B\mu_M^2\mu_T^2(\mu_I\mu_T+\gamma k_T)^2 k_B r_A \alpha_C\alpha_M\delta\mu_V(\rho+\rho^{th}),\\
c_2 &= -n\beta\mu_M^2\mu_T^2\{k_B^2 r_A^2\alpha_C\alpha_M\beta\delta\rho(k_T\gamma+\mu_I\mu_T)^2+\mu_B^2(k_M\alpha_M+\mu_M\mu_V)[2k_T\alpha_M\gamma\mu_A\mu_C\\
&\quad + k_M n N r_V\alpha_C\beta\mu_T + 2\alpha_M\mu_A\mu_C\mu_I\mu_T + n r_V\beta\mu_C\mu_M\mu_T - 2N\alpha_C\mu_A\mu_V k_T\gamma\\
&\quad - 2N\alpha_C\mu_A\mu_V\mu_I\mu_T)][k_T\gamma+\mu_T(\mu_I+\sigma)]\\
&\quad - k_B r_A\mu_B(k_T\gamma+\mu_I\mu_T)[-k_T\gamma\alpha_M\beta\mu_C\mu_M + 2k_T\gamma N\alpha_C\beta\mu_M\mu_V\\
&\quad - k_T\gamma\alpha_C\alpha_M\delta\mu_A\mu_V\rho + k_M\alpha_C\alpha_M\beta k_T N\gamma + k_M\alpha_C\alpha_M\beta n r_V\delta\mu_T\rho\\
&\quad + k_M\alpha_C\alpha_M\beta N\mu_T\mu_I + k_M\alpha_C\alpha_M\beta N\mu_T\sigma - \mu_T\alpha_C\beta\mu_M\mu_V n r_V\delta\rho\\
&\quad + 2\mu_T\alpha_C\beta\mu_M\mu_V N(\mu_I+\sigma) - \mu_T\alpha_M\alpha_C\delta\mu_A\mu_I\mu_V\rho - \mu_T\alpha_M\beta\mu_C\mu_M(\mu_I+\sigma)]\},
\end{aligned}$$

and the coefficients of the polynomial $\psi(V^*)$ are

$$\begin{aligned}
c_1 &= -\mu_M^2\mu_T^2\{\mu_A\mu_B^2(k_M\alpha_M+\mu_M\mu_V)\gamma k_T\mu_A(\alpha_M\mu_C - N\alpha_C\mu_V)[k_T\gamma+\mu_T(\mu_I+\sigma)]\\
&\quad + \mu_T\mu_A^2\mu_B^2(k_M\alpha_M+\mu_M\mu_V)[k_T\gamma+\mu_T(\mu_I+\sigma)]\alpha_M\mu_C\mu_I\\
&\quad + 2\mu_A\mu_B^2(k_M\alpha_M+\mu_M\mu_V)[k_T\gamma+\mu_T(\mu_I+\sigma)]n r_V\beta(k_M N\alpha_C+\mu_C\mu_M)\\
&\quad - \mu_A^2\mu_B^2(k_M\alpha_M+\mu_M\mu_V)[k_T\gamma+\mu_T(\mu_I+\sigma)]N\alpha_C\mu_I\mu_V\\
&\quad - k_B^2 r_A^2\alpha_C\beta^2\mu_M(k_T\gamma+\mu_I\mu_T)k_T N\gamma + k_B^2 r_A^2\alpha_C\beta^2\mu_M(k_T\gamma+\mu_I\mu_T)n r_V\delta\mu_T\rho\\
&\quad - k_B^2 r_A^2\alpha_C\beta^2\mu_M(k_T\gamma+\mu_I\mu_T)N\mu_T(\mu_I+\sigma)\}\\
&\quad - k_B r_A\beta\mu_B\mu_M^2\mu_T^2\{\mu_M(k_T\gamma+\mu_I\mu_T)[k_T\gamma\mu_A(\alpha_M\mu_C - 2N\alpha_C\mu_V) + \mu_T\alpha_M\mu_A\mu_C\mu_I\\
&\quad + \mu_T n r_V\beta\mu_C\mu_M - 2\mu_T N\alpha_C\mu_A\mu_I\mu_V + \mu_T n r_V\alpha_C\delta\mu_A\mu_V\rho] + \mu_M\mu_T\sigma\mu_C k_T\alpha_M\gamma\mu_A\\
&\quad + \mu_M\mu_T\sigma\mu_C\alpha_M\mu_A\mu_I\mu_T + \mu_M\mu_T\sigma\mu_C n r_V\beta\mu_M\mu_T - 2N\alpha_C\mu_A\mu_V(k_T\gamma+\mu_I\mu_T)\\
&\quad - k_M\alpha_C k_T^2 N\alpha_M\gamma^2\mu_A - k_M\alpha_C\mu_T^2 n r_V\delta\alpha_M\mu_A\mu_I\rho - k_M\alpha_C\mu_T^2 n^2 r_V^2\delta\beta\mu_M\rho\\
&\quad - k_M\alpha_C\mu_T^2 N\alpha_M\mu_A\mu_I + k_M\alpha_C\mu_T^2 n r_V\beta\mu_M(\mu_I+\sigma) + k_M\alpha_C k_T\gamma\mu_T n N r_V\beta\mu_M\\
&\quad - k_M\alpha_C k_T\gamma\mu_T n r_V\alpha_M\delta\mu_A\rho - k_M\alpha_C k_T\gamma\mu_T N\alpha_M\mu_A(2\mu_I+\sigma)\}\\
c_0 &= r_V\mu_M^2\mu_T^3\mu_B^2\mu_A^2[\mu_T(\mu_I+\sigma)+\gamma k_T](\mu_M\mu_V+\alpha_M k_M)(\mu_M\mu_C+N\alpha_C k_M)(R_0-1),
\end{aligned}$$

where $\alpha_C^{th} = \dfrac{\alpha_M\mu_C}{N\mu_V}$ and $\rho^{th} = \dfrac{(\alpha_C^{th}-\alpha_C)(\mu_M\mu_V+\alpha_M k_M)[(\mu_I+\sigma)\mu_T+\gamma k_T]N\mu_B}{(\mu_I\mu_T+\gamma k_T)k_B r_A\alpha_C\delta\alpha_M}$.

3.C Proof of the Theorem 3.2

We use the direct Lyapunov method to proof the Theorem 3.2. To construct the Lyapunov function, we used a matrix-theoretic method, which is based on the Perron

eigenvector (48) and the Next Generation Matrix (48, 49, 50, 51).

Firstly, we construct the vectors $\mathcal{F}$ and $\mathcal{V}$, where $\mathcal{F}_i$ represents the rate of new infections in the ith disease compartment and $\mathcal{V}_i$ represents the transition terms.

$$\mathcal{F} = \begin{bmatrix} r_A - n\beta VA \\ r_V I - \beta AV \\ \delta n\beta AV \\ \rho\alpha_C MC \end{bmatrix}, \qquad \mathcal{V} = \begin{bmatrix} \mu_A A \\ \mu_V V + \alpha_M MV \\ \mu_C C + N\alpha_C MC \\ (\sigma + \mu_I)I + \gamma TI \end{bmatrix}$$

Based on (49, 50) we defined two 4×4 matrices,

$$\mathbb{F} = \left[\frac{\partial \mathcal{F}_i}{\partial x_j}(0, y_0)\right] \quad \text{and} \quad \mathbb{V} = \left[\frac{\partial \mathcal{V}_i}{\partial x_j}(0, y_0)\right].$$

So, the inputs of matrices $\mathbb{F}$ and $\mathbb{V}$ are

$$\mathbb{F} = \begin{bmatrix} 0 & -n\beta VA^0 & 0 & 0 \\ 0 & -\beta A^0 & 0 & r_V \\ 0 & \delta n\beta A^0 & 0 & 0 \\ 0 & 0 & \rho\alpha_C M^0 & 0 \end{bmatrix},$$

$$\mathbb{V} = \begin{bmatrix} \mu_A & 0 & 0 & 0 \\ 0 & \mu_V + \alpha_C M^0 & 0 & 0 \\ 0 & 0 & \mu_C + N\alpha_C M^0 & 0 \\ 0 & 0 & 0 & \mu_I + \sigma + \gamma T^0 \end{bmatrix}.$$

Let $\mathbb{G} = \mathbb{V}^{-1}\mathbb{F}$ and ω be the left eigenvector of the non-negative matrix $\mathbb{V}^{-1}\mathbb{F}$ corresponding to the eigenvalue $\rho(\mathbb{V}^{-1}\mathbb{F}) = \rho(\mathbb{F}\mathbb{V}^{-1}) = \lambda$, where $\mathbb{F}\mathbb{V}^{-1}$ is the next generation matrix (51) of the model (3.2). We obtain

$$\omega^T = \begin{bmatrix} 0 & 1 & \dfrac{\rho\alpha_C M^0 r_V}{\lambda^2(\mu_I + \sigma + \gamma T^0)(\mu_V + \alpha_M M^0)} & \dfrac{r_V}{\lambda(\mu_V + \alpha_M M^0)} \end{bmatrix},$$

and the characteristic polynomial of the matrix $\mathbb{G}$ is given by $\Lambda(x) = x^3 + \dfrac{A^0\beta}{\mu_V + \alpha_M M^0}x^2 - \dfrac{A^0\beta n r_V \alpha_C \delta \rho M^0}{(\mu_C + N\alpha_C M^0)(\mu_V + \alpha_M M^0)(\mu_I + \sigma + \gamma T^0)}$. According to Yang and Greenhalgh (2015) we can define $R_0^* = \dfrac{A^0\beta n r_V \alpha_C \delta \rho M^0}{(\mu_C + N\alpha_C M^0)(\mu_V + \alpha_M M^0)(\mu_I + \sigma + \gamma T^0)} - \dfrac{A^0\beta}{\mu_V + \alpha_M M^0} = R_0$. Then R_0^* is a threshold value for the disease to disappear in the sense that

(i) $R_0^* > 1$ if and only if $\lambda > 1$

(ii) $R_0^* = 1$ if and only if $\lambda = 1$

(iii) $R_0^* < 1$ if and only if $\lambda < 1$.

We take $Q : \Gamma \to \mathbb{R}$, where $\Gamma = \{(B, A, V, C, M, I, T) \in \mathbb{R}_+^7 : M \leqslant M^0, A \leqslant A^0, V \geqslant 0, I \geqslant 0\}$ and

$$Q = \frac{1}{\mu_V + \alpha_M M^0} V + \frac{\rho \alpha_C M^0 r_V}{\lambda^2(\mu_I + \sigma + \gamma T^0)(\mu_V + \alpha_M M^0)(\mu_C + N\alpha_C M^0)} C + \frac{r_V}{\lambda(\mu_V + \alpha_M M^0)} I.$$

Notice that $Q(W^0) = 0$ and $Q > 0$ in $\Gamma - \{W^0\}$. Besides that, the derivative function of Q is given by

$$\begin{aligned}
\frac{dQ}{dt} &= \frac{1}{\mu_V + \alpha_M M^0}\frac{dV}{dt} + \frac{\rho \alpha_C M^0 r_V}{\lambda^2(\mu_I + \sigma + \gamma T^0)(\mu_V + \alpha_M M^0)(\mu_C + N\alpha_C M^0)}\frac{dC}{dt} \\
&\quad + \frac{r_V}{\lambda(\mu_V + \alpha_M M^0)}\frac{dI}{dt} \\
&= \frac{1}{\mu_V + \alpha_M M^0}\left(r_V I - \mu_V V - \alpha_M M V - \beta A V\right) \\
&\quad + \frac{\rho \alpha_C M^0 r_V}{\lambda^2(\mu_I + \sigma + \gamma T^0)(\mu_V + \alpha_M M^0)(\mu_C + N\alpha_C M^0)}\left(\delta n \beta V A - N\alpha_C M C - \mu_C C\right) \\
&\quad + \frac{r_V}{\lambda(\mu_V + \alpha_M M^0)}[\rho \alpha_C C M - (\mu_I + \sigma) I - \gamma T I],
\end{aligned}$$

which can be rewritten as

$$\frac{dQ}{dt} = q_V V + q_C C + q_I I,$$

where

$$\begin{aligned}
q_V &= -\frac{\mu_V}{\mu_V + \alpha_M M^0} - \frac{\alpha_M M}{\mu_V + \alpha_M M^0} - \frac{\beta A}{\mu_V + \alpha_M M^0} \\
&\quad + \frac{1}{\lambda^2}\frac{\rho \alpha_C r_V M^0 n \delta \beta A}{(\mu_I + \sigma + \gamma T^0)(\mu_V + \alpha_M M^0)(\mu_C + N\alpha_C M^0)} \\
q_C &= \frac{r_V \rho \alpha_C M}{(\mu_I + \sigma + \gamma T^0)(\mu_V + \alpha_M M^0)} \\
&\quad - \frac{1}{\lambda^2}\frac{\rho \alpha_C r_V M^0 (N\alpha_C M + \mu_C)}{\lambda^2(\mu_I + \sigma + \gamma T^0)(\mu_V + \alpha_M M^0)(\mu_C + N\alpha_C M^0)} \\
q_I &= -\frac{r_V}{(\mu_V + \alpha_M M^0)}\left[\frac{\mu_I + \sigma + \gamma T}{\lambda(\mu_I + \sigma + \gamma T^0)} - 1\right].
\end{aligned}$$

Using the assumptions $M \leqslant M^0$, $A \leqslant A^0$, $T \leqslant T^0$, $\Lambda(\lambda) = 0$, and $\lambda < 1$ we obtain

$$q_V = \lambda \frac{A}{A^0} - 1 \leqslant 0 \tag{3.14}$$

$$q_C = -\frac{r_V \rho \alpha_C M}{\lambda(\mu_I + \sigma + \gamma T^0)(\mu_V + \alpha_M M^0)} \left(\frac{M^0}{\lambda} - M \right) \leqslant 0 \tag{3.15}$$

$$q_I \leqslant -\frac{r_V}{\mu_V + \alpha_M M^0} \left(\frac{1}{\lambda} - 1 \right) \leqslant 0. \tag{3.16}$$

Therefore, $Q' \leqslant 0$ in $\Gamma - \{W^0\}$ if and only if $R_0 < 1$. So, we conclude by LaSalle's invariance principle (53), the equilibrium point W^0 is globally asymptotically stable. □

4 Conclusões

Neste trabalho foram estudados dois modelos matemáticos, com o propósito de descrever o fênomeno reforço dependente de anticorpos, e analisar o efeito das células de memória durante uma infecção secundária por vírus de dengue heterólogo.

No Capítulo 1, estudou-se um modelo simplificado que aborda a interação somente das células plasma, a célula alvo (macrófagos) e o vírus da dengue. O foco neste trabalho foi avaliar o efeito da capacidade de suporte para a proliferação das células plasmáticas, isto é, analisar o efeito de uma proliferação limitada para estas células. Foi encontrado que quanto maior a capacidade das células plasmáticas de se proliferarem, maior será a possibilidade do vírus da dengue não ser eliminado pela ação do sistema imune. Encontramos que a proliferação de células plasmáticas juntamente com a inoculação do vírus têm um papel fundamental na ocorrência do fenômeno reforço dependente de anticorpos. Foi feita uma análise de sensibilidade com o objetivo de analisar quais parâmetros influenciavam mais os limiares R_0 e Q. Encontramos que a taxa de engolfamento do complexo imune por macrófagos, a proporção de macrófagos infectados e a taxa de fagocitose do vírus por macrófagos são os parâmetros que mais influenciam o número de reprodutibilidade basal, enquanto que a taxa de proliferação das células plasmáticas juntamente com todos os parâmetros citados anteriormente influenciam o fator de enfraquecimento do ADE.

No Capítulo 2 foi feito uma comparação entre as abordagens determinística e estocástica para simular a dinâmica do ADE apresentada no capítulo anterior. Encontramos que além do valor de R_0 importante para determinar a estabilidade dos pontos de equilíbrio, a condição inicial do sistema tem um papel fundamental nas simulações estocásticas. Vimos que há situações que a curva média das simulações estocásticas se aproxima da curva determinística ou não, dependendo do valor da condição inicial. A abordagem estocástica é uma ferramenta útil para simular sistemas, estudar tempo de extinção de uma determinada infecção, investigar a probabilidade de um determinado evento ocorrer, entre outros aspectos. Entretanto, sem uma análise matemática do respectivo modelo determinístico, extrair conclusões da dinâmica estudada pode ser complexo. Portanto, concluímos que a abordagem de simulação estocástica é uma ótima abordagem para simular sistemas biológicos, mas para a compreensão da dinâmica do fenômeno de interesse é necessário uma análise do respectivo modelo determinístico. Em modelos de alta complexidade analítica é interessante ao menos estudar o ponto trivial e obter analiticamente algum resultado acerca do limiar R_0, importante para determinar a existência e estabilidade dos pontos de equilíbrios.

No Capítulo 3 foram introduzidas novas variáveis, a fim de analisar a dinâmica do ADE de forma mais detalhada. Neste caso, além das variáveis já descritas no Capítulo 1, introduzimos as células T de memória, a formação do complexo antígeno-anticorpo e a liberação de anticorpos pelas células B de memória. Observou-se que a proliferação das células B é o principal responsável pela ocorrência do fenômeno ADE. Caso as células B de memória tenham uma alta proliferação, é possível o vírus da dengue persistir e alcançar uma alta carga viral, mesmo para uma baixa inoculação do vírus. A existência de uma maior quantidade de células T de memória se mostrou eficaz no controle viral, sendo possível diminuir a concentração de vírus ou até mesmo eliminar a possibilidade do ADE. As análises dos dois modelos foram feitas sob o ponto de vista qualitativo.

Trabalhos futuros

Como trabalho futuro pretende-se continuar a investigação do fenômeno reforço dependente de anticorpos incorporando novas varíaveis ou parâmetros no modelo apresentado no Capítulo 3. Por exemplo, considerando capacidades de suporte para a proliferação das células B e T de memória e a inclusão como varíavel dinâmica de citocinas pró-inflamatórias associadas com a severidade da dengue.

Referências

1 RUBIO, F. A.; YANG, H. M. A mathematical model to describe antibody-dependent enhancement and assess the effect of limiting cloning for plasma cells in heterologous secondary dengue infection. *preprint*, 2020.

2 GILLESPIE, D. T. Exact stochastic simulation of coupled chemical reactions. *The journal of physical chemistry*, ACS Publications, v. 81, n. 25, p. 2340–2361, 1977.

3 ORGANIZATION World Health. *Epidemiology*. 2019. Disponível em: <https://www.who.int/denguecontrol/epidemiology/en/>.

4 CONTROL, C. for D.; PREVENTION. *Dengue and Dengue Hemorrhagic Fever*. 2009. Disponível em: <https://www.cdc.gov/dengue/resources/denguedhf-information-for-health-care-practitioners_2009.pdf>.

5 NET, D. V. *Dengue Virus*. 2019. Disponível em: <http://www.denguevirusnet.com/dengue-virus.html>.

6 JOHN, A. L. S.; RATHORE, A. P. Adaptive immune responses to primary and secondary dengue virus infections. *Nature Reviews Immunology*, Nature Publishing Group, p. 1, 2019.

7 BORGES, M. B.; MARCHEVSKY, R. S.; PEREIRA, R. C.; MENDES, Y. da S.; MENDES, L. G. A.; DINIZ-MENDES, L.; CRUZ, M. A.; TAHMAOUI, O.; BAUDART, S.; FREIRE, M. et al. Detection of post-vaccination enhanced dengue virus infection in macaques: An improved model for early assessment of dengue vaccines. *PLoS pathogens*, Public Library of Science, v. 15, n. 4, p. e1007721, 2019.

8 HAWKES, R. Enhancement of the infectivity of arboviruses by specific antisera produced in domestic fowls. *Australian Journal of Experimental Biology and Medical Science*, Wiley Online Library, v. 42, n. 4, p. 465–482, 1964.

9 HALSTEAD, S.; O'ROURKE, E. Antibody-enhanced dengue virus infection in primate leukocytes. *Nature*, Nature Publishing Group, v. 265, n. 5596, p. 739, 1977.

10 CASTILLO, J. A.; URCUQUI-INCHIMA, S. Mechanisms of monocyte cell death triggered by dengue virus infection. *Apoptosis*, Springer, p. 1–11, 2018.

11 ROBERTS, K.; ALBERTS, B.; JOHNSON, A.; WALTER, P.; HUNT, T. *Molecular biology of the cell*. [S.l.]: New York: Garland Science, 2002.

12 ABBAS, A. K.; LICHTMAN, A. H.; PILLAI, S. *Imunologia celular e molecular*. [S.l.]: Elsevier Brasil, 2015.

13 DÖRNER, T.; RADBRUCH, A. Selecting b cells and plasma cells to memory. *The Journal of experimental medicine*, The Rockefeller University Press, v. 201, n. 4, p. 497, 2005.

14 ONG, E. Z.; ZHANG, S. L.; TAN, H. C.; GAN, E. S.; CHAN, K. R.; OOI, E. E. Dengue virus compartmentalization during antibody-enhanced infection. *Scientific reports*, Nature Publishing Group, v. 7, n. 1, p. 1–9, 2017.

15 GÓMEZ, M. C.; YANG, H. M. A simple mathematical model to describe antibody-dependent enhancement in heterologous secondary infection in dengue. *Mathematical medicine and biology: a journal of the IMA*, Oxford University Press, v. 36, n. 4, p. 411–438, 2019.

16 MAK, T. W.; SAUNDERS, M. E. *The immune response: basic and clinical principles*. [S.l.]: Academic Press, 2005.

17 CHEN, Y.-C.; WANG, S.-Y. Activation of terminally differentiated human monocytes/macrophages by dengue virus: productive infection, hierarchical production of innate cytokines and chemokines, and the synergistic effect of lipopolysaccharide. *Journal of virology*, Am Soc Microbiol, v. 76, n. 19, p. 9877–9887, 2002.

18 ALBERTS, B.; BRAY, D.; LEWIS, L.; RAFF, M.; ROBERTS, K.; WATSON, J. *Molecular Biology of The Cell*. [S.l.]: Garland Publishing Inc., New York & London, 1983.

19 COURAGEOT, M.-P.; CATTEAU, A.; DESPRES, P. Mechanisms of dengue virus-induced cell death. *Adv Virus Res*, v. 60, p. 157–186, 2003.

20 KOU, Z.; LIM, J. Y.; BELTRAMELLO, M.; QUINN, M.; CHEN, H.; LIU, S.-n.; MARTNEZ-SOBRIDO, L.; DIAMOND, M. S.; SCHLESINGER, J. J.; SILVA, A. de et al. Human antibodies against dengue enhance dengue viral infectivity without suppressing type i interferon secretion in primary human monocytes. *Virology*, Elsevier, v. 410, n. 1, p. 240–247, 2011.

21 SITHISARN, P.; SUKSANPAISAN, L.; THEPPARIT, C.; SMITH, D. R. Behavior of the dengue virus in solution. *Journal of medical virology*, Wiley Online Library, v. 71, n. 4, p. 532–539, 2003.

22 EDELSTEIN-KESHET, L. *Mathematical models in biology*. [S.l.]: SIAM, 2005.

23 MARINO, S.; HOGUE, I. B.; RAY, C. J.; KIRSCHNER, D. E. A methodology for performing global uncertainty and sensitivity analysis in systems biology. *Journal of theoretical biology*, Elsevier, v. 254, n. 1, p. 178–196, 2008.

24 MCKAY, M. D.; BECKMAN, R. J.; CONOVER, W. J. A comparison of three methods for selecting values of input variables in the analysis of output from a computer code. *Technometrics*, Taylor & Francis Group, v. 42, n. 1, p. 55–61, 2000.

25 BLOWER, S. M.; DOWLATABADI, H. Sensitivity and uncertainty analysis of complex models of disease transmission: an hiv model, as an example. *International Statistical Review/Revue Internationale de Statistique*, JSTOR, p. 229–243, 1994.

26 GOMERO, B. Latin hypercube sampling and partial rank correlation coefficient analysis applied to an optimal control problem. 2012.

27 FOUNDATION, T. R. *The R Project for Statistical Computing*. Disponível em: <https://www.r-project.org/>.

28 YANG, H. M. A mathematical model for malaria transmission relating global warming and local socioeconomic conditions. *Revista de saude publica*, SciELO Public Health, v. 35, p. 224–231, 2001.

29 TIRADO, S. M. C.; YOON, K.-J. Antibody-dependent enhancement of virus infection and disease. *Viral immunology*, Mary Ann Liebert, Inc., v. 16, n. 1, p. 69–86, 2003.

30 NIKIN-BEERS, R.; CIUPE, S. M. The role of antibody in enhancing dengue virus infection. *Mathematical biosciences*, Elsevier, v. 263, p. 83–92, 2015.

31 CAMPOS, J. L. S.; MONGKOLSAPAYA, J.; SCREATON, G. R. The immune response against flaviviruses. *Nature immunology*, Nature Publishing Group, v. 19, n. 11, p. 1189, 2018.

32 MAIDANA, N.; YANG, H. A spatial model to describe the dengue propagation. *TEMA (São Carlos)*, v. 8, n. 1, p. 83–92, 2007.

33 YANG, H. M. The transovarial transmission in the dynamics of dengue infection: Epidemiological implications and thresholds. *Mathematical biosciences*, Elsevier, v. 286, p. 1–15, 2017.

34 ESTEVA, L.; YANG, H. M. Assessing the effects of temperature and dengue virus load on dengue transmission. *Journal of Biological Systems*, World Scientific, v. 23, n. 04, p. 1550027, 2015.

35 SUN, W.; XUE, L.; YAN, X. Stability of a dengue epidemic model with independent stochastic perturbations. *Journal of Mathematical Analysis and Applications*, Elsevier, v. 468, n. 2, p. 998–1017, 2018.

36 DIN, A.; KHAN, T.; LI, Y.; TAHIR, H.; KHAN, A.; KHAN, W. A. Mathematical analysis of dengue stochastic epidemic model. *Results in Physics*, Elsevier, v. 20, p. 103719, 2021.

37 OTERO, M.; SOLARI, H. G. Stochastic eco-epidemiological model of dengue disease transmission by aedes aegypti mosquito. *Mathematical biosciences*, Elsevier, v. 223, n. 1, p. 32–46, 2010.

38 FOUNDATION, P. S. *Welcome to Python.org*. Disponível em: <https://www.python.org/about/>.

39 NÅSELL, I. *Extinction and quasi-stationarity in the stochastic logistic SIS model*. [S.l.]: Springer, 2011.

40 DEJNIRATTISAI, W.; SUPASA, P.; WONGWIWAT, W.; ROUVINSKI, A.; BARBA-SPAETH, G.; DUANGCHINDA, T.; SAKUNTABHAI, A.; CAO-LORMEAU, V.-M.; MALASIT, P.; REY, F. A. et al. Dengue virus sero-cross-reactivity drives antibody-dependent enhancement of infection with zika virus. *Nature immunology*, Nature Publishing Group, v. 17, n. 9, p. 1102, 2016.

41 COSTA, V. V.; FAGUNDES, C. T.; SOUZA, D. G.; TEIXEIRA, M. M. Inflammatory and innate immune responses in dengue infection: protection versus disease induction. *The American journal of pathology*, Elsevier, v. 182, n. 6, p. 1950–1961, 2013.

42 MEHLHOP, E.; NELSON, S.; JOST, C. A.; GORLATOV, S.; JOHNSON, S.; FREMONT, D. H.; DIAMOND, M. S.; PIERSON, T. C. Complement protein c1q reduces the stoichiometric threshold for antibody-mediated neutralization of west nile virus. *Cell host & microbe*, Elsevier, v. 6, n. 4, p. 381–391, 2009.

43 CIUPE, S. M.; RIBEIRO, R. M.; NELSON, P. W.; DUSHEIKO, G.; PERELSON, A. S. The role of cells refractory to productive infection in acute hepatitis b viral dynamics. *Proceedings of the National Academy of Sciences*, National Acad Sciences, v. 104, n. 12, p. 5050–5055, 2007.

44 NIKIN-BEERS, R.; CIUPE, S. M. Modelling original antigenic sin in dengue viral infection. *Mathematical medicine and biology: a journal of the IMA*, Oxford University Press, v. 35, n. 2, p. 257–272, 2017.

45 MATHEW, A.; TOWNSLEY, E.; ENNIS, F. A. Elucidating the role of t cells in protection against and pathogenesis of dengue virus infections. *Future microbiology*, Future Medicine, v. 9, n. 3, p. 411–425, 2014.

46 MONGKOLSAPAYA, J.; DUANGCHINDA, T.; DEJNIRATTISAI, W.; VASANAWATHANA, S.; AVIRUTNAN, P.; JAIRUNGSRI, A.; KHEMNU, N.; TANGTHAWORNCHAIKUL, N.; CHOTIYARNWONG, P.; SAE-JANG, K. et al. T cell responses in dengue hemorrhagic fever: are cross-reactive t cells suboptimal? *The Journal of Immunology*, Am Assoc Immnol, v. 176, n. 6, p. 3821–3829, 2006.

47 SRIKIATKHACHORN, A.; MATHEW, A.; ROTHMAN, A. L. Immune-mediated cytokine storm and its role in severe dengue. In: SPRINGER. *Seminars in immunopathology*. [S.l.], 2017. v. 39, n. 5, p. 563–574.

48 SHUAI, Z.; DRIESSCHE, P. van den. Global stability of infectious disease models using lyapunov functions. *SIAM Journal on Applied Mathematics*, SIAM, v. 73, n. 4, p. 1513–1532, 2013.

49 DRIESSCHE, P. Van den; WATMOUGH, J. Further notes on the basic reproduction number. In: *Mathematical epidemiology*. [S.l.]: Springer, 2008. p. 159–178.

50 DRIESSCHE, P. Van den; WATMOUGH, J. Reproduction numbers and sub-threshold endemic equilibria for compartmental models of disease transmission. *Mathematical biosciences*, Elsevier, v. 180, n. 1-2, p. 29–48, 2002.

51 DIEKMANN, O.; HEESTERBEEK, J.; ROBERTS, M. G. The construction of next-generation matrices for compartmental epidemic models. *Journal of the Royal Society Interface*, The Royal Society, v. 7, n. 47, p. 873–885, 2009.

52 YANG, H. M.; GREENHALGH, D. Proof of conjecture in: The basic reproduction number obtained from jacobian and next generation matrices—a case study of dengue transmission modelling. *Applied Mathematics and Computation*, Elsevier, v. 265, p. 103–107, 2015.

53 LASALLE, J. P. *The stability of dynamical systems*. [S.l.]: Siam, 1976. v. 25.